The Role of Fractional Rainfall Coverage in Atmospheric General Circulation Model Hydrologic Processes

by

Gavin Gong

B.E. The Cooper Union for the
Advancement of Science and Art
1991

Submitted to the Department of Civil and Environmental Engineering
in partial fulfillment of the requirements for the degree of

Master of Science in Civil and Environmental Engineering

at the

MASSACHUSETTS INSTITUTE OF TECHNOLOGY

May 1994

Author . . . .
Department of Civil and Environmental Engineering
May 13, 1994

Certified by . . . .
Dara Entekhabi
Assistant Professor of Civil and Environmental Engineering
Thesis Supervisor

Accepted by . . . .
Joseph M. Sussman
Chairman, Departmental Committee on Graduate Students

The Role of Fractional Rainfall Coverage in Atmospheric General Circulation Model Hydrologic Processes

by

Gavin Gong

B.E. The Cooper Union for the
Advancement of Science and Art
1991

Abstract

Simulated climates using numerical atmospheric General Circulation Models (GCMs) have been shown to be highly sensitive to the fraction of GCM grid area assumed to be wetted during rain events. A conditional probability approach is utilized to estimate this fractional wetting parameter using point precipitation data. The methodology is applied to obtain monthly estimates for 39 Goddard Institute for Space Studies (GISS) 4°x5° GCM grid areas over the contiguous United States.

The regional and seasonal variations in fractional wetting obtained over the U.S. are tested for their impact on the land surface hydrology parameterization of climate models. A simplified, one-dimensional climate model designed for hydrologic screening is used to make preliminary assessments of the influence of fractional wetting, and to identify the interactions and feedbacks involved. The GISS GCM is then utilized to ascertain the impact on a full GCM, with all of its inherent uncertainties. A small but justifiable effect on hydrologic and climatic parameters is detected.

The reliability of observational data sets used for GCM validation is also discussed. Biases between different data sources, and compatibility between point measurements and GCM grid-average parameters, are found to be important factors. Validation of the GCM simulations involving improved land surface hydrology and realistic fractional wetting variations is conducted using critically analyzed observations. These validations are performed at relatively fine scales involving individual grids and monthly annual cycles. The GCM simulations are found to have great difficulty reproducing the hydrologic and climatic patterns observed at these scales.

Thesis Supervisor: Dara Entekhabi
Title: Assistant Professor of Civil and Environmental Engineering

Acknowledgments

Contents

List of Figures

8

9

List of Tables

Chapter 1

Introduction

1.1 Background and Motivation

1.1.1 Climate Simulation with General Circulation Models

The increasing attention given to changes in the global climate caused by natural and man-made phenomena has fueled current attempts to understand the exceedingly complex climatic system. General Circulation Models (GCMs) currently hold the greatest potential for developing this insight. These three-dimensional numerical models attempt to solve the fundamental physical equations that govern atmospheric fluid flow, and also try to incorporate many of the physical processes that interact with the atmospheric dynamics, such as solar and terrestrial radiation, precipitation, land surface hydrology and ocean dynamics. Changes in the initial and boundary conditions of these mathematical models, representing such perturbations as increased atmospheric carbon dioxide, deforestation and volcanic eruptions, can easily be implemented and their effects on the climate system diagnosed.

At their present state, GCMs do have some significant limitations. The climate system consists of the atmosphere, hydrosphere, cryosphere, biosphere and land surface, and all interactions and feedbacks between these regimes (see Figure 1-1). This intricate and highly coupled system covers a wide range of scales in both time and space. In order to be computationally efficient, global numerical grids used by

Climate components

Atmosphere

Hydrosphere

Cryosphere

Land surface

Biosphere

Changes of
solar radiation

SPACE

Terrestrial
radiation

$H_2O, N_2, O_2, CO_2, O_3$ etc

Aerosol

ATMOSPHERE

Clouds

Atmosphere
land
coupling

Atmosphere
ice
coupling

Heat
exchange

Wind
stress

Evaporation

ICE
SHEETS
SNOW

LAND

BIOMASS

SEA-ICE

Ice
ocean
coupling

OCEAN

EARTH

Changes of
atmospheric
composition

Changes of land features
orography, vegetation,
albedo, etc.

Changes of ocean basin
shape, salinity, etc.

Figure 1-1: Schematic representation of the components and physical processes that make up the climate system. [Source: GARP, 1975]

17

GCM dynamics are unavoidably coarse relative to the spatial scales at which many of the climate's physical processes occur. This causes many important processes to be modeled too simply or altogether ignored in GCMs. For example, typical GCM grids today have a horizontal resolution of about 4° latitude by 5° longitude, which covers an area of roughly $2.5 \times 10^5 km^2$. These grid cells are considered to be homogeneous units with respect to physical processes occurring within the grid. However, observed precipitation processes usually cover a much smaller area of about $10^4 km^2$, and contain substantial spatial intermittency [*Waymire and Gupta*, 1981]. Clearly it is nearly impossible to model actual rainstorms within a GCM grid. Since the physical processes involved cannot be authentically represented in these models, they must be parameterized i.e. simplified relations must be developed in lieu of physically-based equations to approximate their behavior.

Another drawback is the poor treatment of ocean dynamics. Many GCMs simply prescribe seasonally fixed sea surface temperatures at the ocean surface, since they vary slightly and slowly relative to the atmosphere and land surface; oceans thus act as a thermal reservoir and stabilizing factor. However, because of the dominance of oceans over the globe, the circulation of ocean waters and associated temperature variations can have a major impact on climate. The interaction of atmospheric and ocean circulation has thus far received little attention, and is complicated by the vastly different time scales at which the two processes occur.

Increased computational capabilities have allowed for some recent improvements upon these limitations. Not only have grid resolutions improved, but more intricate and realistic physical parameterizations, and more efficient ocean circulation couplings, have been developed for implementation in GCMs. As the sophistication of computational tools continues to expand, major improvements in GCM simulated climate are expected, which has created a period of great promise and anticipation in the field of climate modeling.

1.1.2 Global and Regional Hydrology using GCMs

In addition to climate change investigations, mature GCMs can be of great value to the field of hydrology. The increasing demand on water resources due to diminishing supplies and burgeoning global population has led to the development of large-scale water resource projects, such as diversion from natural sources for irrigation and human consumption. These projects have a much larger scope than traditional hydrology, which focuses on rainfall-runoff processes at the catchment scale. They not only influence the local climate, but have the potential to affect the climate in other parts of the world as well. Consequently, global hydrology has emerged recently as a field of scientific investigation [*Eagleson*, 1986]. A general understanding of the atmospheric branch of the hydrologic cycle and the role of water in the overall climate system is desired to ascertain the regional and global impact of large water resource systems via teleconnections, i.e. the propagation and interaction of climate features over broad temporal and spatial scales. These systems can be modeled as a change in the land surface boundary condition over one or more grids.

GCMs can become an effective experimental tool for studying global hydrology, if a number of provisions are met. First, effective land surface hydrology parameterizations must be incorporated. Since climate models have to consider each land surface grid area as a homogeneous hydrologic unit, parameterizations must account somehow for the variability of rainfall and other processes within a grid area. They also must realistically approximate all interactions between the land surface and atmosphere, including surface runoff and vegetative transpiration. Second, GCMs must be validated at scales applicable to regional and global hydrology. To this point GCM validation has focused on general climatic features, using primarily annual averages at global and zonal spatial scales. Hydrologic analysis requires validation at continental and even grid scales to study the regional consequences of land surface boundary changes over a single grid. Annual cycles must also be accurately modeled, due to such seasonally varying influences as growing seasons and snowfall. Thus the incorporation of reliable land surface hydrology parameterizations into GCMs, and their validation at finer spatial and temporal scales, is critical to their utilization

in global hydrology, as well as overall climate simulations.

1.2 Current Land Surface Hydrology Parameterizations and the Influence of Fractional Rainfall Coverage

1.2.1 Overview of Land Surface Hydrology Parameterizations

Preliminary land surface hydrology parameterizations in GCMs were rather simple; runoff and evapotranspiration dependence on surface moisture conditions were typically treated using linear functions that had no clear physical basis and made no attempt to consider the spatial variability of rainfall and other processes within a grid area [Carson, 1982]. These schemes were designed for computational simplicity and based on the belief that the land surface plays a passive role in atmospheric circulation.

The hydrology parameterization in the Goddard Institute for Space Studies (GISS) GCM [GISS Model-II; Hansen et al., 1983] is typical of this ideology. The primary features are the empirical determination of runoff and evapotranspiration for a grid area as linear functions of the relative soil saturation. Runoff Q is taken as a fraction of the precipitation P that reaches the surface. This fraction is called the runoff ratio R, and is assumed to equal one-half the relative soil saturation s. Should a saturation value of 1 be reached, all additional precipitation becomes runoff.

$$Q = R\,P \qquad 0 \leq R \leq 1 \qquad (1.1)$$

$$R = \begin{cases} \frac{1}{2}s & 0 \leq s < 1 \\ 1 & s = 1 \end{cases} \qquad (1.2)$$

Evapotranspiration from the surface is taken as a fraction of the climatically controlled potential evaporation e_P. This fraction is called the evapotranspiration effi-

20

ciency β, and is assumed to be exactly equal to s.

$$e \;=\; \beta \, e_P \qquad 0 \leq \beta \leq 1 \qquad\qquad (1.3)$$

$$\beta \;=\; s \qquad\qquad 0 \leq s \leq 1 \qquad\qquad (1.4)$$

With this simple scheme, no physical infiltration capacities are used, and phenomena such as Horton and Dunne runoff cannot be distinguished. Also, evapotranspiration is always controlled by the soil unless it is fully saturated. No threshold or wilting points are modeled.

Ever since its recognition as an active component in climate processes [*Eagleson*, 1986], the parameterization of land surface hydrology in atmospheric general circulation models (GCMs) has steadily improved, evolving along two basic paths. One approach is to statistically account for subgrid-scale variability in various model parameters due to the unavoidably coarse resolution of climate models. The basic concept, illustrated in Figure 1-2, is to say that a point parameter such as precipitation intensity or soil saturation varies spatially throughout the grid area according to some probability density function. The value maintained by the climate model for the grid as a whole represents the expected value of the distribution, i.e. the mean over the entire grid area. Thus for the exponential distribution shown in Figure 1-2, a majority of the land surface points within the grid area experience rainfall around the mean intensity of 1.0mm/hr, but some points receive rainfall of substantially higher intensity. Older land surface schemes presumed the mean grid value generated by the model atmosphere to be uniform over the entire large grid area. Using a distribution is more realistic, since typical rainstorms consist of large areas with low intensity and smaller areas with high intensities.

Warrilow et al. [1986] first introduced subgrid-scale spatial variability in rainfall when determining the infiltration rate. *Entekhabi and Eagleson* [1989] devised a statistical-dynamical approach which incorporates physically based equations of soil physics and uses probability distributions to account for the sub-grid variability of rainfall and soil moisture. *Famiglietti and Wood* [1990] followed a similar approach

f_i (I)

Exponential distribution for
precipitation intensity I

f_i (I) = A exp[-AI]

area = 1.0

I

E[I] = A^{-1} = 1.0 mm/hr
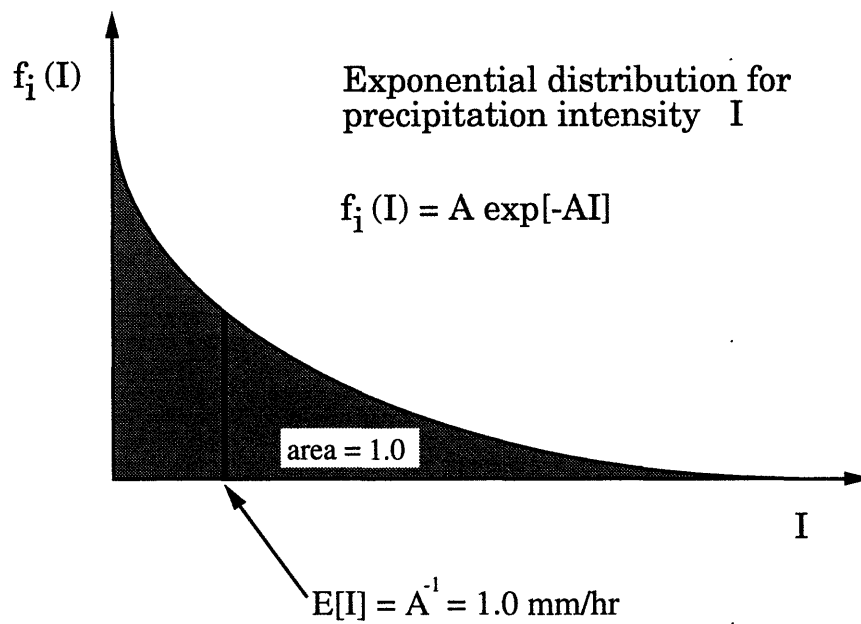
Figure 1-2: Illustration of the statistical-dynamical representation of subgrid spatial variability. An exponential probability density function is used to describe spatial precipitation intensity variations within a GCM grid area.

to parameterizing the land surface response.

The second approach is to accurately model the complex vegetation processes at the land surface boundary. The Simple Biosphere Model [*SiB; Sellers et al.,* 1986] and Biosphere Atmosphere Transfer Scheme [*BATS; Dickinson et al.,* 1986] use resistance formulations to incorporate more realistic surface vegetation and soil moisture diffusion. Figure 1-3 illustrates the different processes accounted for in the SiB model. These sophisticated soil-vegetation-atmosphere transfer (SVAT) models still consider the grid area as a homogeneous hydrologic unit. The subdivision of the GCM grid area into several patches, each with a different set of SVAT parameters, represents an improvement since large-scale variations in vegetation type may be included [*Koster and Suarez,* 1992; *Avissar and Pielke,* 1989]. However, spatial variability of rain intensities and soil moisture conditions occur on a hydrologic scale that is still considerably smaller than these patches. These SVAT models sacrifice adequate representation of spatial variability in favor of modeling vegetation processes in full detail.

1.2.2 Influence of the Fractional Wetting Parameter, $\bar{\kappa}$

One of the most important variables required by some of these improved formulations is the fractional wetting parameter $\bar{\kappa}$. This parameter represents the average fraction of a GCM land surface grid area that actually experiences precipitation during events, and thus accounts for the fact that realistic rainfall events cover only a portion of a grid area. For virtually all current GCMs, model precipitation is assumed to fall uniformly over the entire model grid area for land surface calculations. This is unrealistic, especially for moist-convective type storms which occur at scales much smaller than a typical grid area. Modeled rainfall therefore incorrectly gets distributed over the entire grid area, resulting in very low rainfall intensities. Low intensities are more susceptible to complete infiltration and interception, which consequently leads to exceedingly low surface runoff. By restricting rainfall to only a fraction of the grid area using $\bar{\kappa}$, the model precipitation is concentrated into

ATMOSPHERIC BOUNDARY LAYER
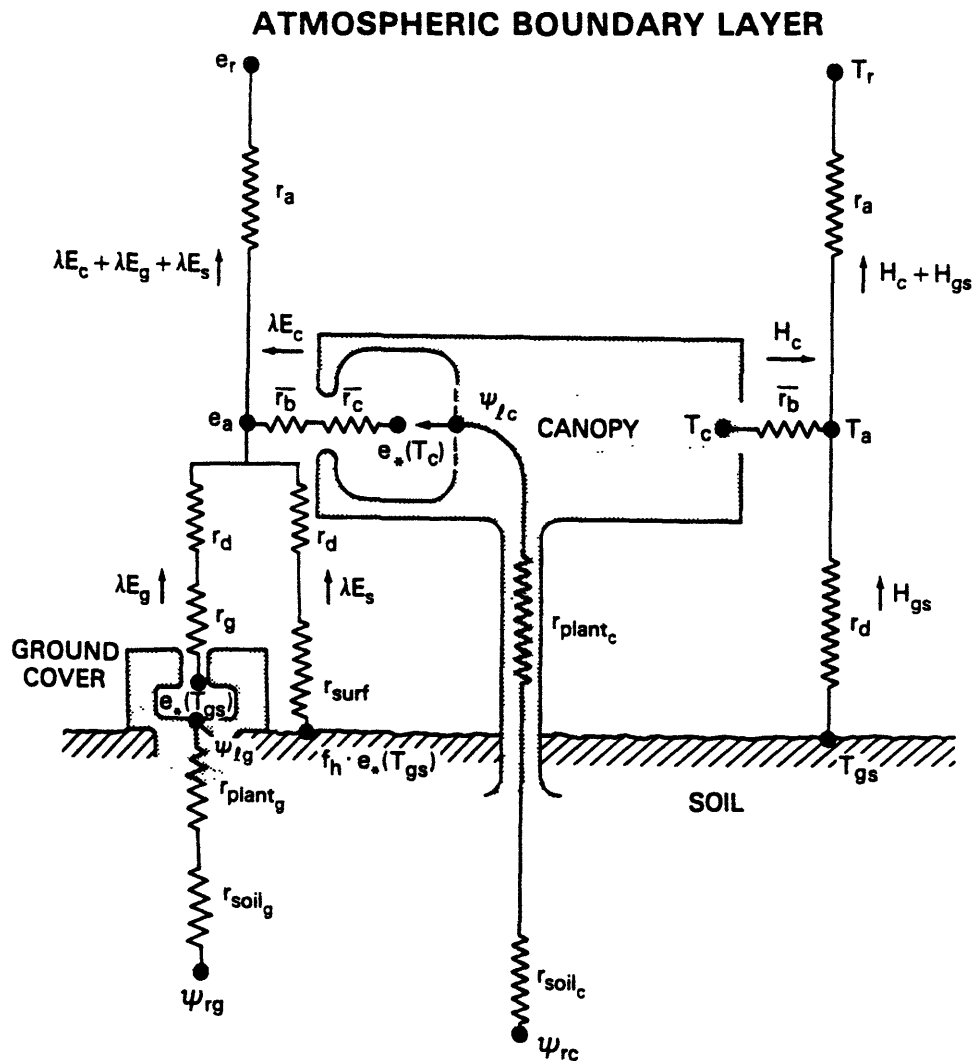
Figure 1-3: Illustration of the land surface and vegetation processes modeled in the Simple Biosphere Model (SiB). [Source: *Sellers et al.*, 1986]

smaller areas of higher intensity, which is more likely to produce infiltration-excess runoff. Thus fractional wetting serves as an important link between true rainfall characteristics and their homogeneous representation in climate models.

Pitman et al. [1990] and *Thomas and Henderson-Sellers* [1991] studied various land surface hydrology schemes and recognize their sensitivity to variations in fractional wetting. *Johnson et al.* [1993] used the GISS GCM and the parameterization of *Entekhabi and Eagleson* [1989] to show that broad $\bar{\kappa}$ variations have a significant influence on simulated climates, in terms of both water and heat balance.

Currently most parameterization schemes that use fractional wetting representations simply prescribe for all grid areas one value of $\bar{\kappa}$, or two values if different precipitation mechanisms are distinguished. However $\bar{\kappa}$ is intuitively expected to have geographic and seasonal variations. Many factors such as local and seasonal climate influence the local fractional wetting. For example, localized summertime moist convective storms should produce a different $\bar{\kappa}$ value than large baroclinic disturbances. The intuitive variability of $\bar{\kappa}$ and its importance to GCM land surface hydrology suggests that the current practice of prescribing uniform values is an unwarranted approximation. An actual determination of fractional wetting values including geographic and seasonal variability is clearly needed.

Unfortunately, relatively little attention has been given to this issue thus far. *Braud et al.* [1993] and *Lopez et al.* [1989] used fractional wetting as a means of obtaining information on individual storms such as mean areal rainfall and rainfall volume. $\bar{\kappa}$ is obtained by either setting up a dense experimental rain gage network over a small area and simply determining the number of gages that record precipitation during storms, or by collecting weather radar data over a short period of time corresponding to the storm. *Eagleson and Qinliang* [1985] theoretically derived moments of catchment storm coverage by generating storms over a catchment to determine the probability of storm coverage. *Eagleson* [1984] used a Poisson arrival process to model rainfall over a catchment and derive expressions for fractional wetting statistics based on rain gage data within the catchment. However, most of these studies are performed at the catchment scale and attempt to resolve individual

storm events. GCM grid areas are orders of magnitude larger than catchments, and model precipitation cannot resolve specific events within the grid area.

Some recent efforts however have been made to obtain fractional wetting values explicitly for use in GCM land surface hydrology parameterizations. *Eltahir and Bras* [1993] used the apparent linear relation between storm volume and storm area (effectively assuming constant rainfall intensity for all events) to obtain $\bar{\kappa}$ as a function of the grid rainfall volume generated by the model. Here fractional wetting is dependent on the model-generated incident precipitation forcing, and is not a characteristic of the regional climate. *Gupta and Waymire* [1993] suggest a procedure for obtaining $\bar{\kappa}$ for a grid area using GARP (Global Atmospheric Research Program) Atlantic Tropical Experiment (GATE) rainfall data and the theory of random cascades for modeling rainfall. However, this procedure makes use of radar data, which has limited availability and measures atmospheric droplet spectra as opposed to surface precipitation conditions.

Collier [1993] used similar ideas to obtain values of $\bar{\kappa}$ corresponding to various rainfall types and model-generated precipitation volumes. An expression for the fraction of grid area with precipitation greater than a specified intensity was derived using either an exponential or log-normal distribution for rainfall. These theoretical expressions were compared to hourly radar observations of individual storms over northwestern Europe, collected by the Commission of the European Communities (CEC) COST-73 Weather Radar Networking Project. A 100km x 100km area was moved over particular precipitation fields to follow each observed storm. The radar observations were found to match best with the log-normally derived expression. A fit of this expression to the observations yielded significantly different $\bar{\kappa}$ values for a variety of storm types (showers, frontal, and thunderstorms/line convection) with hourly rainfall depths ranging from 0.2mm to 1.2mm. The range of $\bar{\kappa}$ values obtained for this study over northwestern Europe was 0.2–0.8.

1.3 Overview of Research

The primary goal of this research is to thoroughly investigate the role of fractional wetting in GCM land surface hydrology parameterizations and simulated climate. Relevant research studies to this point have only considered general sensitivities to uniformly prescribed values of $\bar{\kappa}$. For example, *Johnson et al.* [1993] reports significant climate changes between prescribed values of 0.6 and 0.15 for moist convective rainfall. Recent estimation procedures have yet to be implemented into GCMs. Overall, fractional wetting has not been given explicit or sufficient attention in the context of climate models, despite its apparent influence.

A simple methodology for obtaining monthly estimates of $\bar{\kappa}$ that exhibit geographic and seasonal variability will be developed here which differs from previous attempts discussed above. This procedure uses a probabilistic approach and utilizes long term hourly raingage observations as the data source. The methodology is applied to the Goddard Institute for Space Studies (GISS) $4°\times5°$ GCM grids over the contiguous United States, where extensive precipitation observations are readily available.

The influence of the range of fractional wetting values estimated over the U.S. will be investigated using a variety of experimental tools based upon the GISS GCM Model-II at $4°\times5°$ resolution with the statistical-dynamical land surface hydrology parameterization of *Entekhabi and Eagleson* [1989]. First, the sensitivity of the scheme to the fractional wetting values estimated over the U.S. will be studied analytically, over anticipated values of relevant hydrologic parameters, such as precipitation and soil saturation. Second, a simple one-dimensional climate model developed for the screening of hydrologic processes will be utilized to determine if the observed fractional wetting variations have a significant influence on simulated climate. Although broad variations have been shown to have a significant effect, the estimated seasonal and regional $\bar{\kappa}$ values are substantially smaller in both magnitude and range, and their effect may be masked by inherent climate variability and feedback processes. Finally, the effect of the *Entekhabi and Eagleson* [1989]

27

scheme and the U.S. $\bar{\kappa}$ estimates on the GISS GCM Model-II simulated climate will be analyzed. Further masking of the effect of fractional wetting is expected, due to the increased variability and complexity in a full GCM and the limited duration runs necessitated by computational time constraints. The GISS 4°x5° Model-II with the *Entekhabi and Eagleson* [1989] hydrology parameterization requires roughly six hours to simulate one model month using either an IBM mainframe computer or a workstation platform. The sequential analysis applied in this research begins within a simple analytical environment to determine the primary effect of fractional wetting, then incorporates increasing amounts of climatic interactions and feedbacks to determine precisely how realistic $\bar{\kappa}$ variations influence simulated climate.

The GCM analyses will focus exclusively on grids representing the contiguous U.S. *Johnson et al.* [1993] has already shown the global influence of improved land surface hydrology on simulated climate. What is required now is a validation at finer scales useful to regional and global hydrology. Also, fractional wetting variations are only introduced over the U.S., so that is where the greatest effect on simulated climate is expected. The analysis will investigate changes over individual U.S. grids, and also the full annual cycle of hydrologic and climatic diagnostics. This study thus represents the first attempt to validate GCMs at these scales and assess the utility of GCMs for hydrologic purposes.

As is the case with any GCM validation exercise, the selection of observation data sets with which to compare the model simulations is an important factor. Observations of hydrologic and climatic variables are far from consistent, and can vary greatly depending on the data source, quality, assumptions made and estimation procedure. These issues become particularly relevant when validating at scales of individual grids and months. Thus a secondary aim of this research is to investigate and determine critical factors associated with observational data sets used for GCM validation studies. This data comparison study will also concentrate on the contiguous U.S.

Chapter 2

Regional and Seasonal Estimates of Fractional Storm Wetting Based on Station Precipitation Observations

2.1 Distributed Fractional Wetting Estimates Using Station Precipitation Observations

2.1.1 Precipitation Data

A procedure is developed here which uses hourly data from long term precipitation station records to obtain reliable observation-based monthly estimates of fractional wetting for individual GCM grid areas. Using standard point precipitation data as the source for $\bar{\kappa}$ estimates has significant advantages over previously mentioned methods. The data is usually reliable and is readily accessible, particularly over North America. The procedure for estimating $\bar{\kappa}$ uses rain-no rain information only; any gage bias in depth measurements is not directly relevant. Raingage networks producing this data are very broad in space and time, unlike experimental networks that usually focus on specific regions and sample over limited time periods. However, the sparsity of these long term records prohibits the direct assessment of fractional wetting that is possible with denser experimental networks.

The utilization of this type of raingage data is particularly beneficial in that $\bar{\kappa}$ can be obtained for many different grid areas to assess its geographic variability.

Also, the information that is obtained reflects actual conditions at the land surface, as opposed to atmospheric droplet distribution conditions measured by radar scans. Since the land surface hydrology parameterization serves to partition precipitation incident on the surface, it is imperative that the precipitation at the surface be accurately portrayed.

2.1.2 A Conditional Probability Approach for $\bar{\kappa}$

The fractional wetting parameter $\bar{\kappa}$ represents the fractional area with precipitation for a GCM grid area, averaged over all times in which precipitation occurs there. Using Figure 2-1, fractional wetting can be expressed for a time period T as

$$\bar{\kappa} = \frac{1}{T_p} \int_{t-\frac{T_p}{2}}^{t+\frac{T_p}{2}} \frac{A_t}{A} dt = \frac{1}{T_p} \int_{t-\frac{T_p}{2}}^{t+\frac{T_p}{2}} \kappa \, dt \qquad (2.1)$$

where A_t is the area that experiences precipitation at time t, A is the area of the GCM grid, and T_p represents the total amount of time in which precipitation occurs within the grid area. A_t/A represents the instantaneous fractional wetting for time t, κ. Note that T_p is less than the total period T, since there are times when no part of the grid area receives precipitation. Figure 2-1 depicts a rainfall event occurring over the grid area as a group of smaller individual storm areas [*Waymire and Gupta*, 1981]. The sum of these areas within the grid boundaries comprises A_t.

In this paper, a robust estimation scheme is introduced to estimate $\bar{\kappa}$ from a probabilistic perspective of storm arrivals and distributions. The procedure makes minimal assumptions regarding the original precipitation process and is designed for application to standard surface precipitation gage network records. The assumptions that are introduced due to the probabilistic approach are that the precipitation is a homogeneous random field within a finite grid area and that the gages are randomly distributed within the grid boundaries. If the grid resolution is small, the assumption that the climate and thus the precipitation mechanism within the grid area are homogeneous is appropriate. In this application, we use areas of 4° latitude by 5° longitude; the scale of such an area is smaller than the major gradients in cli-

30

rainfall area at time t, A_t

X

A

GCM grid

any random point i
within the grid
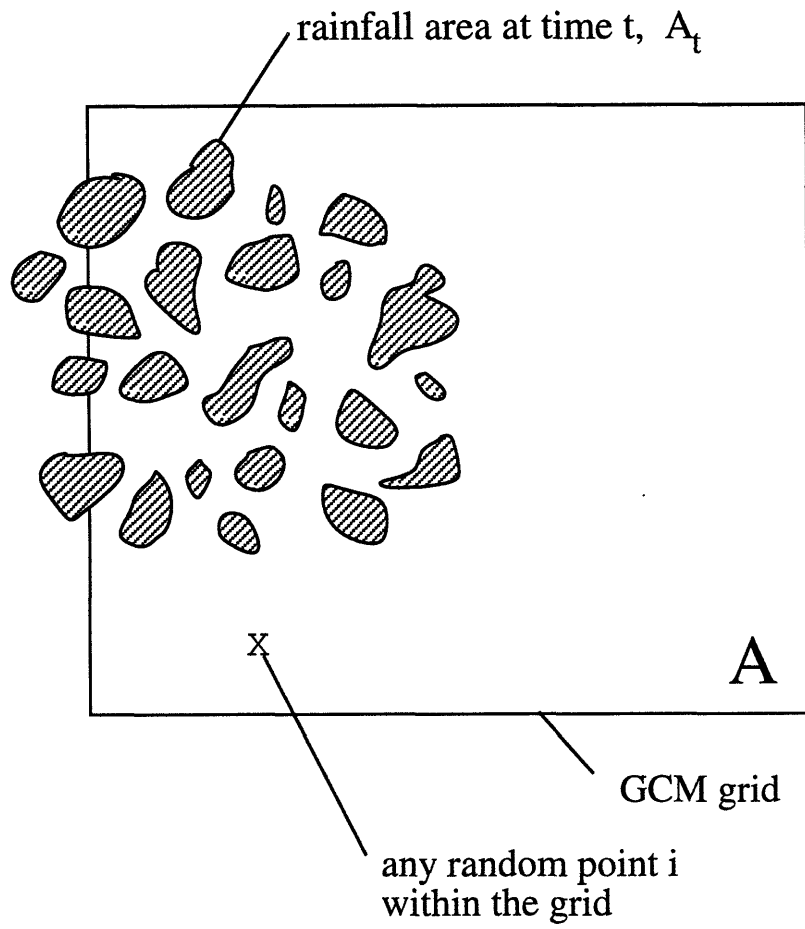
Figure 2-1: Schematic representation of instantaneous rainfall coverage over a GCM
grid area

mate. Sharp orographic features and coastal effects are present in some locations on very small scales (tens of kilometers); these features are lost to both this estimation scheme as well as the atmospheric models that use the parameters estimated here. In time, the application of the estimation procedure to precipitation records for each month of the year reduces the effects of the seasonal cycle; within a one-month period, the climate and the precipitation mechanisms associated with it may safely be assumed to be statistically homogeneous.

From a probabilistic perspective, fractional wetting may be quantified using a basic conditional probability relation. It can be expressed as the probability that rainfall occurs at a particular point within a grid area, provided that rain falls somewhere in the grid area. If it is known that rainfall occurs somewhere in the grid area, then the probability that a particular point experiences this rainfall is simply the area with rain over the total grid area, i.e. the fractional wetting parameter. Define events P_i and G such that P_i represents rainfall occurring at location i in the grid area at any time t, and G represents rainfall occurring anywhere in the grid area at the same arbitrary time t. Thus from elementary conditional probability laws

$$\bar{\kappa} = Prob[P_i|G]$$
$$= \frac{Prob[P_i \cap G]}{Prob[G]} \tag{2.2}$$

Since rainfall at a particular point in the grid area necessitates rainfall occurring somewhere within the grid boundaries, the event P_i is a subset of the larger event G. Using probabilistic sample space and the algebra of events as illustrated in Figure 2-2, the event P_i is said to be *included* in event G. Also, since all points i lie in the grid area, the event G is equal to the union of all events P_i. Therefore

$$Prob[G] = Prob[P_1 \cup P_2 \cup ... \cup P_i \cup ...] \tag{2.3}$$

Under this condition the axioms of the algebra of events leads to [*Drake,* 1967]

$$Prob[P_i \cap G] = Prob[P_i \cap (P_1 \cup P_2 \cup ... \cup P_i \cup ...)]$$

32
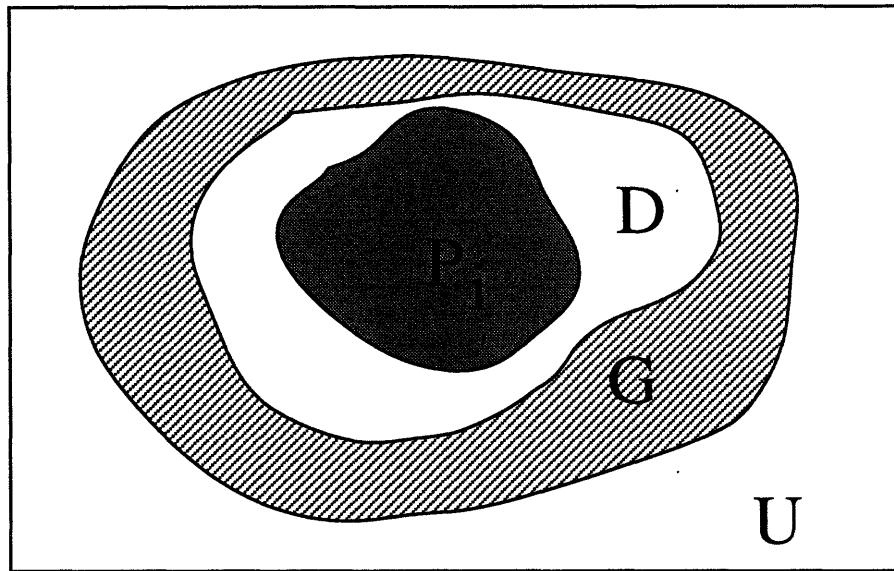
Figure 2-2: Sample space diagram describing the relationship between events P_i, D and G, where U represents the universal set.

$$= Prob[P_i] \qquad\qquad . \qquad\qquad (2.4)$$

This relation is also directly observable in Figure 2-2, where the overlapping area between events P_i and G is simply P_i. Substituting into (2.2),

$$\bar{\kappa} = \frac{Prob[P_i]}{Prob[G]} \qquad\qquad (2.5)$$

This conditional probability model makes the assumption that any point i within the grid area has an equal chance of experiencing precipitation, so that $Prob[P_i]$ will be the same for all points in the grid area.

2.1.3 Estimation of $\bar{\kappa}$ using Point Precipitation

$Prob[P_i]$ and $Prob[G]$ can be estimated for a grid area using hourly point precipitation data records from the network of all available stations in the grid area. If a rainfall station has a sufficiently long continuous data record, $Prob[P_i]$ for that station is the temporal fraction of hours in its data record in which precipitation greater than the hundredth-of-inch threshold was recorded. A single value of $Prob[P_i]$ for the grid area can be obtained by simply averaging the values for every station in the grid area, as long as each station is subject to the same period of record, and assuming that the stations are independent (i.e. randomly located) and within a stationary random precipitation field. This estimation of $Prob[P_i]$ can be expressed mathematically as

$$Prob[P_i] \approx \frac{1}{n}\frac{1}{T}\sum_{i=1}^{n}\sum_{t=1}^{T} Z_{it} \qquad\qquad (2.6)$$

where n is the number of stations in the network, T is the number of hours in the data record, and Z_{it} takes on a value of 1 when rain occurs at station i in hour t, and is 0 otherwise.

The estimation of $Prob[G]$ uses the same principles behind the approximation of $Prob[P_i]$; here the estimate is the fraction of hours in which precipitation was recorded in any of the n stations in the grid area's station network. However this

expression only serves as an adequate approximation of $Prob[G]$ when the grid area has enough stations in its network to detect every storm that occurs in the relatively large area. For example, if a grid area has only five raingages, it is very likely that some events may fall in between the gages and thus never be detected. Introduce the event D which represents rainfall that is detected by the network of n stations. The fraction of hours with precipitation at any station is actually an estimate of $Prob[D]$, which can be expressed mathematically as

$$Prob[D] \approx \frac{1}{T} \sum_{t=1}^{T} [1 - \prod_{i=1}^{n} (1 - Z_{ij})] \qquad (2.7)$$

As indicated in Figure 2-2, the event D is also included but not coincident with event G, since all stations in the network are by definition located within the grid boundaries. Note that if n is high, $Prob[D] \approx Prob[G]$ and the raingage-based approximations serve as a good estimate of $\bar{\kappa}$. In general, networks of long-term hourly raingages are not dense enough to detect all storms. Thus D and G represent significantly different events, and the expression

$$\frac{Prob[P_i]}{Prob[D]} \approx \frac{\frac{1}{n} \frac{1}{T} \sum_{i=1}^{n} \sum_{t=1}^{T} Z_{it}}{\frac{1}{T} \sum_{t=1}^{T} [1 - \prod_{i=1}^{n} (1 - Z_{ij})]} \cdot \qquad (2.8)$$

results in a biased estimate of $\bar{\kappa}$.

This bias can be corrected by incorporating $Prob[D]$ into the original probabilistic expression for $\bar{\kappa}$ in (2.5) in the form,

$$\bar{\kappa} = \frac{Prob[P_i]}{Prob[D]} \frac{Prob[D]}{Prob[G]} \qquad (2.9)$$

The term $Prob[P_i]/Prob[D]$ can be obtained from precipitation data using (2.8), and is symbolized by $\bar{\kappa}^*$, where the asterisk denotes that it is a biased estimate of fractional wetting. Since both P_i and D are included in G, the conditional probability relation applied to P_i and G can also be applied to D and G. The resulting expression for $\bar{\kappa}$ is

$$\bar{\kappa} = \bar{\kappa}^* Prob[D|G] \qquad (2.10)$$

35

The term $Prob[D|G]$ expresses the probability that the network detects a storm given that a storm occurs over the grid area. It represents a correction factor that acts upon the biased estimate $\bar{\kappa}^*$, and is a function of n. By definition this probabilistic expression is less than one, which means that $\bar{\kappa}^*$ is an overestimate of $\bar{\kappa}$. Note that both $\bar{\kappa}^*$ and $Prob[D|G]$ are dependent on the number of stations n in the network.

This correction factor is obtained using the basic probabilistic definition of fractional wetting in (2.2). Consider again Figure 2-1, which depicts a storm occurring somewhere in a grid area at a particular time t. The point i can represent one of the stations in the grid area's network, since the stations are randomly located. For station i at rainy time t, the probability that precipitation is recorded has been defined as κ. Similarly for any other station in the grid area, the probability of recording precipitation at time t is κ. This can be thought of as a simple Bernoulli process. Introducing the binomial random variable y which represents the number of stations that record rain at time t, the probability mass function of y_0 out of n stations detecting precipitation given that there is precipitation over the grid area is

$$P_y(y_0) = \binom{n}{y_0} \kappa^{y_0} (1 - \kappa)^{n-y_0} \tag{2.11}$$

The probability that this storm is detected by the network at time t is simply the probability that at least one station records rain.

$$
\begin{aligned}
P[y \geq 1] &= 1 - P_y(0) \\
&= 1 - (1 - \kappa)^n
\end{aligned}
\tag{2.12}
$$

The overall probability of rain at a point given rain in the grid area, $Prob[P_i|G]$, has been defined as $\bar{\kappa}$, where κ represents instantaneous probability at time t within the averaging period. Analogously, the overall probability of rain in the network given rain in the grid area is

$$Prob[D|G] = \overline{1 - (1 - \kappa)^n} \tag{2.13}$$

Derivation of the probability that the finite gage network detects the storm given

36

that the storm has occured has been developed based on the assumption that the precipitation gages are randomly located within the grid area. The true (unknown but to be estimated) value of fractional wetting in (2.13) is included in this probabilistically-derived correction factor. The smaller the storm scale, the smaller is the probability that the network may detect it successfully, i.e. storms may fall entirely in between gages and avoid detection. Equation (2.13) also suggests that no matter what the storm scale, if a large number of stations are present (large n), then the network is unlikely to be biased.

In order to derive this simple bias-correction, a major assumption on the spatial geometry of storms has been made. Precipitating areas A_t are considered to be intermittent in space and the decorrelation distance is smaller than the mean intergage distance. It will be shown later, via a monte carlo study in Section 2.3, that the estimates of fractional wetting are fairly insensitive to this assumption. In a pair of the monte carlo simulations, the two extreme situations defining the outer envelope of spatial storm structure conditions are considered. In the first, it is assumed that the precipitating area is intermittent; at each timestep the grid area with rain is randomly dispersed throughout the grid area. This corresponds to the Bernoulli process used in (2.11). The estimation of $\bar{\kappa}$ using the simulated raingage records is verified. At the other extreme of possible spatial storm structure, it is assumed that the storm area A_t is spatially intact and that precipitating regions are contiguous; this corresponds to the largest spatial correlation lengths for isotropic fields. These simulations will be discussed in detail in Section 2.3. Since fractional wetting is small (i.e. large grid areas relative to storm size), these two extremes define a rather narrow range of conditions. Any additional bias introduced by this intermittency assumption will grow if $\bar{\kappa}$ is large and care must be exercised in this respect. As it will be shown by both the application to observations in Section 2.2 and the monte carlo study in Section 2.3, the range of conditions over which the bias-correction is applied is within the acceptable limits of the applicability for this remarkably simple approach to estimating fractional wetting.

Equation (2.13) relates the bias correction factor $Prob[D|G]$ to the number of

37

stations n and the instantaneous fractional wetting κ, which will vary within the averaging period from event to event and from hour to hour within an event. Thus κ can be considered as a random variable with mean $\bar{\kappa}$. This variability about the mean climatic value $\bar{\kappa}$ for a specified grid area and month is accounted for by using a beta distribution $\beta(1, b)$ to represent κ

$$
\begin{aligned}
f_\kappa(\kappa_0) &= b(1 - \kappa_0)^{b-1} \quad 0 < \kappa_0 \leq 1 \\
where \ E[\kappa] &= \bar{\kappa} = \frac{1}{1+b}
\end{aligned}
\tag{2.14}
$$

This methodology is not restricted to a $\beta(1, b)$ distribution for κ. Some variability should be included to emphasize that $\bar{\kappa}$ is a mean value and that each hour with rain in the averaging period has an instantaneous fractional wetting that may vary around this value. A $\beta(1, b)$ distribution was selected because its values are limited to between 0 and 1 (as is κ) and its probability curve exhibits a sharp, smooth decay as κ increases from 0. This is the expected shape of the κ PDF for two reasons. Recent literature regarding the distribution of rainstorm areas suggests some sort of decaying function with increasing area [*Eagleson*, 1984]. Fractional wetting is expected to bear some resemblance to rainstorm area, since the grid area is fixed. Also, boundary effects (i.e. storms that only partially fall over the grid area) serve to reduce the area with rain at each hour, which leads to the sharply decaying $\beta(1, b)$ function with much of its probability mass at very low values of κ and consequently a low value for $\bar{\kappa}$.

Using (2.14), the correction factor of (2.13) can now be expressed

$$
\begin{aligned}
Prob[D|G] &= \overline{1 - (1 - \kappa)^n} \\
&= E[1] - E[(1 - \kappa)^n] \\
&= 1 - \frac{b}{n+b}
\end{aligned}
\tag{2.15}
$$

38

Substituting for b using $\bar{\kappa}$ from (2.14), then substituting (2.15) into (2.10) yields

$$\bar{\kappa} = \frac{n\bar{\kappa}^* - 1}{n - 1} \qquad (2.16)$$

Equation (2.16) expresses $\bar{\kappa}$ for a grid area as a function of the biased estimate from precipitation station data $\bar{\kappa}^*$ and the number of stations n in the grid area's network. For an infinitely dense network, l'Hopital's rule can be applied to (2.16) to show that

$$\lim_{n \to \infty} \bar{\kappa} = \bar{\kappa}^*$$

The advantage of the bias correction is that the estimation procedure becomes equally applicable to dense or sparse networks.

Using this estimation procedure geographic and seasonal variations in the fractional wetting parameter can be directly ascertained. Monthly fractional wetting estimates can be obtained for each grid area, from which possible annual cycles in $\bar{\kappa}$ and other characteristic features can be detected for particular climates.

There are several major assumptions in these derivations that must be clearly stated. The foremost assumption is that over a grid area, precipitation occurs as a space-time homogeneous random field. Since the 4°x5° grid area is relatively small, this assumption is adequate unless sharp gradients in the precipitation climatology are locally present. An example of a situation where sharp gradients are found is at locations with large orographic barriers. Sometimes even topographically featureless landscapes have strong precipitation gradients; examples of these situations are the southern U.S. Plains (Oklahoma-Kansas) and the semi-arid regions of West Africa. It is important to note that the GCM grid area for which the parameter $\bar{\kappa}$ is estimated also treats such areas as space-time homogeneous climates.

Also, the estimates of the spatial parameter $\bar{\kappa}$ are based on records of rain-no rain for gage observations that are assumed to be randomly located within the grid area. Although gages are in reality located based on practicality and accessibility and are usually in urban areas, the sparsity of the long term raingage network within the grid area makes it reasonable to assume uncorrelated gages. The measuring sensitivity

of the observing instrument is also a critical factor. For hourly observations, a threshold of 0.01 inches is used to indicate precipitation during that period. More detailed study is need beyond this preliminary introduction to the methodology in order to further explore the sensitivity of the parameter $\bar{\kappa}$ to the characteristics of the precipitation record such as data quality, aggregation period (one hour is used here), grid area definition and other implicit factors.

2.2 Estimates of Fractional Wetting over the Contiguous United States

Seasonal estimates of fractional wetting using the procedure described in Section 2 are made for fixed rectangular grid areas over the contiguous United States corresponding to the Goddard Institute for Space Studies (GISS) 4°x5° atmospheric GCM. An hourly precipitation station data set collected by the National Climatic Data Center [*Earthinfo*, 1989] is used, and a fifteen year period from 1971 through 1985 is selected for study. A total of 1546 stations distributed over all 48 contiguous states are considered. Figure 2-3 shows the grid partitioning for this study, and the number of stations available in each grid area. As seen in Figure 2-3 network density varies over a large range; therefore the degree of bias contained in $\bar{\kappa}^*$ varies considerably for each grid area, and the correction factor becomes imperative for obtaining accurate and consistent values.

Note that significant portions of some grid areas consist of water bodies or foreign countries, neither of which is covered by the precipitation data. The fractional wetting estimates for these grid areas actually represent a smaller parcel of land equal to the portion of land in the grid area within United States borders. Therefore only grids with at least 50% of its surface area falling over the U.S. are included in this study. It is assumed that the amount of monitored land surface in these grids is sufficient to represent grid-wide conditions.

Estimates of climatic fractional wetting $\bar{\kappa}$ over all grid areas are made for the

RAIN GAGE NETWORK DENSITIES
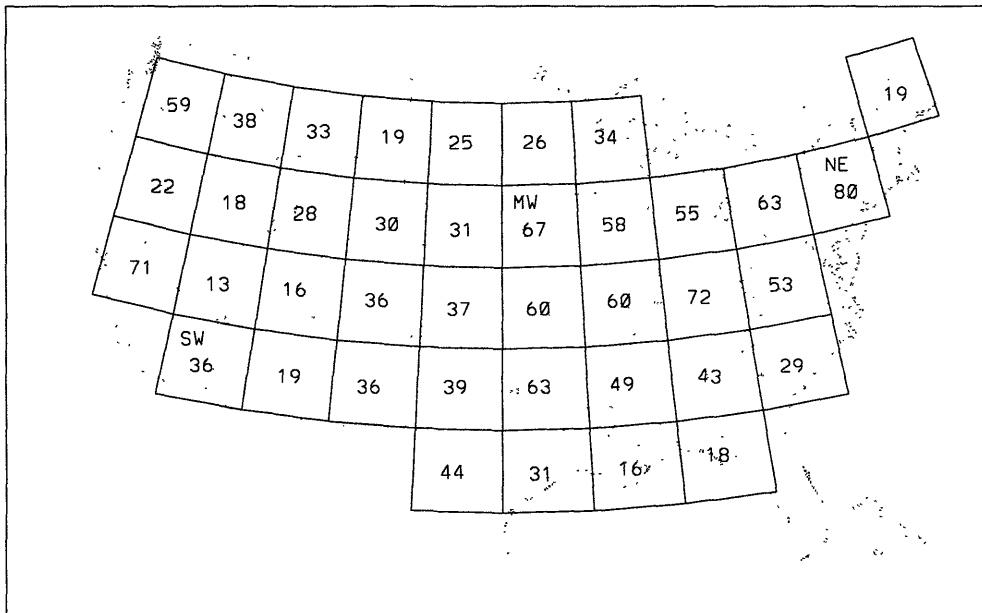
Figure 2-3: Grid partitioning and number of available precipitation stations for GISS 4°x5° GCM grid areas over the contiguous United States

a) FRACTIONAL WETTING: JANUARY

.135 .081 .046 .059 .047 .069 .062 .169
.128 .076 .047 .046 .054 .064 .082 .078 .094 .117
.156 .069 .079 .043 .067 .097 .091 .106 .115
.114 .074 .060 .063 .101 .122 .145 .154
.091 .147 .168 .142

b) FRACTIONAL WETTING: JULY

.044 .044 .043 .045 .047 .062 .063 .114
.044 .039 .029 .047 .051 .059 .066 .058 .068 .076
.027 .036 .037 .042 .049 .052 .053 .058 .060
.020 .036 .036 .039 .047 .048 .060 .067
.053 .052 .060 .068
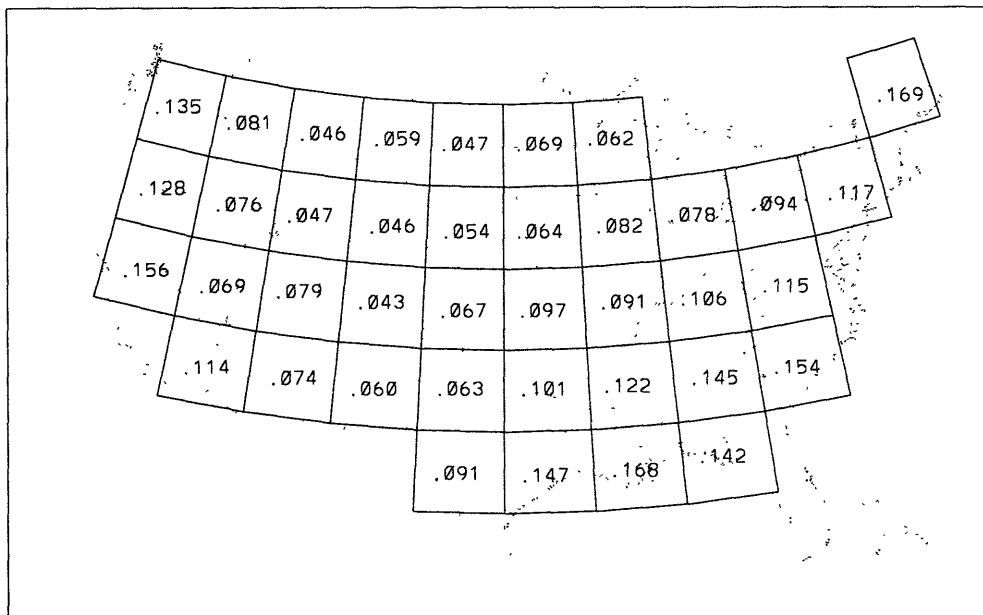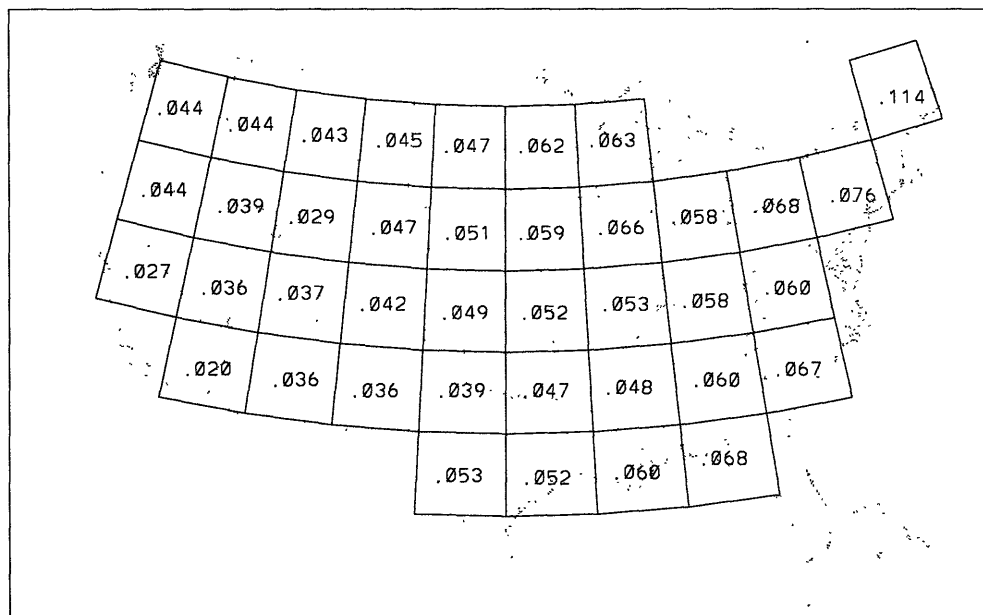
Figure 2-4: Estimated fractional wetting values $\bar{\kappa}$ for GISS 4°x5° GCM grid areas over the contiguous United States in a) January and b) July

42

twelve months of the year; values for January and July are shown in Figure 2-4. Values for all twelve months are provided in Appendix A. The most noticeable feature in this figure is that the estimated values are as a whole lower than what has typically been prescribed in GCMs. Most current GCM modelers assume a uniform $\bar{\kappa}$ value between .10 and .15 for moist convective rainfall based on literature and intuition about storm scales [*Johnson et al.*, 1993]. Some of the January estimates (Figure 2-4a) are in this range, but many are substantially lower than .10. For July (Figure 2-4b), almost all values are below .10, and some are but a few percent. An explanation for this discrepancy is the intermittent nature of rainfall in time and space. Storms are comprised of smaller individual areas that grow, move and dissipate within the life of a storm. This factor may have been insufficiently considered in the prescribed values, while the observation-based estimates are able to account for it.

Significant geographic variations are apparent within each month. General regions can be detected in Figure 2-4 with distinctly different ranges of $\bar{\kappa}$ values. For example, in January the northern plains have noticeably lower $\bar{\kappa}$ values than the eastern half of the U.S. and the northwest corner. In July extremely low values exist in the southwestern states. These geographic variations in fractional wetting are indicative of different regional climatic regimes. Regions with similar $\bar{\kappa}$ values can potentially be correlated to meteorological and topographical characteristics shared by these regions.

A distinct disparity also exists between January and July values, with $\bar{\kappa}$ being almost one half lower on average in July than in January (.094 in January vs. .051 in July). This indicates strong seasonal variations in fractional wetting, which can be understood by considering the seasonal variations in dominant precipitation mechanisms. Large scale and low intensity precipitation events such as those associated with synoptic and baroclinic disturbances are characterized by relatively large fractional wetting values; they usually occur in the wintertime in mid-latitudes. Moist convective rainfall events are brief, localized storms caused by differential heating at the land surface. They are associated with small fractional wetting values, and

43

usually occur in the summertime in mid-latitudes.

The seasonal and regional variations in $\bar{\kappa}$ estimated here reflect the patterns of the governing precipitation regime across the continental United States. The estimated values of $\bar{\kappa}$ are lower for regions and months where precipitation is primarily due to mesoscale convective activity. Even though radar loops (multiple times images) of mesoscale convective complexes show broad moving bands of rain over areas comparable to the grid areas defined here, the areas of activity are intermittent in time; in any one hour, a small fraction of the area is wetted. The estimated values of $\bar{\kappa}$ are generally larger for regions and months dominated by mid-latitude baroclinic (synoptic-scale) disturbances. The precipitation in such weather systems is generally more diffuse in both space and time.

Seasonal and regional variations can be shown more clearly by displaying monthly $\bar{\kappa}$ values for individual grid areas. Figure 2-5 shows the annual $\bar{\kappa}$ cycle for three grid areas, located in the southwest (SW), midwest (MW), and northeast (NE) United States (see Figure 2-3). The NE and SW grid areas exhibit a fairly smooth annual cycle that peaks in the winter and ebbs in the summer, as expected. However, the SW grid area's annual cycle covers a much larger range than that of the NE grid area. In particular, the SW grid area has a much lower summertime minimum than the NE grid area. The MW grid area has a clear semi-annual cycle with peaks in the spring and autumn. *Bradley and Smith* [1993] show that when precipitation events in the midwestern plains are stratified according to a measure of severity, the extreme events have a bimodal seasonal frequency as well. The two seasons of high fractional wetting values for the MW grid area in Figure 2-5 coincide with the *Bradley and Smith* [1993] classification of squall-line precipitation extreme event climatology over this region.

The fractional wetting estimates obtained above required hourly data in order to resolve individual storm areas, and also to correspond with the hourly time step used in many current GCMs. Estimates can also be obtained using larger, aggregated time periods. $\bar{\kappa}$ is expected to increase with larger time periods, since for a large period of say 12 hours, many individual rain-areas can appear, translate and dissipate in the

44
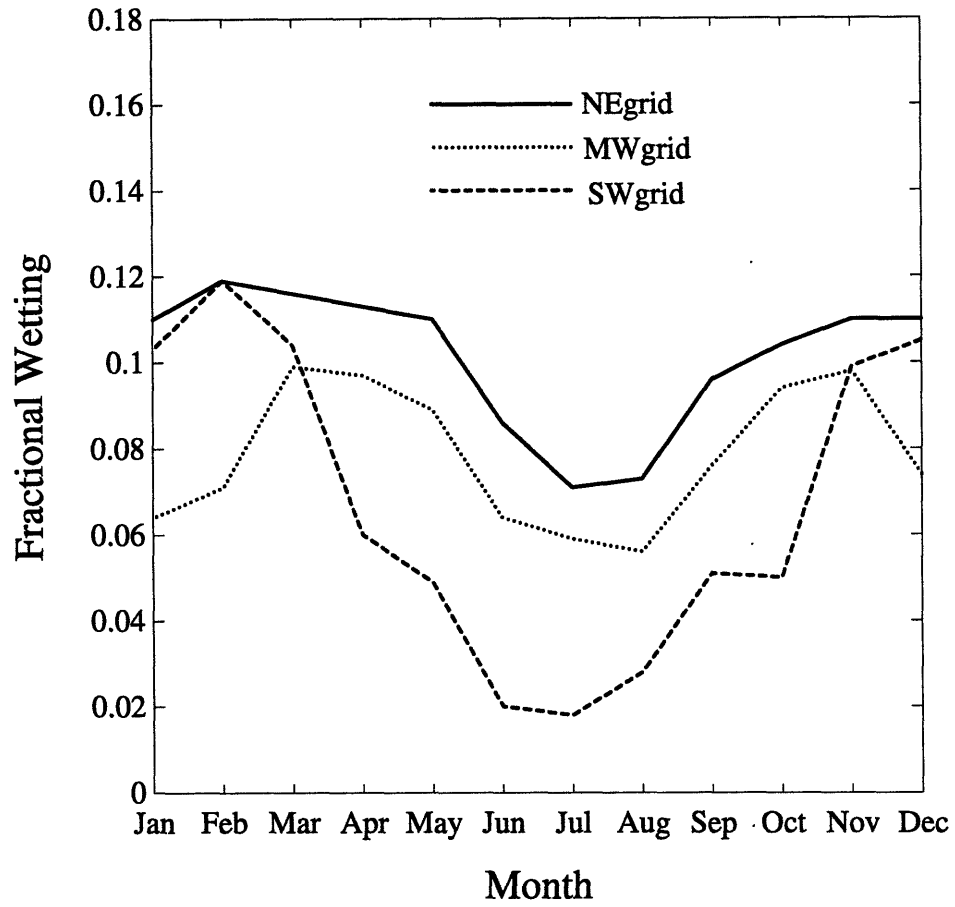
Figure 2-5: Annual cycle of estimated fractional wetting values $\bar{\kappa}$ for the NE, MW and SW grid areas

grid area, which serves to increase the total area wetted within the 12 hour period. It has been argued that the characteristically low values of fractional wetting at the hourly time scale are due to the intermittent nature of precipitation in space and time. It may thus be expected that longer aggregation periods will integrate over this temporal intermittency and significantly increase the fractional wetting estimate. Figure 2-6 illustrates this feature; in the April and October months when the extreme convective storms over this region occur, the temporal intermittency is large as indicated by the rapid growth in fractional wetting if rain records are viewed in terms of longer averaging periods. The winter precipitation is derived from synoptic-scale frontal features with steadier (less time-intermittent) precipitation. Correspondingly, as evident in Figure 2-6, the January fractional wetting estimates for this region do not grow as appreciably if longer averaging periods are considered.

2.3 Testing with Monte Carlo Simulations

A synthetic study was performed to test the estimation procedure and assumptions of Section 2 using monte carlo simulations. A GCM grid area is portrayed using a square coordinate system with a large number of nodes. The station network is created by locating stations at various nodes selected in a random manner. A long sequence of realistic storm areas is generated over the grid area; storm arrivals follow a Poisson process and storm durations are sampled from an exponential distribution. Each simulated storm is given a homogeneous square shape whose area is sampled from a smoothly decaying distribution that has a maximum value and non-zero minimum value. The probability distribution function for storm area A is taken from *Eagleson* [1984] as

$$f_A(A_0) = \frac{D}{2}\varepsilon^{\frac{D}{2}}[1 - (\frac{\varepsilon}{A_m})^{\frac{D}{2}}]^{-1}A_0^{-(1+\frac{D}{2})} \quad \varepsilon \leq A_0 \leq A_m \qquad (2.17)$$

where ε is the minimum storm area, A_m is the maximum storm area, and D is a fractal dimension. Typically A_m is much greater than ε, and D is about 1.35. These storm characteristics were selected because they capture fairly well the general fea-
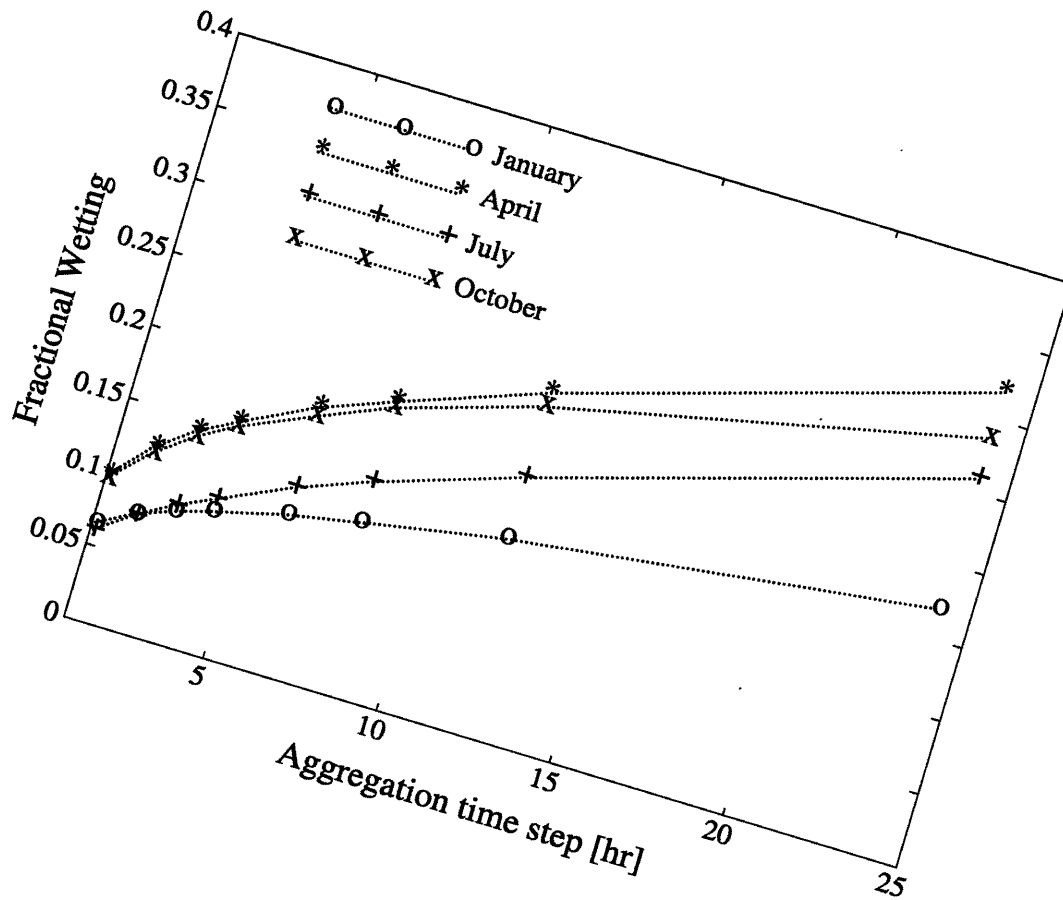
Figure 2-6: Fractional wetting values using aggregated time periods for January, April, July and October over the MW grid area

47

tures of mesoscale storm structure found in the literature [*Eagleson*, 1984; *Eagleson*, 1978]. Whenever a storm arrives it is randomly placed such that some portion of the storm is in the grid area.

This synthetic environment and storm sequence can be used to generate data records for each station. The synthetic time-series data can be used to estimate fractional wetting for the simulated grid area using the conditional probability relations of Section 2.1. The synthetic environment also enables the calculation of actual instantaneous fractional wetting values κ over the grid area for every hourly timestep with rain. The mean of these areal values can then be compared to the biased estimate $\bar{\kappa}^*$ and the corrected estimate $\bar{\kappa}$ obtained from the synthetic station network. Such an environment provides a means of verifying the estimation procedure. Network density can be varied in this synthetic environment, which enables us to explicitly observe its effect on the bias correction factor.

As mentioned earlier, two sets of simulations are carried out to specifically assess the role of spatial storm structure on the estimation procedure. In one set of experiments, the total grid area with precipitation at each timestep, A_t, is dispersed in a random manner throughout the various coordinate grid elements. This satisfies the storm intermittency assumption mentioned in Section 2.1.3 and illustrated in Figure 2-1. The role of possible large spatial correlation in the precipitating field is examined using a second set of simulations. Here the grid area with precipitation produced by the Poisson storms is kept intact in its simulated location, representing no storm intermittency at all. These two conditions are the enveloping cases for storm spatial structure.

Figure 2-7 shows the results of the first simulation with storm parameter values as listed in Table 2.1. Maximum and minimum storm area values are selected that produce $\bar{\kappa}$ values in the expected range for 4°x5° grid areas determined in Section 2.2. The biased estimates $\bar{\kappa}^*$ clearly show their strong dependence on n. Fractional wetting is severely overestimated by $\bar{\kappa}^*$ at low network densities, and this bias is steadily reduced as n increases. As expected the unbiased (i.e. corrected) $\bar{\kappa}$ estimates yield values very close to the areal mean at all network densities, which

verifies that the final estimate including the correction factor in equation (2.16) is indeed independent of the network density.

Figure 2-8 has the same simulation parameters as Figure 2-7, except that rain at each timestep is not randomly dispersed throughout the grid area. Each rainstorm retained its square shape and contiguity, representing the extreme case of strong spatial correlation in the precipitation field. Here $\bar{\kappa}^*$ is improved slightly over Figure 2-7, but the bias and dependence on n are still prevalent. The corrected $\bar{\kappa}$ estimates do not perform quite as well; they appear to retain a slight residual bias resulting in underestimates of the areal mean. However, a significant improvement over $\bar{\kappa}^*$ is still observed for this extreme case. The primary purpose of these two simulations is to determine the sensitivity of the bias correction factor to the storm area intermittency assumption. As indicated in Figure 2-8, even when no storm intermittency is introduced, a substantial amount of bias correction is still obtained. If a strong sensitivity did exist, these $\bar{\kappa}$ estimates would be no better, and perhaps even worse, than the $\bar{\kappa}^*$ values.

Figures 2-7 and 2-8 show that the estimates of unbiased fractional wetting are fairly robust under assumptions of either intermittent or contiguous precipitating areas within the grid area. Since the grid area is considerably larger than the precipitating areas (small $\bar{\kappa}$ values in the application to the U.S. described in Section 2.2) and the mean inter-gage distance in the network relative to the typical decorrelation length of precipitating areas is large, little bias is introduced by making the assumptions regarding randomized gage location that led to the simple estimation procedure. Barancourt et al. (1992) estimate the decorrelation distance for the precipitation indicator (1 rain or 0 no-rain) for a region in France. They examine various degrees of intermittency and similarly conclude that for small-scale intermittency associated with short-time integration periods, the network finite-density is constraining; consequently simple probabilistic models may be applied to unbias the results.

Actual intermittent rainstorms lie somewhere in between the representations of Figures 2-7 and 2-8, so the procedure developed here for estimating fractional wetting

Table 2.1: Parameter specifications for the monte carlo simulations

Parameter	Value
Grid size	100x100
Length of simulation	60000 hr
Poisson arrival rate	$.02 \ \mathrm{hr}^{-1}$
Mean storm duration	3 hr
Minimum storm area ε	400
Maximum storm area A_m	10000
Fractal dimension	1.35
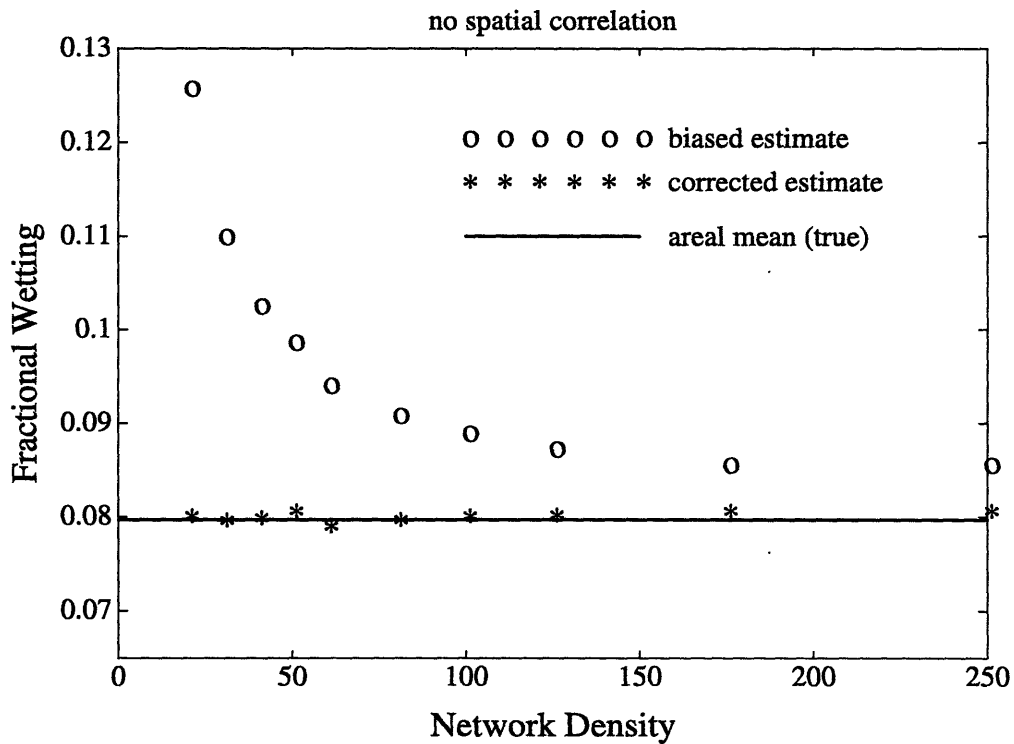
Figure 2-7: Variation in biased ($\bar{\kappa}^*$) and corrected ($\bar{\kappa}$) fractional wetting estimates with network density for a simulation with parameters as specified in Table 2.1. Rain areas are randomly dispersed at each timestep so as to have no spatial correlation.

high spatial correlation

0.13

0.12   o o o o o o biased estimate

        * * * * * * corrected estimate

0.11   ——————— areal mean (true)

0.1

0.09

0.08

0.07

0   50   100   150   200   250

Network Density

Fractional Wetting
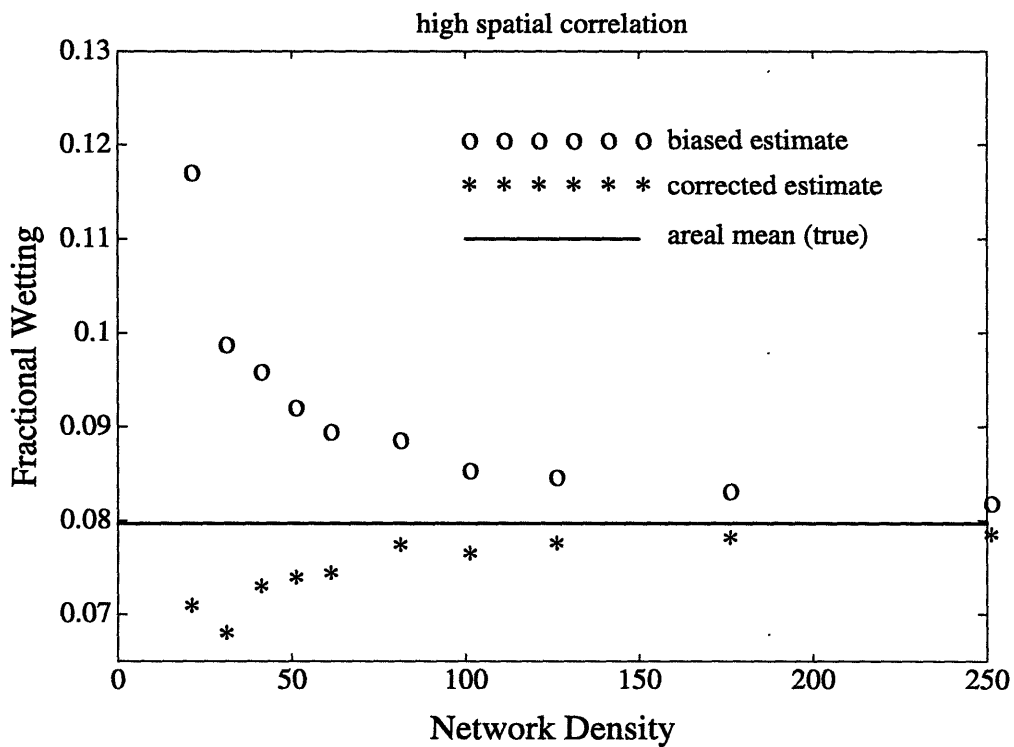
Figure 2-8: Variation in biased ($\bar{\kappa}^*$) and corrected ($\bar{\kappa}$) fractional wetting estimates with network density for a simulation with parameters as specified in Table 2.1. Rain areas are not randomly dispersed at each timestep, but instead retain their square shape and have a high spatial correlation.

in a GCM grid area yields valid results when applied to actual precipitation station records.

2.4 Discussion

The estimation procedure developed here has been shown to produce reliable regional and seasonal estimates of fractional wetting using station precipitation observations. The major assumptions made by this procedure are that rainfall within a grid area and month is a space-time homogeneous random field and that raingages are randomly located in the grid area. A series of monte carlo simulations in a synthetic environment verified the general reliability of these estimates. The estimates that were obtained revealed significant spatial and temporal variability in $\bar{\kappa}$ over the contiguous United States. Different regional climatic regimes are observed that share similar $\bar{\kappa}$ values. Clear unimodal or bimodal annual cycles are observed for individual grid areas. Some estimated values are as low as a few percent, which is substantially less than what has typically been prescribed by GCM modelers. As evidenced by the $\bar{\kappa}$ estimates for aggregated time periods (Figure 2-6), the disparity between the estimates and typically prescribed values may be attributable to the intermittent nature of rainfall in space and time. The relatively low values of these estimates, and their significant seasonal and regional variability, should have an important impact on GCM land surface hydrology parameterizations and the simulated climates produced by GCMs.

An important factor to note for the estimates of $\bar{\kappa}$ based on the procedure outlined here is that they are based on the current climate. When implemented in the GCM, the parameter is specific not only to location and season but to the governing climatic regime. GCM studies of climate change and deforestation, for example, may yield regional climates with altered regimes. In these cases, the parameter $\bar{\kappa}$ based on the historical climate may not be applicable. One solution to this limitation is to correlate the values of seasonal and regional $\bar{\kappa}$ based on the current climate to indicators of the climatic regime (e.g. mean precipitation rate, mean number of

storms per time period, mean storm depth, fraction of time with rain, etc.) and adjust the GCM parameter $\bar{\kappa}$ as the sensitivity experiment progresses. This procedure is also appropriate for transferring the values of $\bar{\kappa}$ estimated here to those regions of the globe where there is poor or nonexistent raingage network coverage. Finally, the described methodology is not restricted to $4°x5°$ grid areas, but is equally applicable to areas of any size since the Bernoulli-based correction factor eliminates the dependence on the number of available gages. In fact, the quality of this fractional wetting estimation procedure should improve for finer resolution GCMs since the validity of the homogeneous random precipitation field assumption improves for smaller land areas.

Chapter 3

Preliminary Investigations of Fractional Wetting in Land Surface Hydrology Parameterizations and Climate Simulations

3.1 Fractional Wetting in the Statistical-dynamical Hydrology Scheme of *Entekhabi and Eagleson* [1989]

3.1.1 Introduction

In this Chapter, the influence of the fractional wetting parameter on land surface hydrology parameterizations and climate simulations is investigated. Specifically, we will analyze fractional wetting as it appears in the statistical-dynamical hydrology scheme of *Entekhabi and Eagleson* [1989]. Following a brief description of this parameterization, its sensitivity to $\bar{\kappa}$ will be studied off-line, i.e. outside of any climate model. Next, a simple one-dimensional climate model will be utilized to determine the influence of expected $\bar{\kappa}$ variations in a system with basic climatic features and feedbacks. These analyses will provide a clearer understanding of the primary effects of fractional wetting variations than may be possible in a full GCM that contains a myriad of competing physical processes and interactions in a complex system.

3.1.2 Improved Parameterization of the Runoff Ratio, R

The basic premise of the *Entekhabi and Eagleson* [1989] hydrology scheme is to develop improved parameterizations for the runoff ratio, R and evapotranspiration efficiency, β, that are physically-based and account for subgrid spatial variability in precipitation and soil saturation. The fractional wetting parameter appears in the expression for R, so that is where our focus will lie. β is not considered in this work.

R is derived by first assuming precipitation intensity to be exponentially distributed in space throughout the wetted fraction $\bar{\kappa}$ of a grid area, with a mean intensity equal to that generated by the climate model precipitation scheme. Spatial relative soil saturation variations in a grid area are expressed using a gamma distribution, with the mean equal to the overall saturation value maintained by the model for that grid. These distributions are incorporated into an expression for the surface infiltration rate based on the linearized unsaturated darcy equation for vertical steady flow. This expression is integrated in space over all possible precipitation and soil saturation values and can be simplified to yield the following four parameter expression for the dimensionless runoff ratio:

$$R = exp[-\frac{1}{E[s]}] + \frac{(1 - exp[-(\bar{\kappa}\,I\,V + \frac{1}{E[s]})])\,(exp[-\bar{\kappa}\,I\,(1 - V)])}{(\bar{\kappa}\,I\,V\,E[s]) + 1} \tag{3.1}$$

where

$$I = \frac{K(1)}{E[P]}$$

$$V = \frac{1}{\Delta z}\frac{d\psi}{ds}\Big|_{s=1}$$

and $K(1)$ is the saturated hydraulic conductivity, $E[P]$ is the grid mean precipitation intensity, $E[s]$ is the grid mean soil saturation, ψ is the matric potential of the soil, and Δz is the thickness of the top soil layer of the model, taken as 10cm. More thorough descriptions of this parameterization can be found in *Johnson et al.* [1993],

and of course *Entekhabi and Eagleson* [1989].

In climate models, land surface-atmosphere interaction is treated as a one-dimensional process in the vertical direction; adjacent surface grid areas have no effect on each other, except through atmospheric transport, i.e. interaction with climate model dynamics. The parameters V and $K(1)$ are soil properties, and do not vary in time for particular grid areas. Therefore the only climatological parameters that can cause the runoff ratio to vary are $E[s]$, $E[P]$, and $\bar{\kappa}$. That is,

$$R = R\left(\, E[s],\quad E[P],\quad \bar{\kappa}\,\right) \qquad (3.2)$$

over a particular grid area. Each parameter will influence R to varying degrees, and the effect is further complicated if all parameters are allowed to vary, as is the case in nature.

3.1.3 Off-line Sensitivity Analysis on R

The analysis begins by studying analytically the sensitivity of R to $E[s]$, $E[P]$, and $\bar{\kappa}$, to determine which of these climatological parameters are the most influential. Equation 3.1 is graphed over the anticipated range of values of its parameters by plotting R against one parameter for constant values of a second parameter, while holding the remaining parameter fixed at a typical value.

The anticipated parameter ranges were diagnosed as follows. Soil saturation is allowed to vary over its entire range of $0 < E[s] \leq 1$, due to the great variety of values that are possible over the thin top layer. Fractional wetting falls in the range $.01 < \bar{\kappa} < .2$, in general accordance to the values estimated over the United States in Chapter 2. Using the general Brooks-Corey type soil hydraulic properties described in *Entekhabi and Eagleson* [1989] and an average soil texture consisting of almost equal parts sand, silt and clay, the parameter V was assigned a typical value of -3.0. This value is negative since the matric potential is defined as a negative number. Saturated hydraulic conductivity over a range of soil textures from pure sand to pure clay varies from $0.3\text{mm/hr} < K(1) < 7.5\text{mm/hr}$. Typical

precipitation intensities were determined using average values from an archived GISS GCM Model-II simulation, and were found to vary roughly from 0.4mm/hr $< E[P] <$ 1.5mm/h r. Consequently, the parameter I varies in the range $0.2 < I <$ 17.0.

Figure 3-1 plots R against $\bar{\kappa}$ for various constant values of $E[s]$, holding I fixed at a typical value of 7.0. R is seen to vary greatly with $\bar{\kappa}$, with increasing sensitivity as $\bar{\kappa}$ values become lower. The expected range of $\bar{\kappa}$ yields values of R over its entire range of possible values at low mean soil saturation values. At high values of $E[s]$ the sensitivity is diminished slightly, but R still covers a range of about 0.6., and the sensitivity gradient is still apparent. Runoff ratio is inversely proportional to fractional wetting in a nonlinear manner. This is reasonable since a decreased area with precipitation concentrates the rainfall and increases the intensity, which increases the likelihood of runoff.

According to Figure 3-1, R is also sensitive to $E[s]$, but not to the degree of $\bar{\kappa}$. Over the entire range of possible $E[s]$ values, the greatest variation in R occurs at higher fixed $\bar{\kappa}$ values; here R varies over a range of about 0.4. At very low values of $\bar{\kappa}$, $E[s]$ has a very small effect on R. This too is reasonable; at extremely low fractional wetting values, the runoff ratio is already near 1. Practically all incoming precipitation will be converted to runoff, regardless of the soil moisture condition. As expected, R is directly proportional to $E[s]$ since wetter soils have less available storage capacity and are less able to infiltrate water.

The sensitivity of R to I is shown in Figure 3-2, holding fractional wetting at an approximate average value of 0.08. Similarly to $\bar{\kappa}$, the runoff ratio appears to be extremely sensitive to I, and consequently to the precipitation intensity $E[P]$. This sensitivity is large over all values of $E[s]$, and especially at dry soil moisture conditions. R is inversely proportional I or directly proportional to $E[P]$, as expected. The extent of sensitivity to mean soil saturation is also apparent in this figure.

This sensitivity analysis clearly shows that in the hydrologically and climatologically expected range of parameter values, the runoff ratio parameterization of *Entekhabi and Eagleson* [1989] is very sensitive to variations in the fractional wet-

58
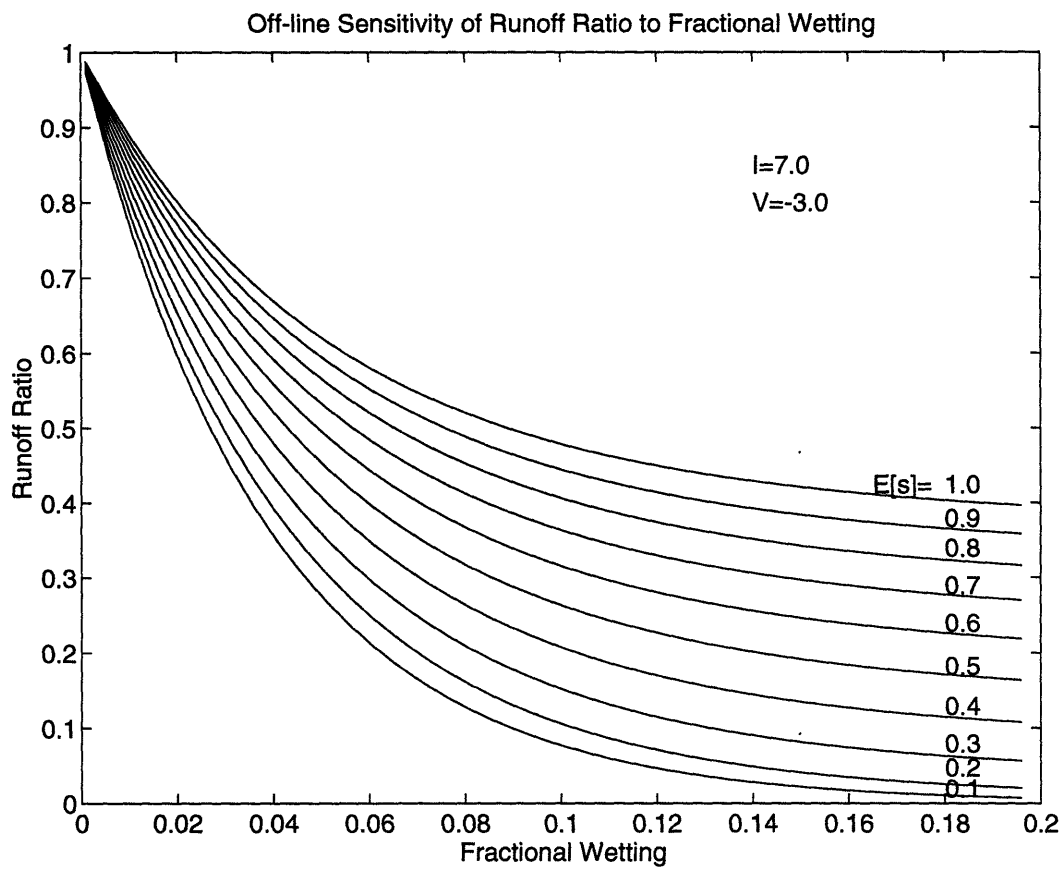
Figure 3-1: Runoff ratio R as a function of fractional wetting $\bar{\kappa}$ at fixed relative mean soil saturation $E[s]$ values, according to the land surface hydrology parameterization of *Entekhabi and Eagleson* [1989]. I is kept constant at 7.0 and $V = -3.0$. The selected parameter values and ranges are typical for the simulated climate.
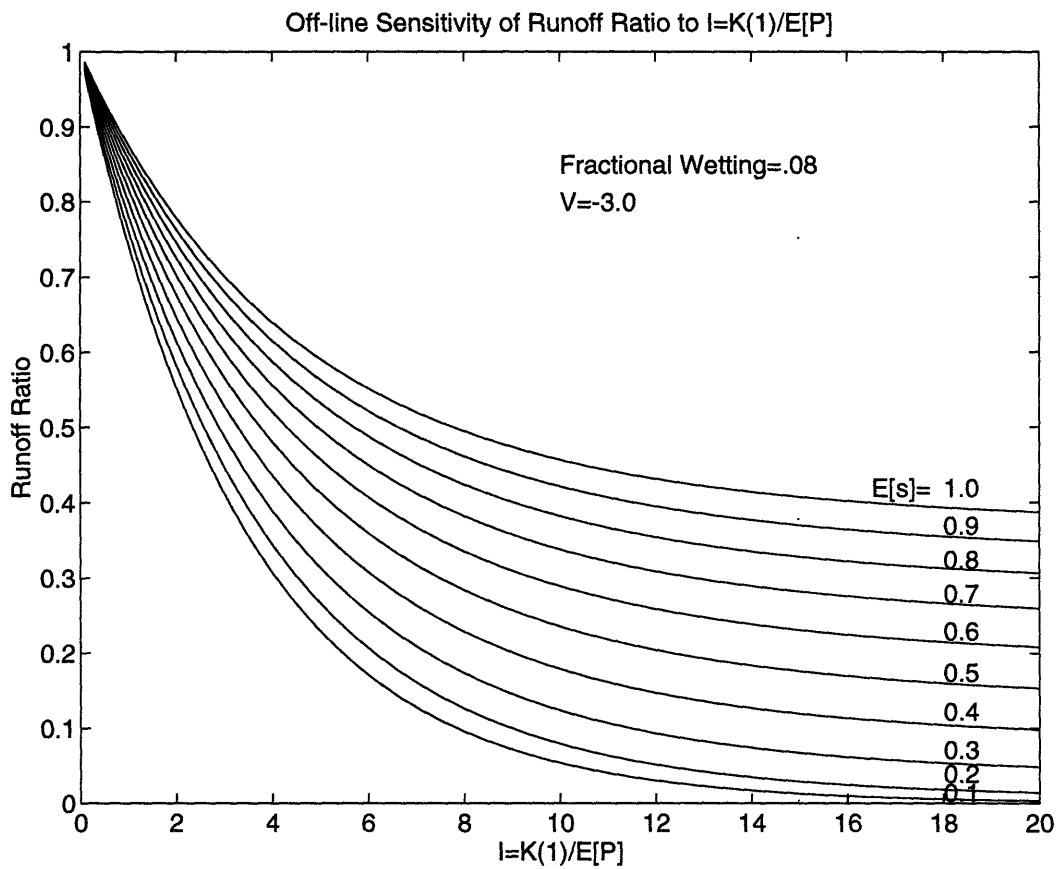
Figure 3-2: Runoff ratio R as a function of I at fixed values of relative mean soil saturation $E[s]$, according to the land surface hydrology parameterization of *Entekhabi and Eagleson* [1989]. $\bar{\kappa}$ is kept constant at 0.08 and $V = -3.0$. The selected parameter values and ranges are typical for the simulated climate.

ting parameter. Grid averaged precipitation intensity has also been identified as having a major influence. Grid averaged soil saturation has a smaller but still noticeable impact. I and $\bar{\kappa}$ appear to be influential to roughly the same degree, which is important since the two parameters are intricately related and highly variable.

In any climate simulation, however, R determines the fate of precipitation falling on the surface by partitioning it into runoff and infiltration. This subsequently influences $E[s]$, and ultimately $E[P]$. Many climatological interactions and feedbacks exist which may cause variations in R due to $\bar{\kappa}$ to alter the other parameters used to determine its value. This may either magnify, suppress or reverse the overall effect on R and the land surface hydrology.

The expected climatic response to a decrease in $\bar{\kappa}$ is depicted in Figure 3-3. The runoff ratio and consequently surface runoff should increase, leading to drier soils and a reduction in evaporation and its associated latent heat flux. This perturbation in the heat budget should be compensated by an increase in the less efficient sensible heat flux. As a result, surface temperatures should rise. Many of these relationships are nonlinear, beginning with initial response of runoff ratio to fractional wetting as indicated in Figure 3-2. In particular, evaporation is nonlinearly related to soil saturation as another part of the *Entekhabi & Eagleson* [1989] land surface hydrology parameterization. Temporal lags may also exist, such as the delay between heat fluxes changes and the response by surface temperature.

Finally, two potential negative feedback processes on R can be readily identified. Since R is directly proportional to $E[s]$, the reduction in soil moisture caused by lowering $\bar{\kappa}$ will in turn decrease R, counteracting the initial increase in R. This feedback may vary in strength, since R is not always very sensitive to $E[s]$. Also, a possible consequence of reduced evaporation is a drier atmosphere, and decreased precipitation: a drier climate. Precipitation intensity $E[P]$ may also be lessened in this drier state, as well as precipitation frequency. R is extremely sensitive to $E[P]$, and they are also directly proportional. Thus R will be reduced in contrast to its preliminary increase. These examples illustrate two of the more immediate potential negative feedbacks. In a system as intricate as the global climate, other less apparent

```
┌─────────────────────────┐
│ Fractional      DOWN    │
│ Wetting                 │
└─────────────────────────┘
            │
            ▼
┌─────────────────────────┐
│ Runoff          UP      │
│ Ratio                   │
└─────────────────────────┘
            │
            ▼
┌─────────────────────────┐
│ Surface         UP      │
│ Runoff                  │
└─────────────────────────┘
            │
            ▼
┌─────────────────────────┐
│ Infiltration    DOWN    │
└─────────────────────────┘
            │
            ▼
┌─────────────────────────┐                    ┌─────────────────────────┐
│ Surface Soil    DOWN    │ ────────────────►  │ Runoff          DOWN    │
│ Saturation              │                    │ Ratio                   │
└─────────────────────────┘                    └─────────────────────────┘
            │
            ▼
┌─────────────────────────┐
│ Surface         DOWN    │ ──────────────┐
│ Evaporation             │               │
└─────────────────────────┘               │
            │                             │
            ▼                             ▼
┌─────────────────────────┐   ┌─────────────────────────┐
│ Latent          DOWN    │   │ Drier Atmosphere        │
│ Heat Flux               │   └─────────────────────────┘
└─────────────────────────┘               │
            │                             ▼
            ▼              ┌─────────────────────────┐
┌─────────────────────────┐   │ Precipitation   DOWN    │
│ Sensible        UP      │   └─────────────────────────┘
│ Heat Flux               │               │
└─────────────────────────┘               ▼
            │              ┌─────────────────────────┐
            ▼              │ Precipitation   DOWN    │
┌─────────────────────────┐   │ Intensity               │
│ Temperatures    UP      │   └─────────────────────────┘
└─────────────────────────┘               │
                                          ▼
                           ┌─────────────────────────┐
                           │ Runoff          DOWN    │
                           │ Ratio                   │
                           └─────────────────────────┘
```
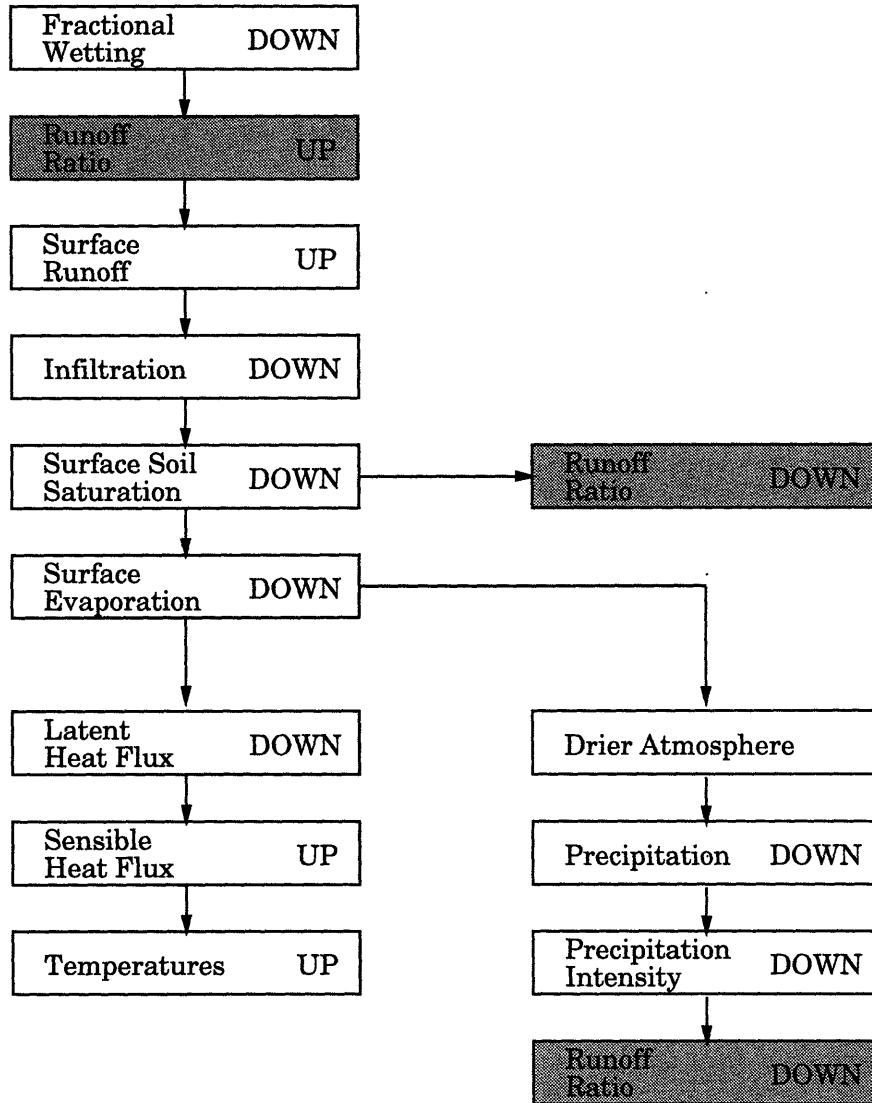
Figure 3-3: Expected climatic response to a reduction in fractional wetting, indicating anticipated negative feedbacks.

feedbacks may also exist.

What results is a very complex relationship between $\bar{\kappa}$ and R, and also the associated hydrologic and climatic parameters such as runoff, evapotranspiration, soil saturation, latent heat flux and even temperature. These features cannot be captured in an off-line analysis. Clearly a climate model containing these interactions and feedbacks is needed to study the importance of these relationships and ascertain the precise climatological effect of fractional wetting variations.

3.2 Utilization of a One-Dimensional Climate Model for Hydrologic Screening

3.2.1 Basic Purpose

The most direct way to investigate the significance of the varying fractional wetting estimates discussed in Chapter 2 is to implement them into a GCM and study the effect on model climate. However, a number of problems arise in such an immediate GCM implementation. The large computational requirements of full GCMs inhibit long or repeated simulation runs that are necessary to fully investigate hydrologic and climatic sensitivity to $\bar{\kappa}$ variations on the order described in Chapter 2. Also, the extensive feedbacks between numerous climate processes included in three-dimensional GCMs make it difficult to ascertain the specific influence of $\bar{\kappa}$ variations on the land surface hydrology parameterization and the climate as a whole. It is preferable to first investigate $\bar{\kappa}$ sensitivities using a simpler model that contains the climatic processes relevant to fractional wetting, yet can isolate its effects and is less computationally burdensome than a full GCM.

Such a model has been developed by *Entekhabi* [1994], and its primary application is to screen various modifications in the landsurface hydrology parameterization of GCMs prior to their implementation. This screening model captures the major climatic processes that interact with the landsurface hydrology. This includes virtually all of the physical parameterizations, such as radiative transfer, clouds, moist

convection and water vapor condensation. The large-scale dynamics of the atmosphere do not play a direct role in landsurface hydrology; therefore the horizontal convergence of heat and moisture is parameterized simply in the screening model, as opposed to numerically solving the equations that govern atmospheric fluid flow over a three-dimensional grid. With the absence of precise lateral dynamics, all remaining modeled processes are vertical processes. Therefore the screening model is essentially a one-dimensional apparatus, which greatly simplifies its computational requirements.

Many of the physical parameterizations used by this screening model are identical to those of the GISS GCM. In fact, this simple model was originally constructed with the goal of being a simplified version of the GISS model that focused on landsurface hydrology components. Thus this screening model is intrinsically linked to, and intended for use in conjunction with, the GISS GCM.

Note that the screening model is in essence a radiative-convective (RC) process model, since the two are very similar in structure. *Henderson-Sellers and McGuffe* [1987] and *Schneider and Dickinson* [1974] describe the general features of an RC model. Like an RC model, the single dimension of the screening model occurs in the vertical direction, and there are a discrete number of atmospheric layers. Fluxes of solar and terrestrial radiation are the primary computational components, along with a convective adjustment based on a critical lapse rate. However, the screening model has a different purpose and emphasis than most RC models, so some features do differ.

RC models are designed to simulate the global average surface temperature, as well as the vertical temperature profile in the atmosphere. Therefore the accurate calculation of radiative streams in each layer is of utmost importance, and fairly thorough schemes are often used. In addition, various parameterizations are often included to incorporate some feedback mechanisms that influence global temperatures but are not internally accounted for, such as the ice-albedo-temperature feedback [*Wang and Stone*, 1980]. Landsurface-atmosphere interactions play a minor role in most of these models.

In the screening model however, interactions between the atmosphere and land-surface are the primary components under investigation. Thus features such as a surface air layer and an interactive soil column are included, and a complete hydrologic cycle is modeled. Radiation streams and atmospheric feedbacks are not stressed as strongly, since accurate global temperatures are not the goal of the screening model. Even though the screening model is similar in structure to a basic RC model, it is designed solely for testing hydrologic sensitivities in the climate, and should not be used interchangeably with other RC-type models.

3.2.2 Brief Model Description

A very brief description of the screening model and its various components is included here, in order to provide a general feel for how the model works. A much more thorough description can be found in *Entekhabi* [1994]. The screening model consists of nine atmospheric layers, with pressure levels centered as in the GISS GCM. At the surface boundary, there are effectively two "grids" of equal area, one representing the landsurface and the other representing the ocean. A simple linear reservoir scheme is used to provide lateral convergence of heat and moisture between the two grids within each layer. This dynamically-linked two grid construction provides a complete hydrologic cycle within the model. The radiation scheme is based on *Hoffman* [1981]. Many of the precipitation and boundary layer processes follow the parameterizations used by the GISS GCM Model-II [*Hansen et al.,* 1983].

Subgrid-scale spatial variability in the landsurface hydrology parameterization is accounted for using the *Entekhabi and Eagleson* [1989] statistical-dynamical scheme. Multiple soil layers are also used in the model, and the *Abramopoulos et al.* [1988] multiple soil layer moisture diffusion scheme is used to update the soil moisture content of each layer. Incoming soil radiation from above the highest atmospheric layer is the only external forcing placed on the model.

The screening model as described above performs perpetual-day simulations, since there is no mechanism to provide for seasonal heat storage. Thus the exter-

nal solar radiation forcing must correspond to a prescribed Julian day. A general sensitivity analysis can be performed on the fractional wetting parameter using this perpetual-day version. The model can also be modified to provide seasonal heat storage and produce simulations that contain an annual cycle. The one-dimensional heat conduction equation is solved for the three-layer system following *Hansen et al.* [1983]. Energy balance is maintained for each layer, and the temperature profile in each layer is represented as a quadratic function of depth. Heat flux equations through each layer are derived and used to update the average temperature in each layer. These equations are given in Appendix B. This inclusion of seasonal heat storage enables the investigation of seasonally varying $\bar{\kappa}$ values in comparison to a constant value throughout the year.

3.3 Fractional Wetting Experiments with the One-Dimensional Screening Model

3.3.1 Model Specifications

The one-dimensional screening model is used to investigate the sensitivity of hydrologic and climatic diagnostic parameters to variations in fractional wetting on the order described in Chapter 2. Three interactive soil layers were modeled, and a non-zero flux condition was placed at the bottom of the lowest layer to represent groundwater flow. A simple parameterization was incorporated based on gravity-controlled flow in unsaturated porous media. Groundwater runoff is modeled as the hydraulic conductivity of the lowest soil layer (a function of relative soil saturation) multiplied by an arbitrarily selected typical bedrock slope. Since the saturated zone is not modeled, it is assumed that the topographic slope is equal to the bedrock slope. These slopes are generally small, so the contribution of groundwater flow to the surface water balance is expected to be small. However, its functional relationship to soil saturation may lead to drier soils, particularly in the lowest layer. Complete parameter specifications for the model are listed in Table 3.1. Representative soil

Table 3.1: Parameter specifications for the one-dimensional screening model

Parameter	Value
Latitude	15N
Fixed Ocean Surface temperature	28C
Cloud temperature standard deviation	3C
Surface Wind Speed (Land)	2 m/s
Surface Wind Speed (Ocean)	5 m/s
Albedo (Land)	.25
Albedo (Ocean)	.35
Soil sand fraction	.30
Soil silt fraction	.35
Soil clay fraction	.35
Soil layer 1 thickness	.10m
Soil layer 2 thickness	.15m
Soil layer 3 thickness	.50m
Soil moisture coeff. of variability	1.0
Bedrock slope	0.00354
Dynamic exchange parameter	1.67 days

hydraulic properties conform with those specified in *Entekhabi and Eagleson* [1989].

As mentioned in Section 3.2.2, a simple cloud cover parameterization is included in the screening model. A brief summary of the cloud parameterization is given in Appendix C. Clouds play a major role in determining short and long wave radiation fluxes. Since radiation is the dominant feature in any RC climate model, cloud cover can affect all aspects of the screening model. This includes land surface processes, since the heat and water balance are coupled through evaporation and its latent heat storage. Even in this simple climate model, atmospheric feedbacks can obscure the effect of hydrologic changes due to fractional wetting. For this reason, many of the screening model simulations performed here will prescribe fixed cloud fractions for each atmospheric layer, based on the average climatology produced by simulations with interactive cloud cover. The fixed cloud simulations, hereafter designated as FIXC, allow for further isolation of hydrologic processes than in interactive cloud simulations, hereafter called INTC.

3.3.2 Perpetual-day simulation experiments

Following the aforementioned sequential analysis procedure, screening model simulations begin with the semplist possible type: A series of nine perpetual-day simulations is performed, each with a different fixed fractional wetting value of $\bar{\kappa} = .02, .04, .06, ..., .18$. The Julian day for all runs was set at 182, or July 1. Each simulation consisted of a 100 day spinup followed by a 600 day collection period, in which daily values of runoff ratio, surface runoff, precipitation, evaporation and top soil layer saturation over the land surface were recorded. Since perpetual-day simulations offer no climatic realism, only a basic sensitivity analysis on the primary hydrologic diagnostics is performed to determine the principal reaction to changes in fractional wetting. Also, all simulations retained the model's original interactive cloud cover parameterization (INTC).

Despite its simplicity compared to GCMs, the screening model is still a very complex and nonlinear system, and some amount of variability in the diagnostic

parameters is still expected. The objective of this sensitivity analysis is to see if small changes in $\bar{\kappa}$ have a significant impact on the mean parameter values over all 600 days. Such small variations in $\bar{\kappa}$ are not expected to produce drastically different diagnostic values. However, they may significantly alter the mean of these parameters.

For each simulation run, the mean over the collection period for each diagnostic parameter is calculated. The results are presented in Figures 3-4–3-6 as graphs showing the changes in mean with $\bar{\kappa}$ for each parameter. Error bars for the mean over a 600 day time series are calculated as

$$1.96\sigma_{\bar{x}} \approx \frac{2\sigma_x}{(600)^{1/2}}$$

where $\bar{x}$ represents the mean of a parameter x, $\sigma_{\bar{x}}$ is the standard deviation of the mean $\bar{x}$ and σ_x is the statistical standard deviation of the 600 samples of x. Assuming a normal distribution for x, $1.96\sigma_{\bar{x}}$ within the mean on both sides represents 95% of the probability mass for $\bar{x}$. Thus we can interpret the graphs as indicating with 95% certainty that the calculated mean value lies within the error bars for each point.

The off-line analysis in section 3.1.3 indicated that functionally, R and $\bar{\kappa}$ are inversely proportional with the absolute value slope increasing as $\bar{\kappa}$ gets smaller. Climatically however, Figure 3-4a indicates a different relationship. Although still inversely proportional, the slope appears to be fairly constant as $\bar{\kappa}$ drops from 0.18 to 0.1. At $\bar{\kappa}$ values below 0.1, no effect on R can be detected due to the large error bars produced by the climate simulations, even though this is functionally the most sensitive region. Also, the mean R values simulated by the model runs cover a very small range. Clearly negative feedbacks are present which counter the expected R-$\bar{\kappa}$ relationship, and they are most influential for $\bar{\kappa}$ below 0.1. These feedbacks can be revealed by analyzing the response of various hydrologic and climatic diagnostics to $\bar{\kappa}$.

Surface runoff (Figure 3-4b) behaves much like R. This is not surprising since runoff is determined directly by the value of R. Soil saturation decreases steadily
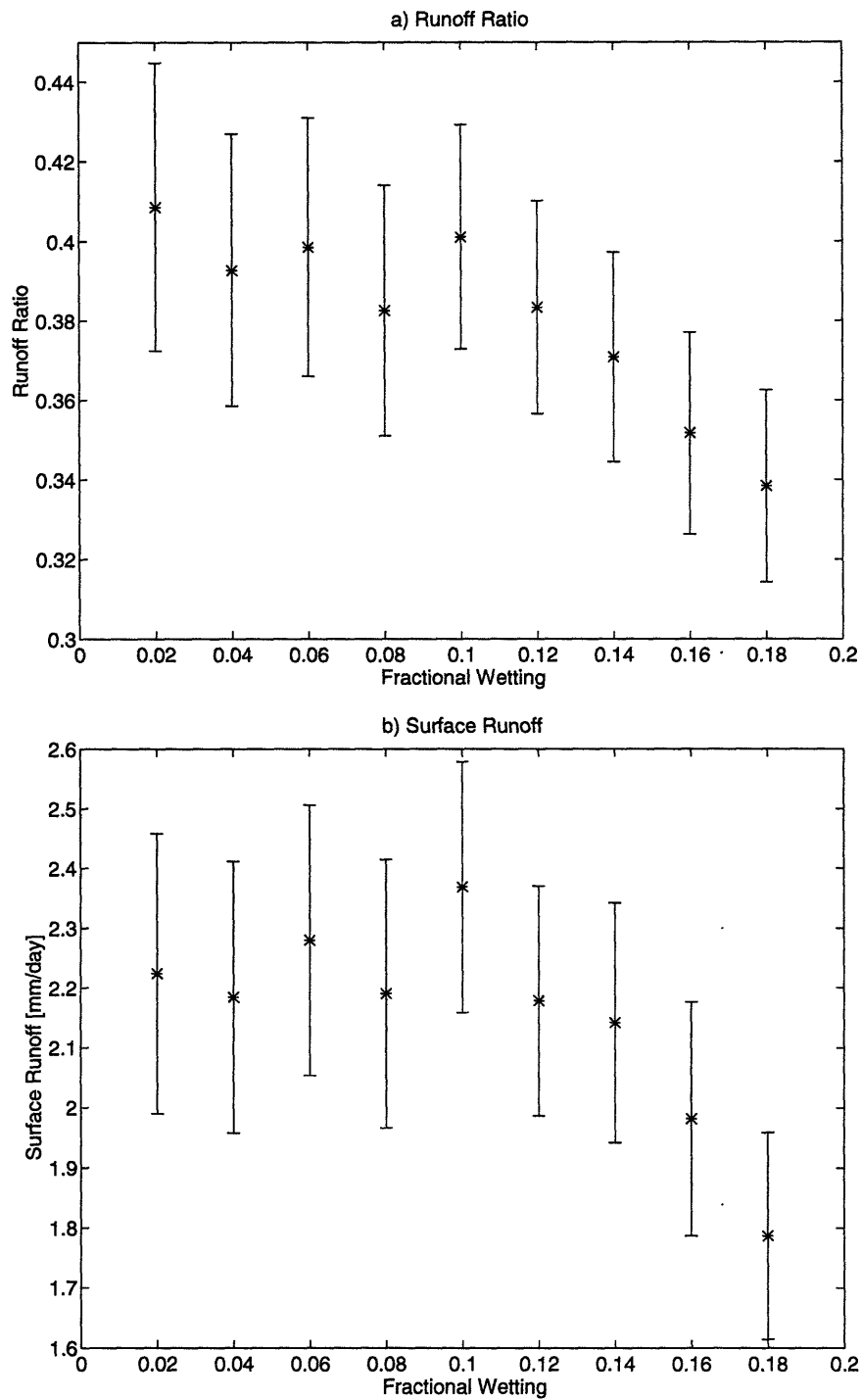
Figure 3-4: Sensitivity of a) runoff ratio and b) land surface runoff to small changes in the fractional wetting parameter $\bar{\kappa}$ produced by perpetual-day screening model simulations.
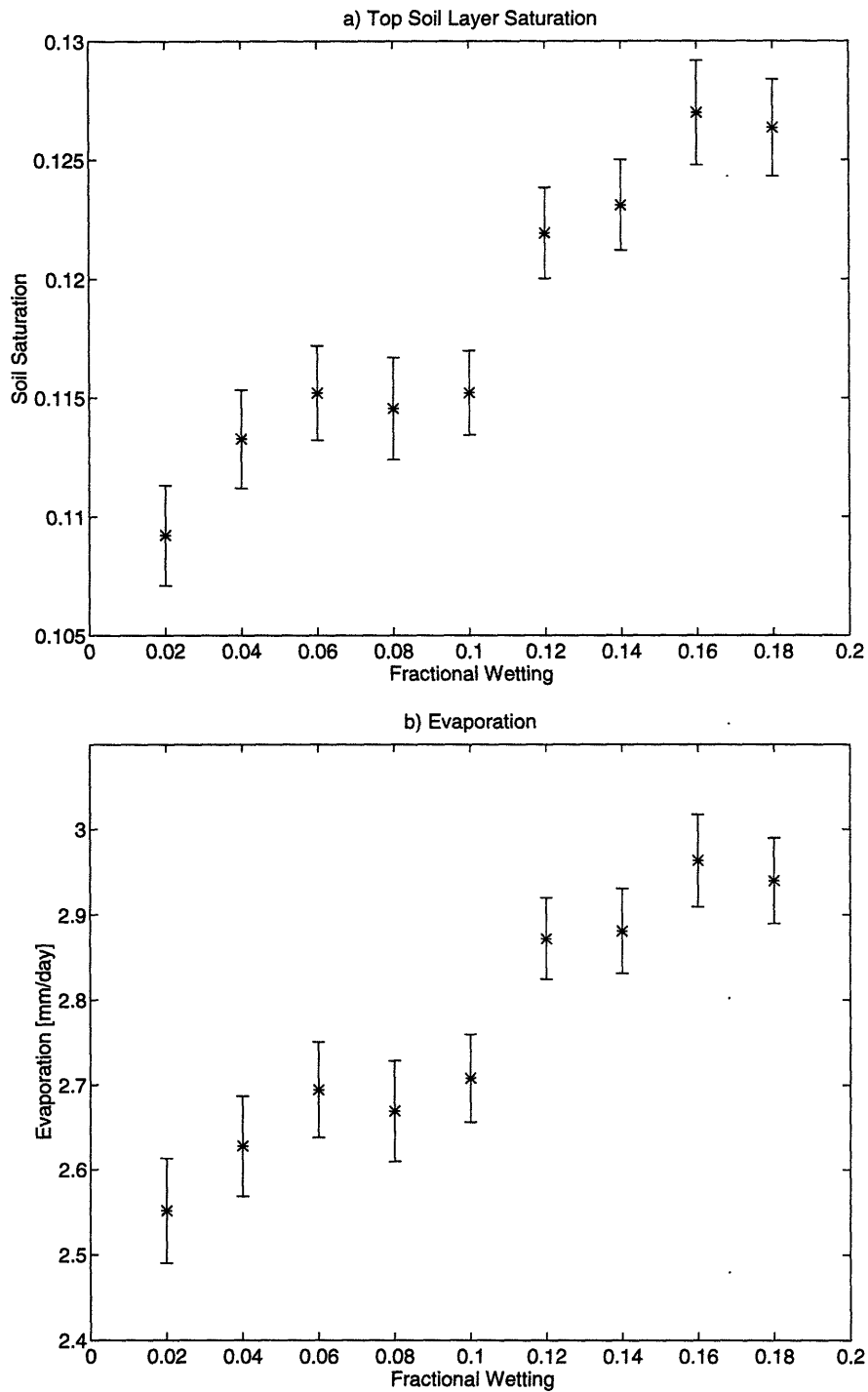
Figure 3-5: Sensitivity of a) top soil layer saturation and b) land surface evaporation to small changes in the fractional wetting parameter $\bar{\kappa}$ produced by perpetual-day screening model simulations.
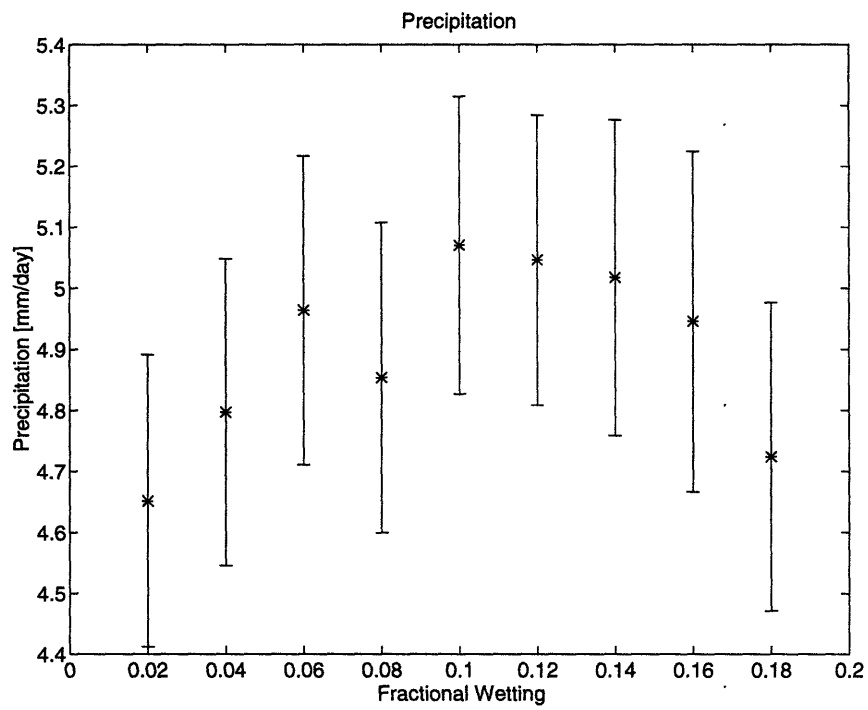
Figure 3-6: Sensitivity of land surface precipitation to small changes in the fractional wetting parameter $\bar{\kappa}$ produced by perpetual-day screening model simulations.

and very significantly as fractional wetting is reduced, as does evaporation since these two parameters are also directly related (Figure 3-5). This steady decrease in soil saturation allows for the negative feedback on R due to $E[s]$ to take effect over all $\bar{\kappa}$ values. According to Figure 3-5a, $E[s]$ only varies within a very small range of about .02 over the nine perpetual-day simulations. The off-line sensitivity analysis indicates that R is not affected by such small changes in $E[s]$, which implies a very weak feedback.

These mean soil saturation values are misleading though, because they represent the average over the entire simulation. Since there are many more hours without rain than with rain in any realistic climate representation, $E[s]$ will be relatively dry due to evaporation and diffusion processes. However, the runoff ratio and fractional wetting parameter only take hold when precipitation occurs, during which the surface soil saturation is expected to be substantially larger. In this wetter environment, soil moisture will vary much more than indicated by $E[s]$. In short, during the timesteps in which R is applied, $E[s]$ can vary significantly in response to changes in $\bar{\kappa}$, allowing for a strong negative soil saturation feedback on R. This factor also explains why the R, runoff and precipitation values have much larger error bars than soil saturation and evaporation values. The first three parameters are only computed during hours in which precipitation occurs, and they are expected to vary considerably over the course of a storm. The latter two parameters include all hours; they contain less variability since climate is dominated by hours without precipitation, which are predominantly dry and slowly varying.

The negative precipitation feedback is also observable, particularly at low $\bar{\kappa}$ values. As seen in Figure 3-6, precipitation, despite its large error bars, clearly begins to decrease when $\bar{\kappa}$ drops below about 0.1. This coincides exactly with the values for which R no longer responds to fractional wetting. The decrease in precipitation affects the runoff ratio parameterization by decreasing R. Since R was shown to be extremely sensitive to precipitation through I, this feedback mechanism is strong enough to counter and nullify the high functional sensitivity between R and $\bar{\kappa}$ at low $\bar{\kappa}$. Above $\bar{\kappa} = 0.1$, the fractional wetting values are not extreme enough to

impact the prectipitaion forcing.

Note that Figure 3-6 presents time averaged precipitation amounts, while runoff ratio is related to the precipitation intensity $E[P]$. The drier climate represented by reduced average precipitation can manifest itself as less intense rainfall, and also less frequent rainfall. Less frequent rainfall of the same intensity will not feed back on R. In reality, both intensity and frequency should be noticeably affected.

In summary, a clear threshold can be seen at $\bar{\kappa}$ equal to about 0.1. Above this fractional wetting value, the precipitation feedback does not take effect, as indicated by the relatively invariant precipitation values seen in Figure 3-6. In this $\bar{\kappa}$ range, only the soil saturation feedback is active, and it serves to linearize the R-$\bar{\kappa}$ relationship. Unfortunately, this conclusion is clouded by the large statistical error bars on R. Extreme low values of $\bar{\kappa}$ below 0.1 however do affect simulated precipitation, which allow the strong precipitation feedback to take effect in conjunction with the soil moisture feedback The result is a dramatic reduction in runoff ratio response to fractional wetting, in a region in which R is theoretically expected to be very sensitive. These perpetual-day simulations have verified the existence of both the precipitation and soil moisture induced negative feedbacks on runoff ratio resulting from changes in fractional wetting.

3.3.3 Seasonally Varying Simulations

Two simulation runs were made with the seasonally varying version of the screening model. The first run, S1, fixed $\bar{\kappa}$ at .08, while the second run, S2, had a different value for each month. These monthly values were selected to conform with the basic seasonal pattern of Figure 2-5, which peaked in the winter and ebbed in the summer. The monthly $\bar{\kappa}$ values were, beginning in January, .14,.13,.11,.08,.05,.03,.02,.03,.05,.08.,11, and .13. Note that the average of these 12 values is .08, the same as the fixed value for run S1. Also, the monthly fractional wetting values vary in a smooth and sinusoidal fashion about the annual mean (see Figure 3-7). Since an annual cycle is modeled in this version, the Julian day and

74
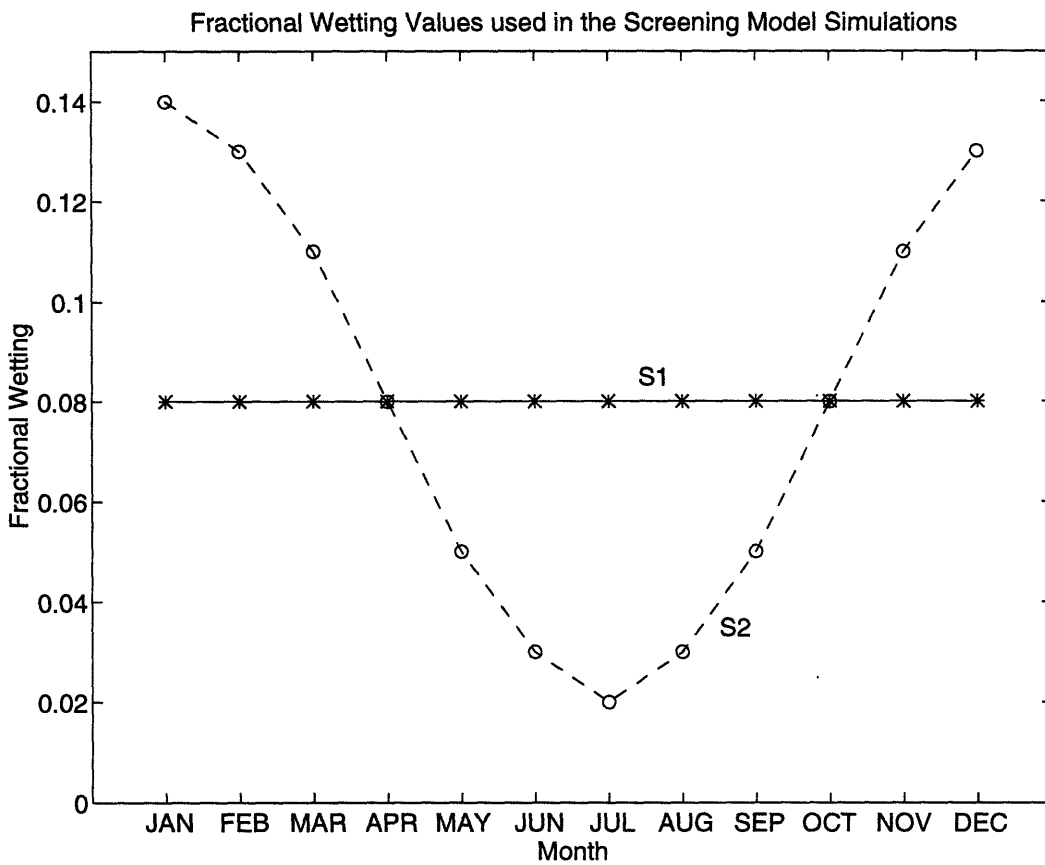
Figure 3-7: Monthly variations in fractional wetting between simulations S1 and S2 for the seasonally varying screening model experiments

solar forcing at each time step were varied accordingly. Each run consisted of a 3 year spinup, followed by a 50 year collection period. Diagnostics were collected very month. A much longer simulation is required here than for the perpetual-day version, in order to obtain an accurate assessment of the full annual cycle.

In addition to being more realistic, these simulations differ from the perpetual-day experiments in fundamental ways. The long-term perpetual-day runs allowed us to analyze and compare the equilibrium climates corresponding to particular fractional wetting values. In these seasonally varying simulations, we are studying the equilibrium climate produced by introducing seasonal variability in $\bar{\kappa}$, and comparing it to the equilibrium climate with no variability. The major anticipated response is a curtailing of the precipitation feedback seen previously when $\bar{\kappa}$ varies below 0.1, since the simulated precipitation is not given enough time to equilibrate to the change in fractional wetting. Here only one month passes before $\bar{\kappa}$ changes again, and the radiative forcing changes even more frequently. The perpetual-day runs gave the model 600 days to react to a single change in $\bar{\kappa}$, all under the same radiative forcing.

Two main objectives can be identified for these seasonally varying screening model simulations. The first objective is to see if the introduction of seasonal $\bar{\kappa}$ variability about an annual mean of 0.8 affects the resultant mean annual climate. This is possible if the model respondsre diffently to $\bar{\kappa}$ values above the mean than to values below the mean. In other words, if a particular climate diagnostic responds nonlinearly to fractional wetting perturbations, the annual mean of that diagnostic produced by simulation S2 will differ from that of S1. Second, the monthly annual cycles of various diagnostics will be studied in detail to assess the direct response of monthly fractional wetting variations. Analysis of the extent of monthly diagnostic changes will also help to determine any nonlinearities and feedbacks that may exist.

Statistical Testing Methodology

The principal method of analysis in this section is to compare the mean value of various diagnostic parameters produced by runs S1 and S2. With extended 50

year simulation lengths, we can reliably calculate sample standard deviations for each month, then use them to determine whether or not the monthly means are statistically different. We will use a standard statistical test on the equality of two unknown true population means when both sample means and standard deviations are known [*Crow et al.*, 1960]. Given two populations x and y, n samples can be taken from each one to yield sample means $\bar{x}$ and $\bar{y}$, and sample standard deviations σ_x and σ_y. The hypothesis that the two population means μ_x and μ_y are equal fails (i.e. the means are not equal) if:

$$|\bar{y} - \bar{x}| > z\left(\frac{\sigma_x}{n} + \frac{\sigma_y}{n}\right)^{\frac{1}{2}} \tag{3.3}$$

Assuming a normal distribution for x and y and applying an equal-tails test, the value of z corresponding to a 5% level of significance is 1.96.

All statistical tests have inherent assumptions and approximations; therefore their results should not be accepted unconditionally. In our 50 year simulations, 50 samples may yield fairly large sample standard deviations, making the test criteria (right-hand side of (3.3)) very rigorous. An even longer simulation of say 200 years would in all likelihood reduce the sample standard deviation. Also, the normal distribution assumption may not be accurate, especially for limited value diagnostics such as runoff ratio, precipitation and soil saturation. Instead of relying solely on the significance tests, our analysis of the seasonally varying screening model simulations will also look for patterns and trends that appear regardless of their statistical significance. This will provide a broader assessment of the influence of seasonal fractional wetting variations.

Mean Annual Climate

We begin by comparing the annual mean produced by runs S1 and S2 using FIXC conditions. For each of the relevant diagnostics, a value is obtained for each year of simulation by taking the average over all twelve months of that year. Taking the mean over all 50 years of a simulation yields the desired annual mean for that

simulation. The difference in annual mean between the two simulations (S2-S1) is presented in Figures 3-8 and 3-9 as solid line bar graphs. All relevant hydrologic and climatic diagnostics are displayed. Superimposed are dotted line bars which indicate the required difference for statistical significance as derminined by the right-hand side of (3.3). These test thresholds are graphed as boitive and negative values since the calculcaluclated mean can increase or decrease.

Figure 3-8a indicates that the annual mean runoff ratio is not statistically altered by introducing seasonal variability in fractional wetting about the same mean, since the difference $R_{S2} - R_{S1}$ is well below its criteria value. This implies that the affect of $\bar{\kappa}$ perturbations above the mean are balanced by perturbation affects below the mean. The off-line analysis showed a greater response by R to lower $\bar{\kappa}$ values. Apparently some of the feedbacks discovered in the perpetual-day simulations are also in effect here, or else Figure 3-8a would have certainly indicated a significant increase in R.

The other hydrologic diagnostics shown in Figure 3-8 also do not indicate a significant change in annual mean, implying that the land surface hydrology as a whole responds equally to positive and negative fractional wetting perturbations. The same holds true for the land surface heat fluxes, as indicated in Figure 3-9a. Shortwave radiation is not affected at all since cloud fractions remain fixed. However, these statistically equal fluxes produce statistically different surface temperatures, as seen in Figure 3-9b. All soil layer and surface air temperatures decrease in response to seasonal fractional wetting variability. In general a decrease in temperatures is the expected response to an overall increase in $\bar{\kappa}$ (see Figure 3-3).

Even though the primary hydrologic diagnostics appear to respond equally to increases and decreases in $\bar{\kappa}$, the resulting cooler climate indicates that fractional wetting values above the mean of 0.8 are ultimately more influential than values below 0.8. Also, a number of annual mean diagnostics are very close to satisfying the chosen statistical criteria, implying that they too may be influenced to some degree. This possibility is evidenced by the fact that although they are statistically insignificant, all hydrologic parameters change in the direction of a wetter climate:

78
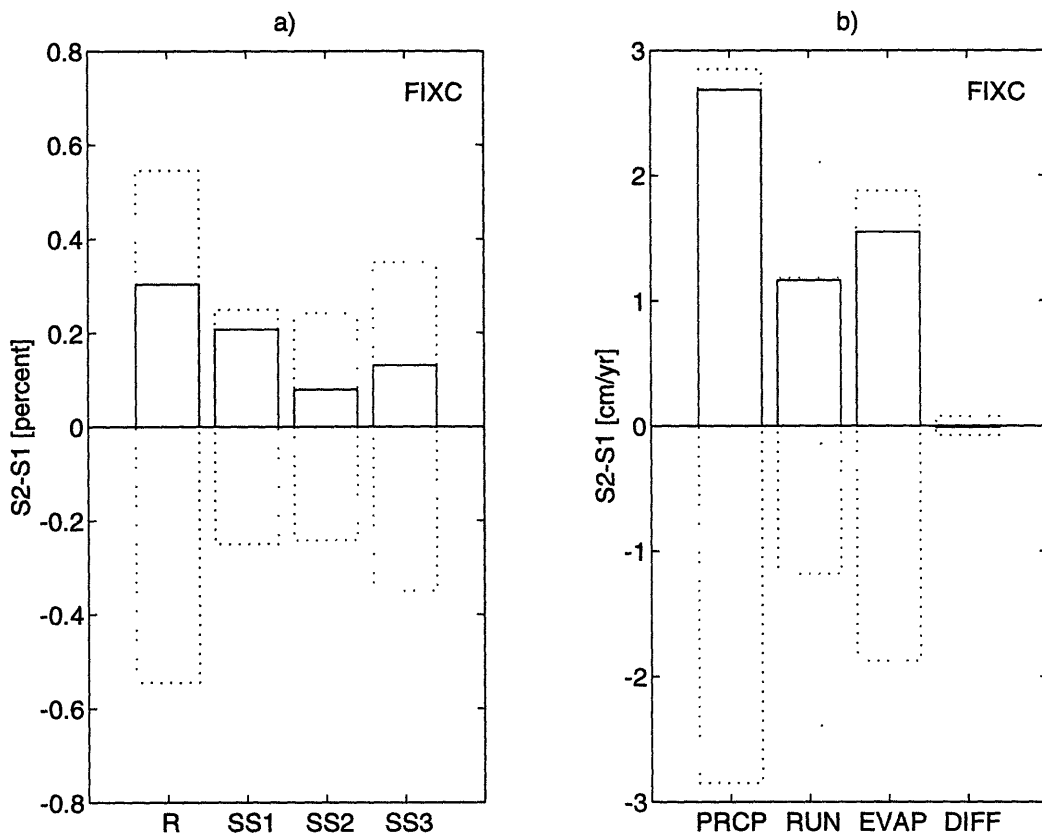
Figure 3-8: Difference (S2-S1) in annual mean hydrologic budget diagnostics for FIXC simulations, with statistical equality criteria. a) runoff ratio and three soil layer saturation states. b) precipitation, surface runoff, evaporation and diffusion between first and second soil layer.
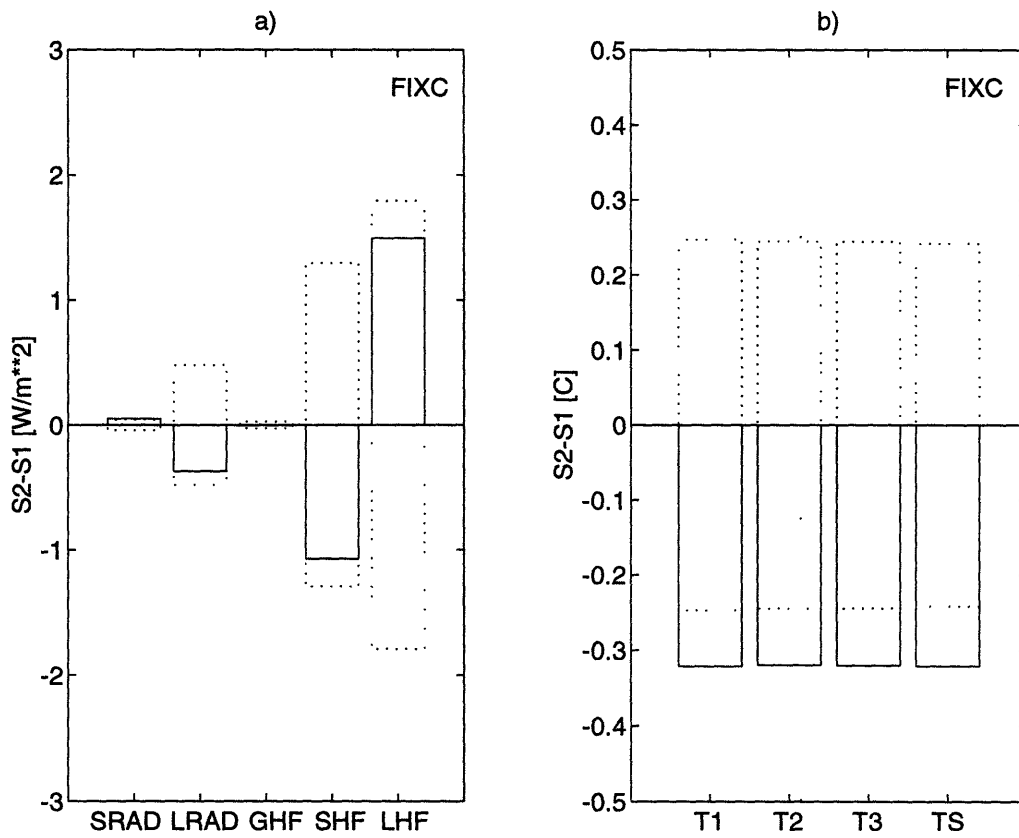
Figure 3-9: Difference (S2-S1) in annual mean heat budget diagnostics for FIXC simulations, with statistical equality criteria. a) incoming solar radiation, net outgoing thermal radiation, ground heat flux, outgoing sensible heat flux and outgoing latent heat flux. b) three soil layer temperatures and surface air temperature.

80

wetter soils, increased precipitation, increased evaporation and latent heat flux, and decreased sensible heat flux. Wetter climates are also expected as a result of an overall increase in $\bar{\kappa}$.

Role of Interactive Cloud Fractions

The annual means produced by runs S1 and S2 using INTC conditions are presented in Figures 3-10 and 3-11 in the same manner as for the FIXC case. The effect of allowing interactive cloud fractions is a severe decrease in the overall response to seasonal $\bar{\kappa}$ perturbations by all hydrologic parameters. The heat fluxes are amplified, and many of them are significantly altered by the $\bar{\kappa}$ variations. With INTC, the significant reduction in incoming solar radiation and net outgoing thermal radiation indicate more clouds, or an increase in atmospheric moisture. Clouds allow less solar radiation to reach the surface, and more water vapor generates more downward longwave radiation to reduce the net upward thermal radiation. Increased clouds represent a wetter climate. The significant decrease in solar radiation and inefficient sensible heat flux leads to significantly cooler surface temperatures, to roughly the same degree seen using FIXC. Thus the INTC simulations also result in a wetter and cooler climate, indicating once again a stronger response to higher fractional wetting values.

Although both the FIXC and INTC cases produce the same decrease in surface temperature, the mechanisms that cause it are different. This clearly shows the influence of clouds on all aspects of both the water and heat balance. They are coupled through the evaporation process, which affects the atmospheric moisture vapor content and subsequently radiation, in addition to the latent flux. With fixed cloud fractions, this coupling to radiation is effectively eliminated. All climatic responses to $\bar{\kappa}$ occur through hydrology and the associated latent heat flux. With interactive cloud fractions, radiation becomes the dominant response mechanism to $\bar{\kappa}$ variations, suppressing hydrologic responses. Due to this atmospheric moisture and cloud fraction coupling, a fundamentally hydrologic perturbation represented by fractional wetting variations affects not the hydrologic fluxes, but instead the radia-
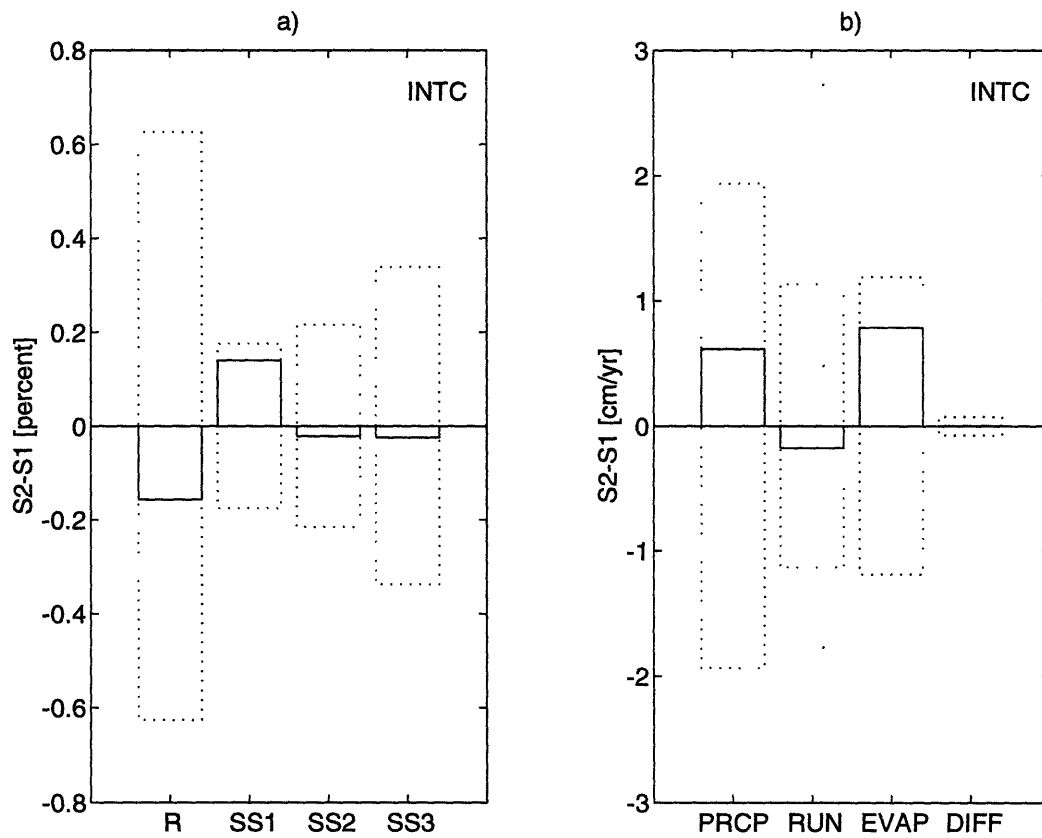
Figure 3-10: Difference (S2-S1) in annual mean hydrologic budget diagnostics for INTC simulations, with statistical equality criteria. a) runoff ratio and three soil layer saturation states. b) precipitation, surface runoff, evaporation and diffusion between first and second soil layer.
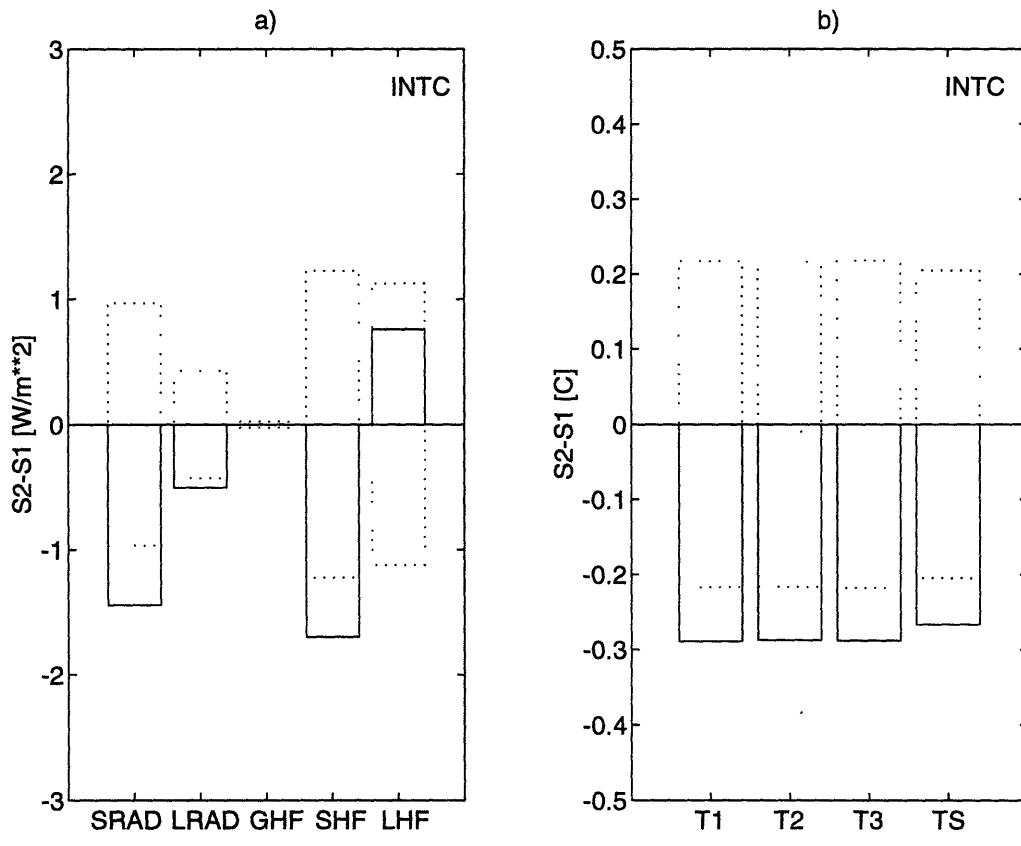
Figure 3-11: Difference (S2-S1) in annual mean heat budget diagnostics for INTC simulations, with statistical equality criteria. a) incoming solar radiation, net outgoing thermal radiation, ground heat flux, outgoing sensible heat flux and outgoing latent heat flux. b) three soil layer temperatures and surface air temperature.

tive fluxes. Therefore fixing cloud fractions serves to further isolate the hydrologic resp onse in the screening model, which is its primary purpose.

Annual Cycles of Model Diagnostics

Investigation of the annual means revealed the existence of negative feedbacks on R in the seasonally varying screening model simulations. They also revealed a greater response to $\bar{\kappa}$ increases above the mean as a consequence of land surface-atmosphere interactions between the heat and moisture budgets. The precise feedbacks and interactions that produce the observed response in annual mean climate can be ascertained by studying the annual cycles of the relevant diagnostic parameters. Only the FIXC case will be presented, in order to specify the land surface hydrologic response to fractional wetting.

The same statistical test can be applied to the difference in monthly mean values, since in a 50 year simulation there are 50 samples for each month. Figures 3-12-3-16 show the annual cycle of the difference between monthly means of runs S1 and S2, with their corresponding statistical criteria for equality. For example, the difference for January would be determined by calculating the mean value over all 50 January samples of run S1, and subtracting it from the mean over all 50 January samples of run S2.

Figure 3-12a shows that R varies in a smooth manner that corresponds very well with the monthly $\bar{\kappa}$ variations seen in Figure 2-5. As expected, positive $\bar{\kappa}$ perturbations decrease R, and negative perturbations increase R. The annual cycle in R is fairly sinusoidal, indicating that in this climate model R responds somewhat linearly to $\bar{\kappa}$, both above and below the mean of 0.8. This verifies the statistically equal annual means seen in Figure 3-8a. Once again, a negative feedback must exist since R is functionally expected to increase by much more in the summer than the amount it decreases in the winter.

The smooth, approximately sinusoidal annual cycle in R appears despite the fact that only four months pass the statistical significance test. Failure to exceed the statistical criteria generally indicates that the difference in mean between the two
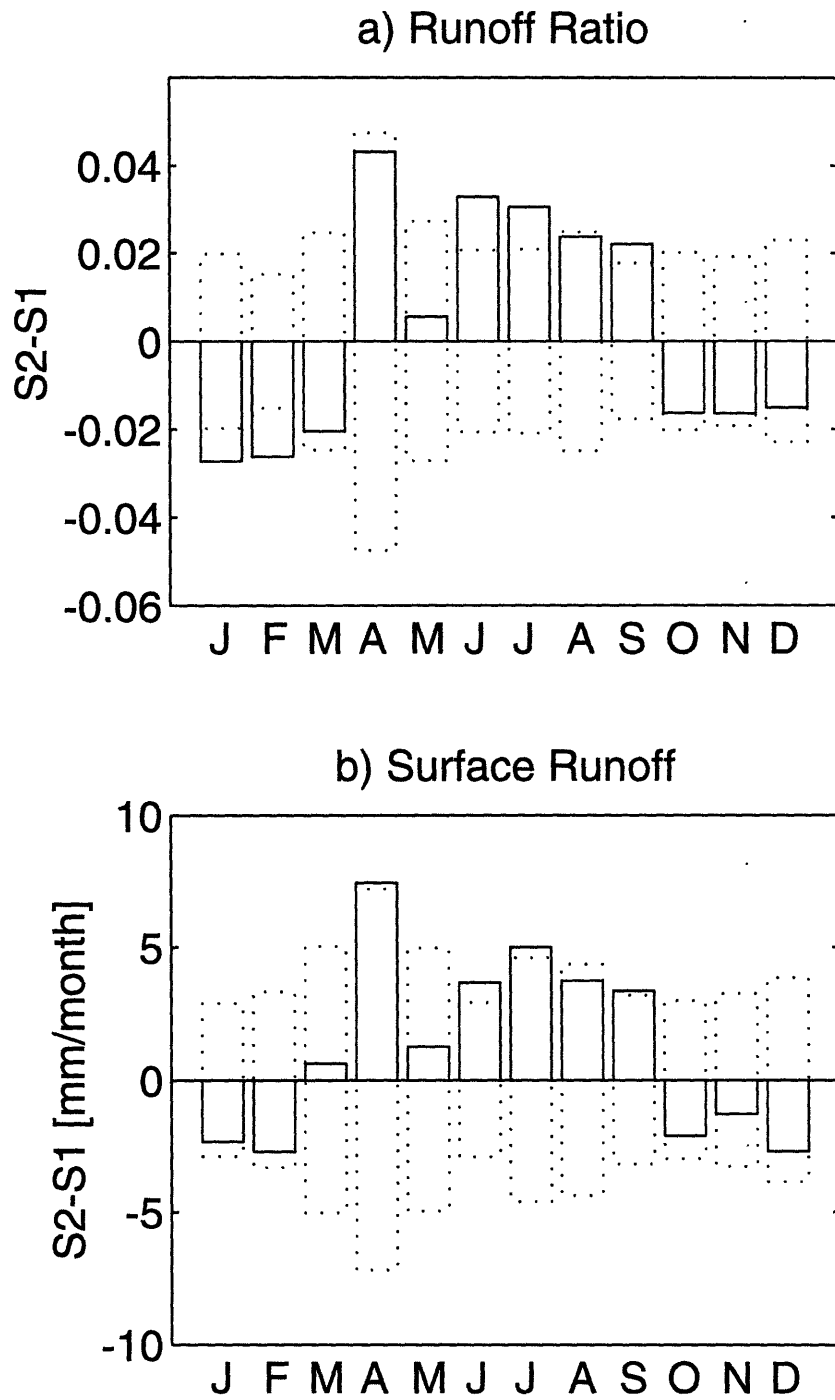
Figure 3-12: Monthly annual cycle of the difference (S2-S1) between seasonally varying FIXC simulations containing fixed (S1) and monthly varying (S2) fractional wetting values, with statistical equality criteria. a) runoff ratio. b) surface runoff.
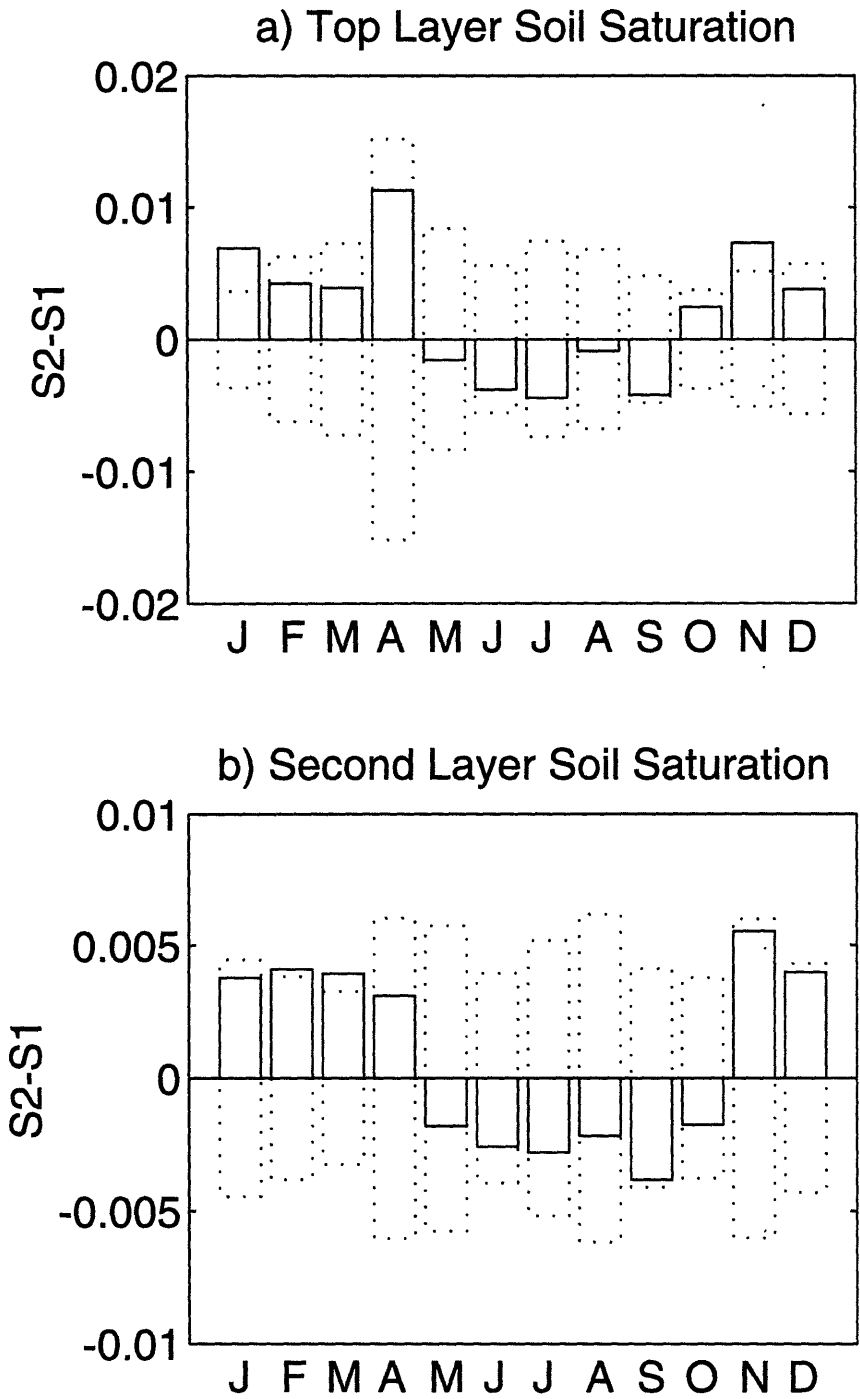
Figure 3-13: Monthly annual cycle of the difference (S2-S1) between seasonally varying FIXC simulations containing fixed (S1) and monthly varying (S2) fractional wetting values, with statistical equality criteria. a) top soil layer saturation. b) second soil layer saturation.
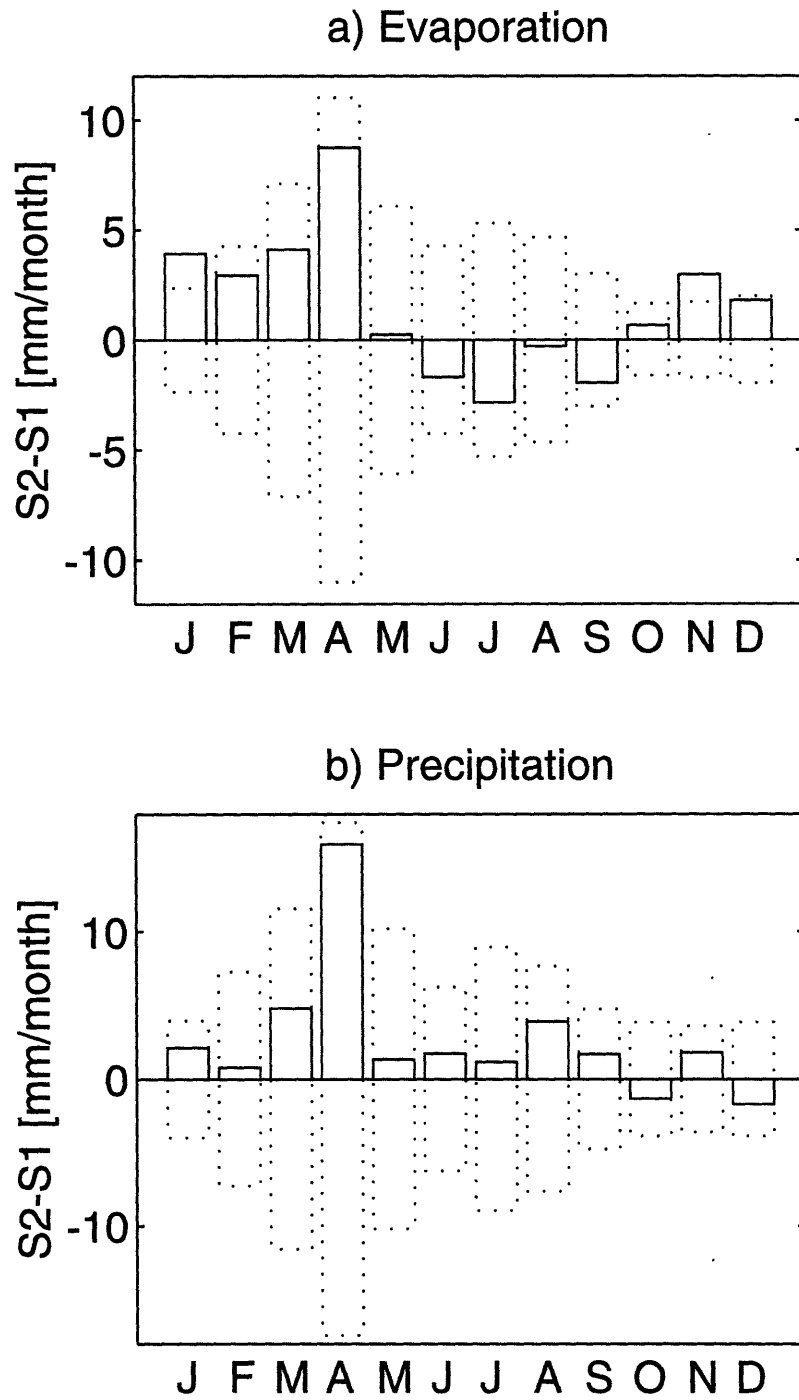
Figure 3-14: Monthly annual cycle of the difference (S2-S1) between seasonally varying FIXC simulations containing fixed (S1) and monthly varying (S2) fractional wetting values, with statistical equality criteria. a) evaporation. b) precipitation.
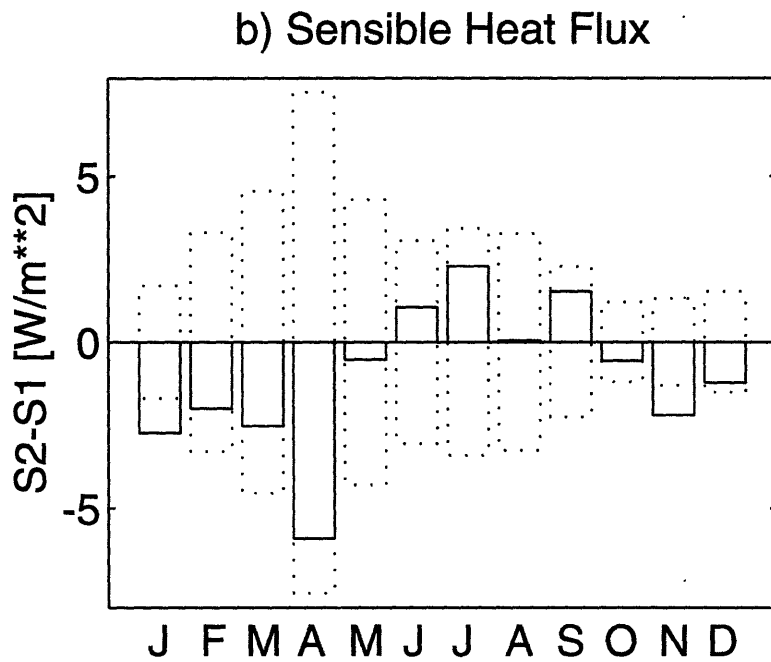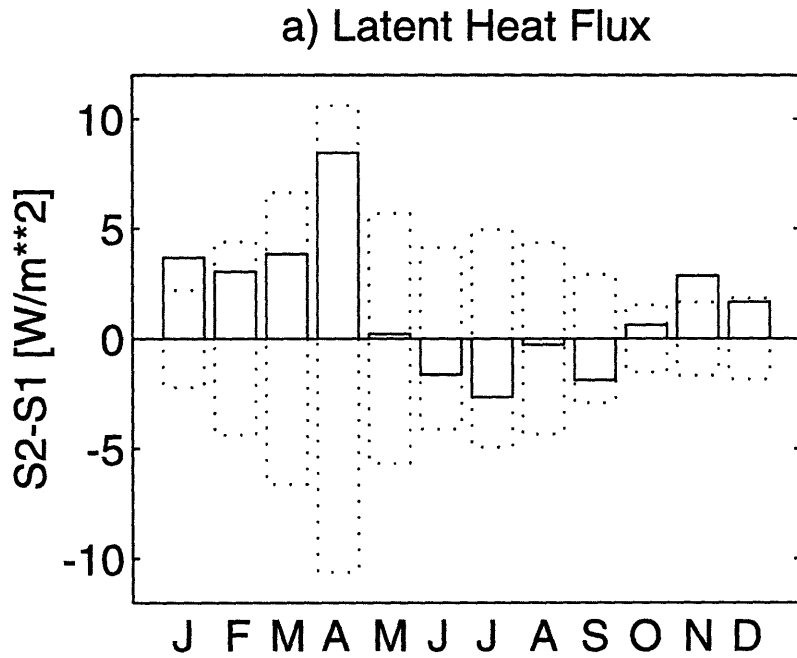
Figure 3-15: Monthly annual cycle of the difference (S2-S1) between seasonally varying FIXC simulations containing fixed (S1) and monthly varying (S2) fractional wetting values, with statistical equality criteria. a) latent heat flux. b) sensible heat flux.
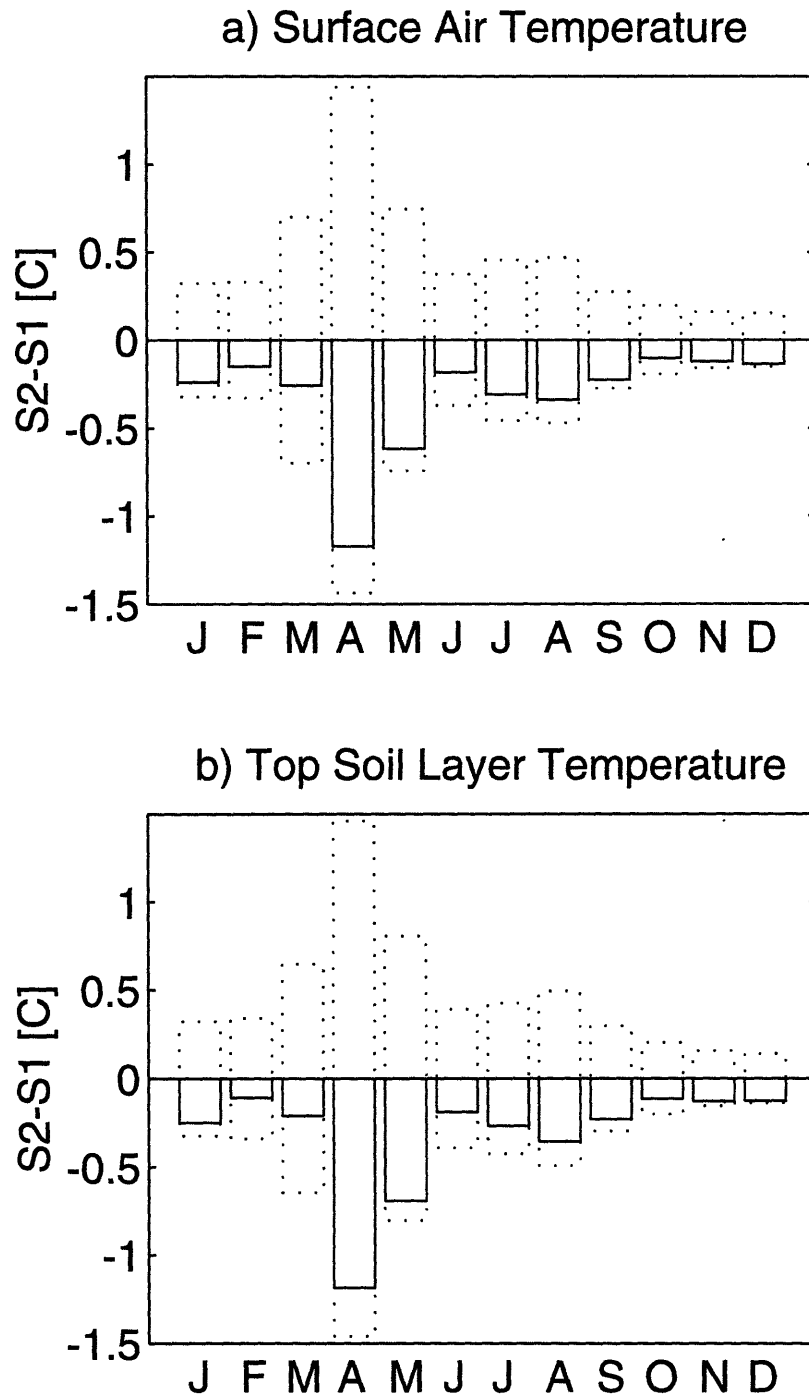
Figure 3-16: Monthly annual cycle of the difference (S2-S1) between seasonally varying FIXC simulations containing fixed (S1) and monthly varying (S2) fractional wetting values, with statistical equality criteria. a) surface air temperature. b) top soil layer temperature.

runs is indistinguishable from the variability contained in each run. If this were the case, then any difference in mean would be attributed to noise, and be equally likely to be positive or negative. In such a situation the clear annual cycle seen in R would not be present. Even though the statistical test for non-equal mean is generally not passed, the trend shown by the difference implies that they are significant. All diagnostics contain the same general amount of significance in their annual cycles. Surface runoff (Figure 3-12b) appears to coincide with runoff ratio, which is expected since R directly affects runoff and infiltration. There does seem to be a slight nonlinearity weighted towards summer months (low $\bar{\kappa}$). A possible explanation for this will be discussed later.

Soil saturation responds directly to infiltration, so it is not surprising that its annual cycle (Figure 3-13) also shows a clear pattern that coincides with R and $\bar{\kappa}$. The responsiveness of $E[s]$ to $\bar{\kappa}$ implies that soil moisture variations are considerable during periods of precipitation. Thus the negative feedback due to soil moisture exists, which causes the "linearization" of R vs. $\bar{\kappa}$.

As shown in Figure 3-14, evaporation also contains a readily apparent annual cycle that agrees with the seasonal response of previous parameters. Evaporation is directly related to soil saturation, so this is expected. Precipitation however, is seen to change very little in response to $\bar{\kappa}$ variations. The difference in monthly mean is far below the statistical criteria for all months, and no clear seastonal patern emerges. Although the land surface responds clearly to $\bar{\kappa}$ variations, its influence does not extend to the atmosphere and precipitation. Since the precipitation is essentially unaltered, the negative feedback due to precipitation intensity changes cannot exist, assuming that precipitation frequency is also unaltered. Therefore the only feedback on R in these seasonally varying simulations is caused by $E[s]$.

This conclusion disagrees with the perpetual-day simulations, in which the precipitation feedback did exist for $\bar{\kappa}$ values below about 0.1. The response to this strong feedback was an elimination of the response by R to $\bar{\kappa}$. If this feedback existed in seasonally varying runs, Figure 3-12a would show no difference in R for the summer months, where $\bar{\kappa}$ is below 0.1. The perpetual-day simulations indicated

90

that the principal effect of the weaker soil moisture feedback was to linearize R vs. $\bar{\kappa}$. Since this is the only existing feedback in the seasonally varying simulations, R is seen to respond directly and evenly to $\bar{\kappa}$.

Although a clear and expected annual cycle is seen for surface soil saturation in response to fractional wetting, the top soil layer appears to respond more to increases in $\bar{\kappa}$ than decreases. The only two months that exceed the statistical criteria occur in the winter, when $\bar{\kappa}$ increases. This effect is not as apparent in the second soil layer, but it is very apparent in the evaporation cycle. This subtle bias towards fractional wetting increases could easily be attributed to noise, except that this characteristic appears and coincides with the annual cycles for the heat budget. Figure 3-15 shown the anuual cycles for latent and sensible heat flux differences. Figure 3-16 presents annual cycles for surface air and top soil layer temperature differences. Latent heat flux coincides exactly with evaporation. Sensible heat flux directly opposes latent heat flux, with the same relative magnitude. If these differences were due simply to statistical noise, these surface fluxes representing both the water and heat budget would not respond to each other to the extent observed.

The ultimate effect of these surface fluxes is a reduction in surface temperatures in all months, reflecting a greater response to increases in fractional wetting. The small and brief decreases in evaporation and latent heat flux seen in the summer are insufficient to cause temperatures to increase, despite the large decrease in $\bar{\kappa}$. Note that although none of the monthly temperatures meet the statistical criteria for non-equal mean, all months do show a decrease. Pure noise would consist of equal and random increases and decreases. Also, the aggregate affect of these statisitically small monthly decreases is a decrease in the annual mean temperature that is statistically significant (Figure 3-9b).

Finally, the precipitation cycle also indicates an increase for virtually every month, despite the very small magnitudes. These tiny monthly increases lead to an annual mean difference that is much closer to the statistical criteria. Thus a slight increase in precipitation over all months representing a greater response to increases in $\bar{\kappa}$ does result, even though it is difficult to see statistically. This slightly wetter

climate serves to increase the total amount of runoff generated, even though the precipitation increase is not large enough to feed back on the runoff ratio. This explains why runoff (Figure 3-12b) appears to respond more to decreases in $\bar{\kappa}$. In truth, surface runoff is simply increased by a slight amount every month due to the wetter climate.

The increased responsiveness to $\bar{\kappa}$ increases over decreases begins to appear with first layer soil saturation. R and runoff, the primary parameters affected by $\bar{\kappa}$, respond equally to positive and negative perturbations. Thus the climatic bias towards increased fractional wetting is produced by the land surface response to changes in R, the partitioning of the precipitation forcing into runoff and infiltration.

A number of factors can be identified which produce this uneven land surface response, due to the physically realistic and nonlinear nature in which the acnd surface is parameterized. First, the soil column is modeled as a three layer system with vertical diffusion. Therefore the first soil layer is influenced not just by infiltration and evaporation from above, but also diffusion from below. Decreasing $\bar{\kappa}$ to extremely low summertime values serves to substantially decrease the top layer soil moisture. Lower soil layers will react to this by diffusing water up to the top layer. This reduces the extent to which soil saturation decreases, and mitigates the effect of decreasing $\bar{\kappa}$. This mitigating effect will be aost prevelant during extreme low top layer soil moisture conditions.

Also, another facet of the *Entekhabi & Eagleson* [1989] statistical-dynamical land surface hydrology parameterization is a complex and nonlinear response by evaporation to soil saturation. Generally, the soil-controlled evaporative demand decreases as the soil becomes drier, reflecting vegetative thresholds and wilting points, and physical exfiltration capacities. As a result wetter soils caused by $\bar{\kappa}$ increases will evaporate proportionally more than drier soils caused by $\bar{\kappa}$ decreases. Increases in fractional wetting therefore generate a greater evaporative response than decreases. The nonlinear physical response of the land surface exfiltration capacity to soil moisture is the mechanism that causes monthly variations in fractional wetting about the same annual mean to ultimately affect the annual mean climate. Thus we

92

see that the thermal and moisture inertia of the land surface at extreme dry conditions reduces the sensitivity to shifts in parameters such as $\bar{\kappa}$.

3.4 Discussion

This chapter began with an off-line sensitivity analysis on the runoff ratio parameterization in the *Entekhabi & Eagleson* [1989] hydrology scheme. R was found to be very sensitive to fractional wetting changes in the expected range of relevant parameters. The sensitivity increased as $\bar{\kappa}$ became smaller. This indicated that the variations in $\bar{\kappa}$ determined in Chapter 2 are expected to affect R and subsequently the land surface and climate. In addition, R was also found to be sensitive to mean soil saturation, and very sensitive to precipitation intensity. In a climate situation, changes in these other parameters may result from the initial $\bar{\kappa}$ perturbation, which could magnify, suppress or reverse the overall response by R.

A simple one-dimensional climate model developed for hydrologng screening was then used to investigate the true climatic impact of fractional wetting. A series of perpetual-day simulations identified two negative feedbacks which acted to inhibit the nonlinear functional response of R to $\bar{\kappa}$. One feedback was caused by soil saturation changes, and the other by precipitation changes. These feedbacks greatly altered the R-$\bar{\kappa}$ relationship expected from the off-line analysis.

Using more realistic seasonally varying simulations, the effect of monthly variations in $\bar{\kappa}$ about the same mean was investigated. In these simulations, the soil saturation feedback was seen to apply, but not the precipitation feedback. The result is a "linearization" of the response by R to $\bar{\kappa}$; R responded equally to positive and negative perturbations in fractional wetting, whereas functionaslly R responded much more to negative perturbations.

Although the primary response of R favored neither increases or decreases in $\bar{\kappa}$, subsequent interaction with the land surface served to inhibit the response to decreases in $\bar{\kappa}$. Consequently, the land surface and its outgoing moisture and heat fluxes respond more to increases in $\bar{\kappa}$ than decreases. As a result, the effect on

surface temperature and precipitation, two parameters not directly associated with fractional wetting, corresponds to an overall increase in $\bar{\kappa}$ over all months. The introduction of seasonal variability in fractional wetting has a complex bit discernible and clear effect on the simulated climate produced by the one-dimensional hydrologic screening climate model.

The major difference between the perpetual-day and seasonally mvarying siulations is the absence of the precipitation feedback in the seasonally varying runs. This can be explained by the time scales for equilibrium associated with the different simulation types as mentioned in the beginning of Section 3.3.3. The perpetual-day simulations ran for 600 days under fixed fractional wetting and solar forcing conditions. This allowed sufficient time for all interactions and feedbacks to equilibrate, including precipitation. Precipitation is expected to require a substantial amount of time to equilibrate, since it does not respond directly to $\bar{\kappa}$, but rather implicitly through moisture fluxes away from the surface. Furthermore, atmospheric residence times and moisture storage, and horizontal and vertical moisture fluxes can also vary and need to equilibrate to the evaporative input.

With seasonally-varying simulations, $\bar{\kappa}$ changes monthly and solar forcing changes every few days. The dominance of radiative processes over moisture fluxes was clearly demonstrated when analyzing the annual mean diagnostics during the interactive cloud cover case. This constantly changing environment prevents precipitation changes from reaching any sort of equilibrium in response to $\bar{\kappa}$ induced changes in R, especially considering the multitude of interactions necessary for fractional wetting changes to affect precipitation. The soil moisture feedback can take effect, since soil moisture will respond almost immediately to changes in the runoff ratio, especially in the top so

Chapter 4

Climate Simulations Using the GISS Atmospheric GCM

4.1 Overview of Experiments

4.1.1 GCMs vs. the Screening Model

The experiments performed using the simplified one-dimensional climate model for hydrologic screening successfully identified the response by the land surface and climate to realistic seasonal variations in the fractional wetting parameter. Although the magnitude of these changes was small, they revealed definite behavioral patterns attributable to feedback mechanisms and nonlinear relationships at the land surface-atmosphere interface. These results justify further investigation of the effects of fractional wetting variations using a full three-dimensional atmospheric GCM.

There are a number of benefits to using a GCM for fractional wetting investigations, and also some potential difficulties. Since the $\bar{\kappa}$ values over the contiguous United States estimated in Chapter 2 correspond to rectangular grid areas for the GISS $4°x5°$ GCM, the simulations can reflect these actual values. The screening model does not represent specific land surface areas, so a reasonable set of $\bar{\kappa}$ values had to be assumed instead. Also, the screening model investigations were limited to seasonal $\bar{\kappa}$ variations. The lateral component of GCMs does not exist in the screening model, which is one dimensional in the vertical direction. Therefore to study the effects of spatial variability in fractional wetting, a full GCM must be

used. Finally, GCM simulation results can be validated against observed data sets to assess the degree to which improved land surface hydrology parameterizations, and in particular realistic fractional wetting variations, improve GCM simulations compared to these observations.

The potential difficulties surrounding the use of GCMs primarily involves their complexity. GCMs attempt to simulate all of them numerous processes and interactions involved in the global climate. Such an ambitious model unavoidably contains a substantial amount of inherent climatic variability in excess of that contained in the screening model, which was constructed to focus on hydrologic processes only. The increased model variability may cloud the changes induced by $\bar{\kappa}$ variatons, and make their precise effect more difficult to identify. This is particularly true in light of the relatively small magnitude of the changes expected due to fractional wetting. A further complicating factor is that numerically solving the equations governing atmospheric fluid flow over the entire global atmosphere makes a GCM much more computationally intensive then the screening model. Consequently, the GCM simulations performed here must be of much shorter duration than the screening model. Shorter simulations make the resulting climate diagnostics less precise, and statistical checks between different simulations virtually impossible.

4.1.2 Model Specifications and Simulations

The GCM simulations performed here utilize an improved version of the GISS GCM Model-II [Hansen, et al., 1983]. The basic model uses a rectangular grid with nine vertical layers and a horizontal resolution of four degrees latitude by five degrees longitude, and prescribes seasonally-fixed sea surface temperatures. The simple, linear land surface hydrology parameterizations for runoff ratio and evapotranspiration efficiency are replaced by the statistical-dynamical scheme of Entekhabi & Eagleson [1989]. Three soil layers are modeled in the land surface component, and a multiple soil layer moisture diffusion scheme developed by Abramopoulos et al. [1988] has been included. Transpiration occurs from all three soil layers by assigning root fractions of .85, .10 and .05, starting from the top layer. Groundwater runoff is in-

96

corporated as described in the screening model of Chapter 3. Average topographical slopes were obtained for each land surface grid by averaging the .5°x.5° topography data set used as a land surface boundary by the GISS GCM.

Analogous to the screening model simulations S1 and S2, two GCM simulations are conducted. The first run, designated SIM1, assigns a fixed value of $\bar{\kappa} = .08$ over all grids and months, and for both moist-convective and supersaturation precipitation mechanisms. $\bar{\kappa} = .08$ was selected since it is essentially the average of all values obtained over the U.S. in Chapter 2. Thus this simulation maintains the standard practice of prescribing a uniform fractional wetting value, but uses a realistic value that is obtained from precipitation observations. Even though this value only represents the contiguous U.S., applying it over all grids still represents an improvement over using an arbitrarily selected value. SIM1 was run for six years, with a two year spinup followed by a four year collection period.

The second run, SIM2, uses the actual $\bar{\kappa}$ values estimated over 39 U.S. grids and twelve months in Chapter 2. All other grids retain the fixed value of .08. This simulation therefore introduces over the U.S. seasonal and regional variations in $\bar{\kappa}$ about the mean value represented in SIM1. Since the only modification from SIM1 involves the $\bar{\kappa}$ variations, SIM2 had only a one year spinup before its four year collection period.

A third simulation is also discussed in this chapter. Designated SIMG, it represents a five year run of the original GISS 4°x5° GCM Model-II which was performed previously by GISS, with monthly diagnostics of basic parameters archived on tape. For consistency with SIM1 and SIM2, the last four years of the archived simulation was used as the collection period. By comparison with SIMG, the effect of introducing the *Entekhabi & Eagleson* [1989] scheme at .5°x.5° resolution in SIM1 and SIM2 can also by studied, along with specific fractional wetting effects.

Diagnostics for SIM1 and SIM2 were also collected on a monthly basis. Since SIM2 only introduces fractional wetting variations over the contiguous U.S., the analysis will focus specifically on this region. The influence of improved land surface hydrology parameterization and broad fractional wetting changes on a global

97

scale has already been demonstrated by *Johnson et al.*, [1993] at 8°x10° resolution. Therefore the goals here are to use a finer horizontal resolution, introduce realistic variability in $\bar{\kappa}$, and validate the simulated climate at finer scales that are useful to global and regional hydrology.

4.2 Influence of Fractional Wetting Variations over the Contiguous United States

4.2.1 Seasonal $\bar{\kappa}$ Variations

We begin by studying the precise impact of realistic fractional wetting variations over the contiguous U.S. The effect of seasonal $\bar{\kappa}$ variations can be investigated in the same manner as with the screening model in Chapter 3. Figure 4-1 shows the monthly annual cycle of $\bar{\kappa}$ values for SIM2 obtained by averaging over all 39 U.S. grid areas. The annual average of all values estimated in Chapter 2 is 0.082. The contiguous U.S. as a whole experiences a clear annual $\bar{\kappa}$ cycle which peaks in the winter and ebbs in the summer, much like what was simulated in the screening model. However, the annual range of $\bar{\kappa}$ values seen here, roughly .05, is noticeably smaller than the range of .12 used in the screening model. Not only are the GCM perturbations less extreme, but they also do not exhibit the same pure sinusoidal pattern. It will be interesting to see to what degree these GCM simulations agree with the screening model simulations.

Simulation Results

The difference in the annual cycles (SIM2-SIM1) is presented for a number of relevant diagnostic parameters in Figures 4-2-4-5. The GCM simulations are each only four years in length, which is insufficient to establish reliable sample standard deviations and determine statistical equality criteria. Therefore, percent differences have been graphed instead for many of these parameters, calculated as 100*(SIM2-
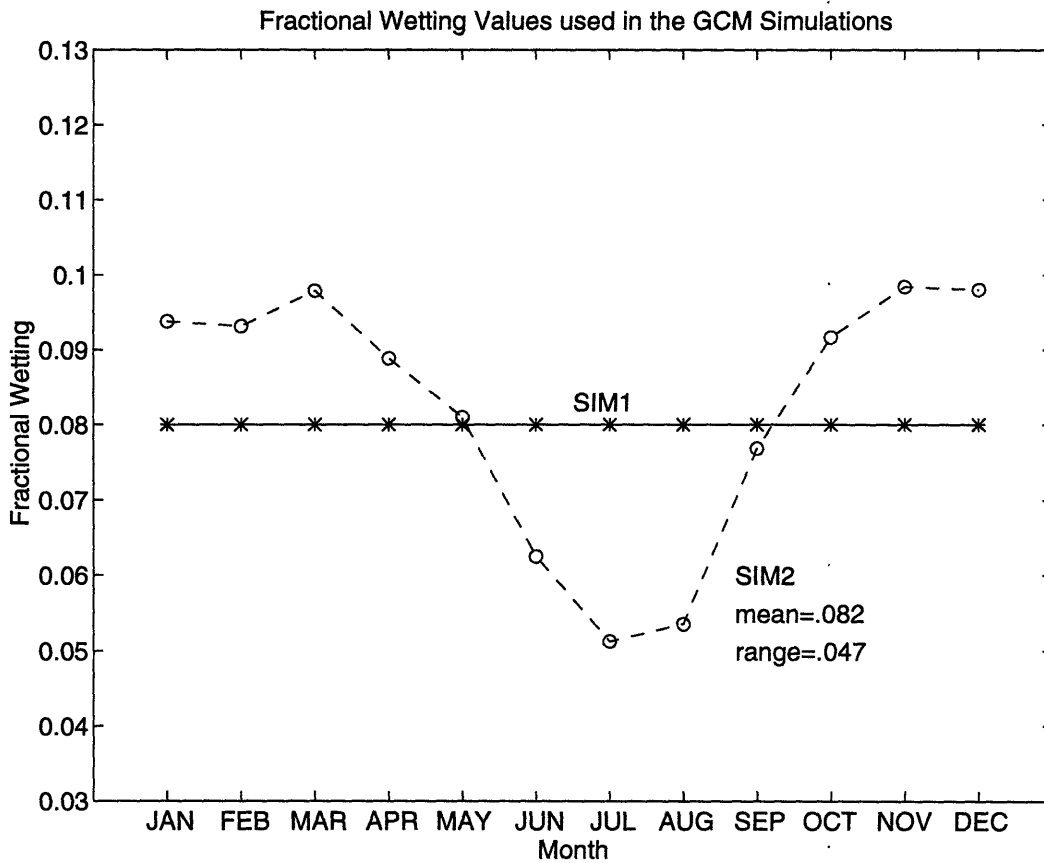
Figure 4-1: Monthly variations in fractional wetting for runs SIM1 and SIM2, averaged over all 39 U.S. grid areas.

a) Runoff Ratio
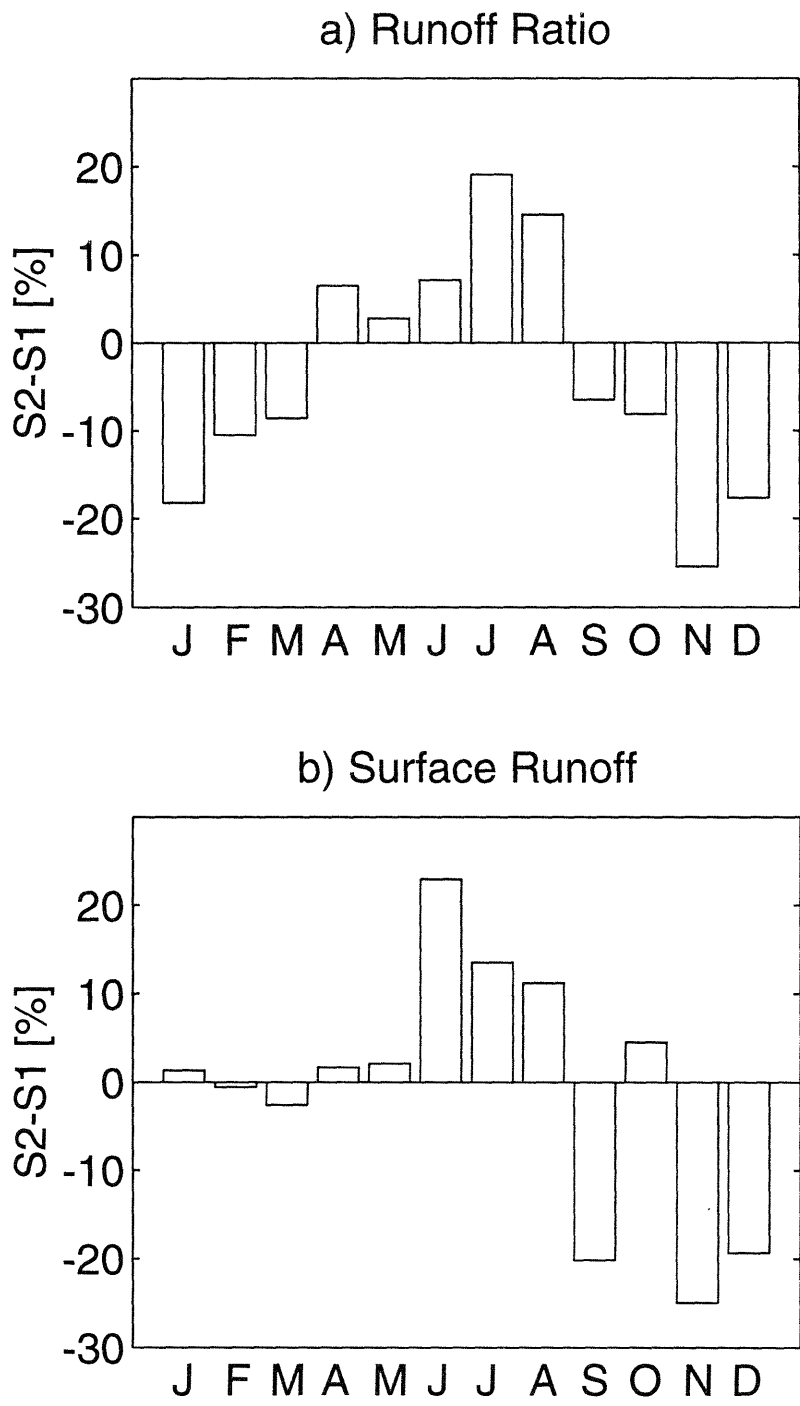
b) Surface Runoff

Figure 4-2: Monthly annual cycle (U.S. average) of the percent difference between GCM runs SIM1 and SIM2 for a) runoff ratio and b) surface runoff.
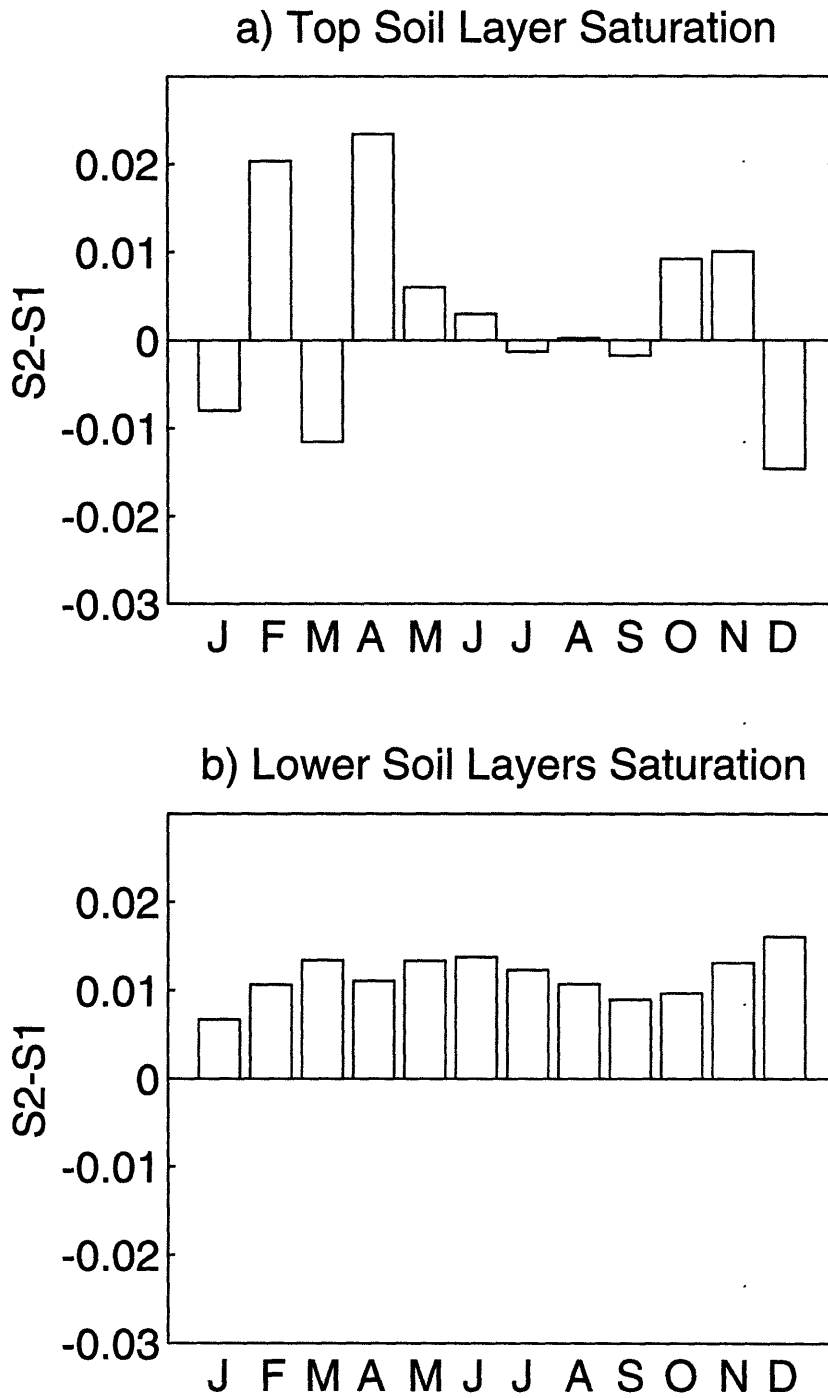
Figure 4-3: Monthly annual cycle (U.S. average) of the difference between GCM runs SIM1 and SIM2 for a) top soil layer saturation and b) combined lower soil layers saturation.
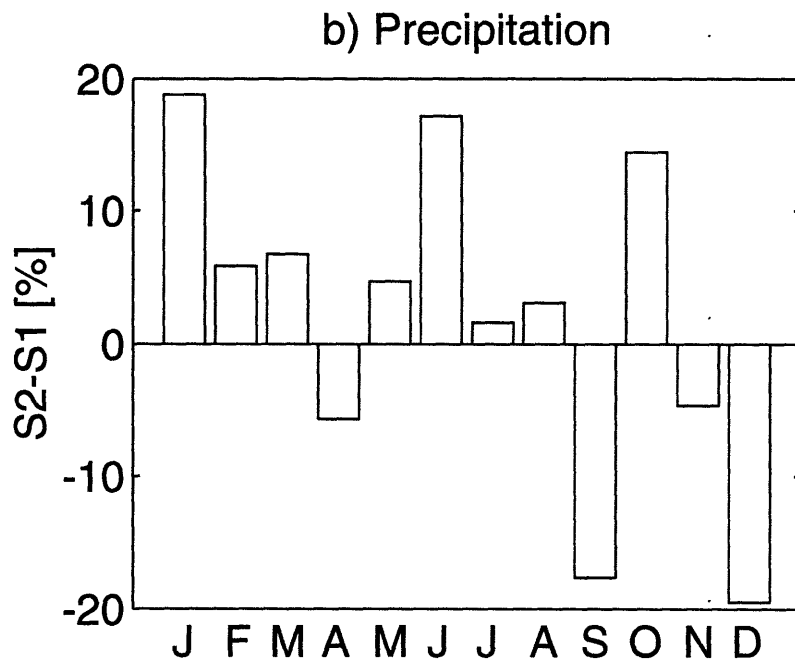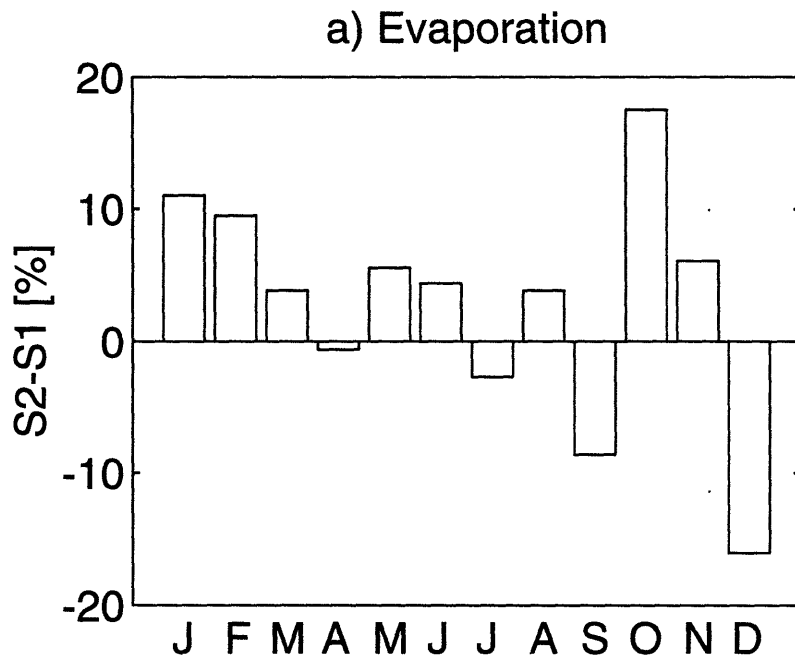
Figure 4-4: Monthly annual cycle (U.S. average) of the percent difference between GCM runs SIM1 and SIM2 for a) land surface evaporation and b) precipitation.

a) Surface Air Temperature

b) Lower Soil Layers Temperature
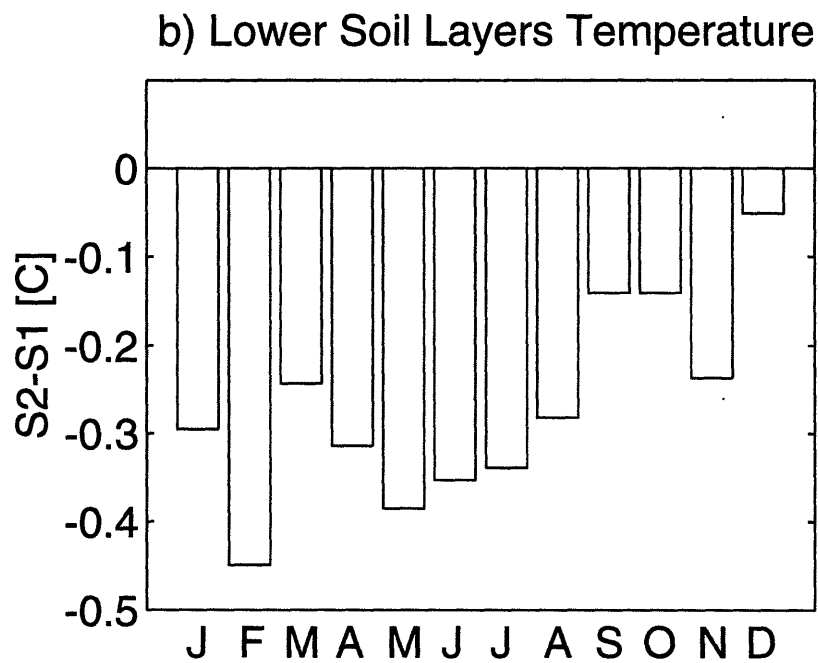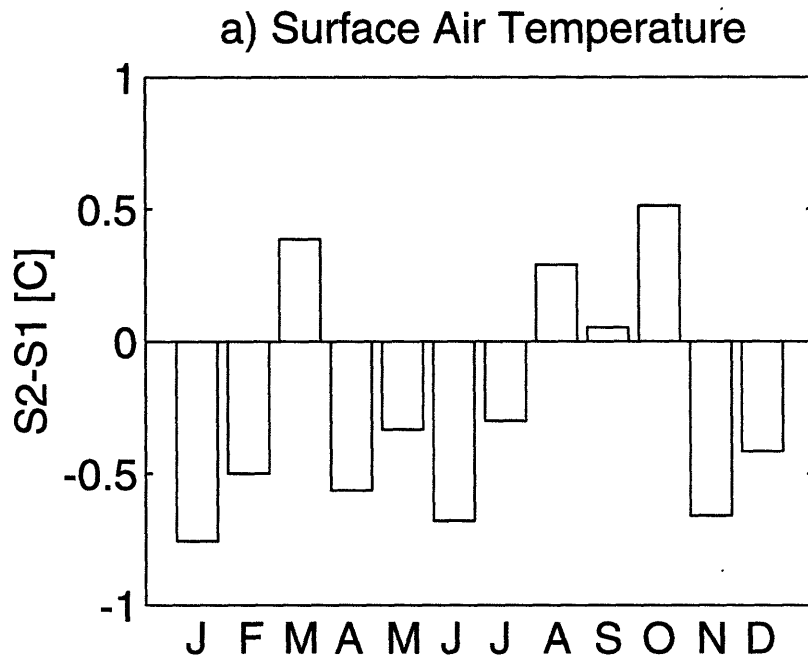
Figure 4-5: Monthly annual cycle (U.S. average) of the difference between GCM runs SIM1 and SIM2 for a) surface air temperature and b) combined lower soil layers temperature.

103

SIM1)/SIM1. This statistic provides some measure at least of the magnitude of the $\bar{\kappa}$ induced changes.

Figure 4-2a shows a strong and direct response by runoff ratio to seasonal fractional wetting variations, much like the screening model. Many months show substantial changes in R, and they correspond with the largest perturbations in $\bar{\kappa}$. For the purposes of this analysis, 15% has been arbitrarily selected as a threshold criteria for significant parameter change. Even in the complex GCM environment, realistically estimated seasonal $\bar{\kappa}$ variations have a clear impact on the partitioning of rainfall into surface runoff and infiltration. This is apparent despite the limited duration of the GCM simulations and the smaller annual range in fractional wetting values.

The actual surface runoff changes are shown in Figure 4-2b. Between the months of June and December, runoff variations respond directly and in many cases significantly to $\bar{\kappa}$ and R, which is in agreement with the screening model simulations. However, between January and May there is a negligible change in surface runoff. This feature is attributable to the fact that snowfall is modeled in the GCM. A substantial portion of the precipitation generated over the U.S. in the winter is snow, which often remains on the surface and accumulates. Therefore it is not subject to partitioning via R, and consequently is not influenced by changes in $\bar{\kappa}$. When this accumulated snow eventually melts, it has been modeled to entirely infiltrate into the soil column until saturation occurs; again R and $\bar{\kappa}$ do not play a role. In the screening model, a latitude of 15° North was used, so that snowfall and snowmelt were nonexistent. The presence and effect of snowfall clearly plays an important role in GCM land surface hydrology.

Soil saturation differences are depicted in Figure 4-3. Figure 4-3a shows the top soil layer, and Figure 4-3b represents the two lower layers combined together. Actual differences are shown for these parameters, since the very low soil saturation values modeled in the summer months cause percent differences to be misleading. Seasonal $\bar{\kappa}$ variations appear to have virtually no effect on the top soil layer in the GCM simulations, whereas a small but definite response was seen in the screening

model. The soil moisture reservoir represented by the lower layers, however, shows a consistently wetter state over all months. Wetter soils are another theoretically expected response to a general increase in fractional wetting. Thus the GCM simulations also appear to be more responsive to increases in $\bar{\kappa}$, which agrees with the results of the screening model.

Evaporation and precipitation are presented in Figure 4-4, in percent difference form. Neither of these hydrologic fluxes exhibit a disiernable pattern in response to the $\bar{\kappa}$ perturbations. Some months exhibit fairly large differences in precipitation, but the noise is very apparent. The slight changes in land surface evaporation are not surprising, since evaporation comes mainly from the top soil layer. However, most months show an increase evaporation, and the largest monthly differences are also increases. Like the lower soil layers, this too may reflect a land surface response that corresponds to an overall increase in fractional wetting. The same cannot be said for precipitation, since fairly large increases and decreases are seen in different months.

Finally, surface air temperature and combined layer two and three soil temperature are presented in Figure 4-5. The top soil layer temperature (not shown) behaves virtually identical to the surface air temperature. Actual differences are used for temperatures due to the small magnitude of the changes expected for temperature. A noticeable decrease in surface air temperature is seen for most months. Months with increases do not appear to represent a disiernable annual pattern or cycle, and are probably attributable to noise. The lower layers show a small but definite decrease in temperature over all months. Although these temperature decreases are small, changes of this magnitude are known to have substantial impacts on overall climate. Also, the clear temperature decrease produced by the screening model is of roughly the same magnitude as seen in these GCM simulations. Once again, this cooler climate implies that seasonal $\bar{\kappa}$ increases dominate over the decreases.

Discussion

The contiguous U.S. modeled by the GISS GCM exhibits a noticeable hydrologic and climatic response to seasonal variations in fractional wetting. This response agrees with that produced by the screening model in many respects, but also contains some differences. The similarities include an immediate and somewhat linear response by the runoff ratio to $\bar{\kappa}$ in both simulations. This indicates the importance of the fractional wetting parameter in the land surface hydrology parameterization of *Entekhabi & Eagleson* [1989]. Both simulation environments also indicate an ultimate climatic response that corresponds to an increase in fractional wetting. In the GCM simulations, this is evidenced primarily by wetter soil saturation in the lower layers, and lower temperatures, over most or all months. In the screening model, lower temperatures and increased precipitation were the major features.

Dissimilarities between the screening model and GCM mainly involve the hydrologic fluxes that lead to the overall cooler and wetter states. In SIM1 and SIM2, the only parameter that exhibits a clear annual cycle that corresponds to the fractional wetting cycle is R. Surface soil saturation and evaporation have no discernible pattern, although these diagnostics have clear cycles in the screening model. GCM runoff differences represent an unusual case, since a pattern is apparent only in the absence of snowfall and snowmelt.

These dissimilarities can be attributed to the characteristics that differentiate the two simulation environments. One initial concern surrounding the GCM simulations is that the effects due to fractional wetting variations would be very difficult to distinguish, due to the increased complexity and inherent variability associated with GCMs. This concern is compounded by the limited duration simulations necessitated by computational constraints, and the fact that the actual annual cycle in $\bar{\kappa}$ over the contiguous U.S. covers a smaller range than that used in the screening model.

The ambiguity in parameters like evaporation (Figure 4-4a), precipitation (Figure 4-4b), top soil layer saturation (Figure 4-3a), and top soil layer temperature (Figure 4-5a) can certainly be attributed to this factor. The large differences seen in a number of individual months may be due simply to noise, which would only

106

be eliminated with simulations of substantially longer duration. Longer runs would produce more reliable mean values, which could then possibly detect cyclical difference patterns in response to the small observed seasonal $\bar{\kappa}$ variations over the U.S.

However, these noisy hydrologic fluxes do not prevent the subsequent climatic states from responding clearly and in agreement with the screening model. One conclusion drawn from the screening model simulations was that the land surface response to extreme small $\bar{\kappa}$ values gets muted, causing the climate to alter towards an overall increase in $\bar{\kappa}$. Run S2 contained a sinusoidal monthly pattern in $\bar{\kappa}$, with an equal number of months above and below the mean of $\bar{\kappa} = .08$. In the GCM runs, SIM2 does not contain a sinusoidal pattern. Most months have a $\bar{\kappa}$ value above .08, and only three months have values substantially below this mean. Chapter 3 also concluded that a number of climate diagnostics require time to equilibrate to a changed value, especially parameters not directly associated with fractional wetting. Thus the limited months with already less influential small $\bar{\kappa}$ values may inhibit remote GCM parameters such as temperature and lower soil layer saturation from recognizing the decreases in $\bar{\kappa}$ at all. As a result, increases in fractional wetting dominate even more strongly in the GCM simulations, which serves to counteract the reduction in mean parameter precision and produce the same ultimate result as the screening model.

A second possible explanation for the discrepancy between hydrologic flux differences in the screening model and GCM simulations involves the role of snowfall and snowmelt. As mentioned before, snow plays an important role in the climatology of the contiguous U.S., whereas it is nonexistent in the screening model. This factor was already used to explain the resulting annual cycle in runoff differences seen in Figure 4-2b. Of course, the presence of snow on the land surface will also affect parameters such as soil moisture and evaporation, since surface snow cover provides an additional reservoir for land surface evaporation, and is assumed to completely infiltrate when it melts. This factor can certainly act to disrupt the annual cycle in these parameters anticipated by the screening model.

The exact effects of snow on land surface hydrologic response are difficult to characterize, in light of the noise and other ambiguities mentioned earlier. Also, the U.S. as a whole contains many regions with different characteristics of snowfall frequency and snow cover duration. Yet another complicating factor involves the intricate but poorly understood and crudely modeled interaction between snowfall and the land surface. Although the presence of snow appears to completely negate the influence of seasonal fractional wetting variations on surface runoff, this is not true for other parameters, due to the aforementioned factors.

In summary, there are some substantial differences between the screening model and GCM simulations. These differences cover a variety of physical phenomena and computational constraints. Some of the differences obscure the effects of seasonal fractional wetting variations, while others may enhance them. Overall though, both sets of simulations show that seasonal $\bar{\kappa}$ variations produce a wetter and cooler climate.

4.2.2 Regional $\bar{\kappa}$ Variations

A major benefit of fractional wetting investigations using a full GCM is the ability to assess the impact of regional variations over different grid areas. The screening model consisted of one large representative land surface grid area, so spatial $\bar{\kappa}$ changes were not possible. Figure 4-6 maps the annual average of individual grid $\bar{\kappa}$ values estimated in Chapter 2 and implemented in run SIM2. To facilitate the analysis, bold lines have been included to distinguish regions in which $\bar{\kappa}$ increases and decreases compared to the value of .08 used in SIM1. This will also be done for all parameter difference maps presented later in this section. For many parameters, percent differences will again be calculated.

Figure 4-6 indicates a decrease in $\bar{\kappa}$ from the arbitrary value of .08 along much of the midsection of the U.S., extending from the Rocky Mountains all the way to the eastern coastline. The dominant increases in $\bar{\kappa}$ occur in the northern plains and west coast, and also the deep south. Very few grid areas exhibit extreme high

SIM2: FRACTIONAL WETTING [%]
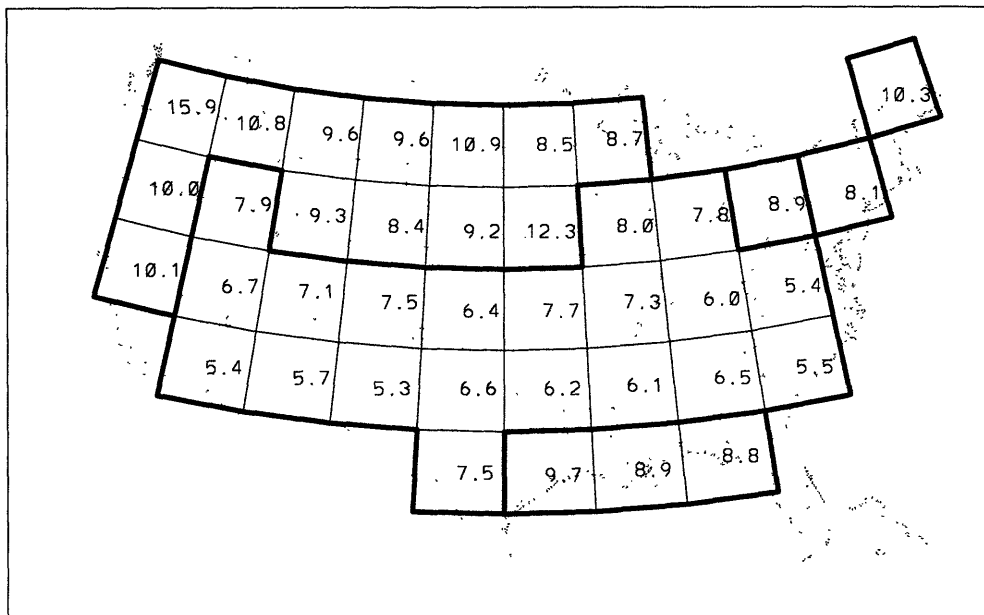
Figure 4-6: GCM grid area map over the contiguous United States showing annual averages of estimated fractional wetting values implemented in run SIM2. Bold lines indicate regions with $\bar{\kappa}$ above or below the SIM1 value of .08.

or low $\bar{\kappa}$ perturbations; however the spatial range over the U.S. is 10.6, which is substantially higher than the annual range seen in the previous section for the U.S. as a whole. Also, there are a roughly equal number of grids above and below 0.08.

The investigation of seasonal fractional wetting variations revealed a direct and somewhat linear response by the runoff ratio to monthly changes in $\bar{\kappa}$, which subsequently affected the land surface response and overall climate. It will be interesting to see if the regional $\bar{\kappa}$ variations depicted in Figure 4-6 have a similarly direct effect on R and other diagnostics. In the same manner as for annual cycles in the previous section, Figures 4-7-4-10 show individual grid area maps of the differences between annual average values of SIM1 and SIM2 for relevant parameters.

Figure 4-7 shows the percent differences for R and surface runoff. Comparison of Figure 4-6 and Figure 4-7a clearly shows that a direct and linear relationship between R and $\bar{\kappa}$ does not exist in these spatial variations. In fact, R and $\bar{\kappa}$ do not appear to be related at all. As exemplified in the seasonal $\bar{\kappa}$ investigations, decreases/increases in $\bar{\kappa}$ should produce increases/decreases in R. If this were true for the spatial variations, the bold lines in Figures 4-6 and 4-7a should at least depict the same pattern; they clearly do not.

This absence of a direct relationship between R and $\bar{\kappa}$ is not entirely unexpected. Each grid is subjected to its own annual cycle in $\bar{\kappa}$, which varies from grid to grid. Seasonal $\bar{\kappa}$ has already been shown to be highly and nonlinearly influential. Also, while the hydrologic processes in each grid occur in only the vertical direction, lateral exchange and transport of moisture does occur in each atmospheric layer. Such teleconnections may allow $\bar{\kappa}$ induced changes in a grid to subsequently affect other grids downwind. These exchanges follow prevailing atmospheric motion, and can traverse the U.S. in a matter of days. This spatial interaction between grids is completely internal and irrelevant when considering the U.S. in entirety, as was done in the seasonal investigations.

The lack of a direct R-$\bar{\kappa}$ relationship however does not imply that regional $\bar{\kappa}$ variations have no impact. Figure 4-7a contains three general regional groupings. A decrease in R is observed for much of the eastern U.S., and also the northwest

110

a) SIM2-SIM1: RUNOFF RATIO [%]

b) SIM2-SIM1: SURFACE RUNOFF [%]

Figure 4-7: GCM grid area map over the contiguous United States showing the percent difference between annual average values of SIM1 and SIM2 for a) runoff ratio and b) surface runoff. Bold lines indicate regions of positive and negative difference.

111

a) SIM2-SIM1: TOP LAYER SOIL SATURATION [%]
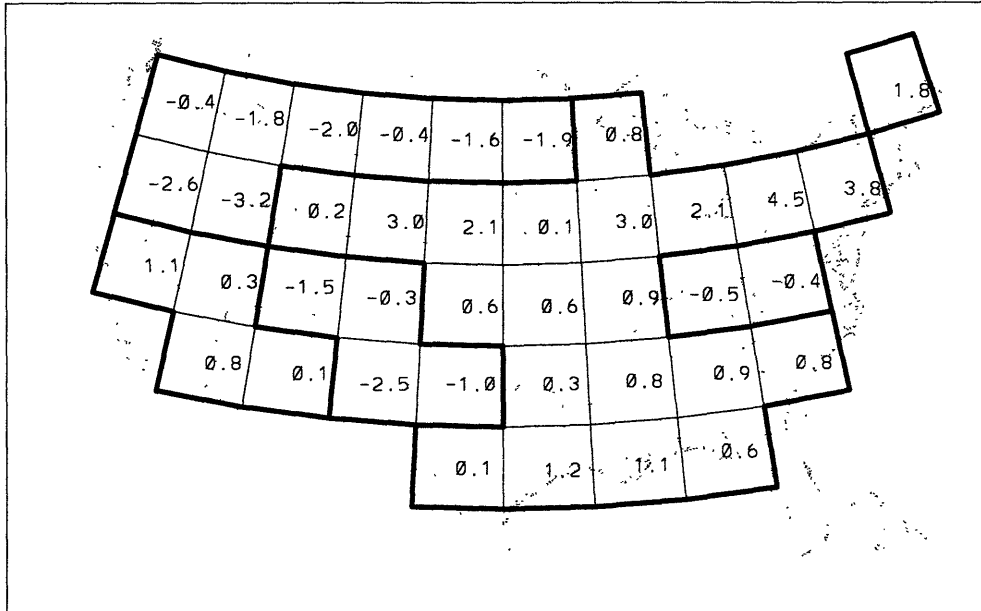
b) SIM2-SIM1: LOWER LAYERS SOIL SATURATION [%]
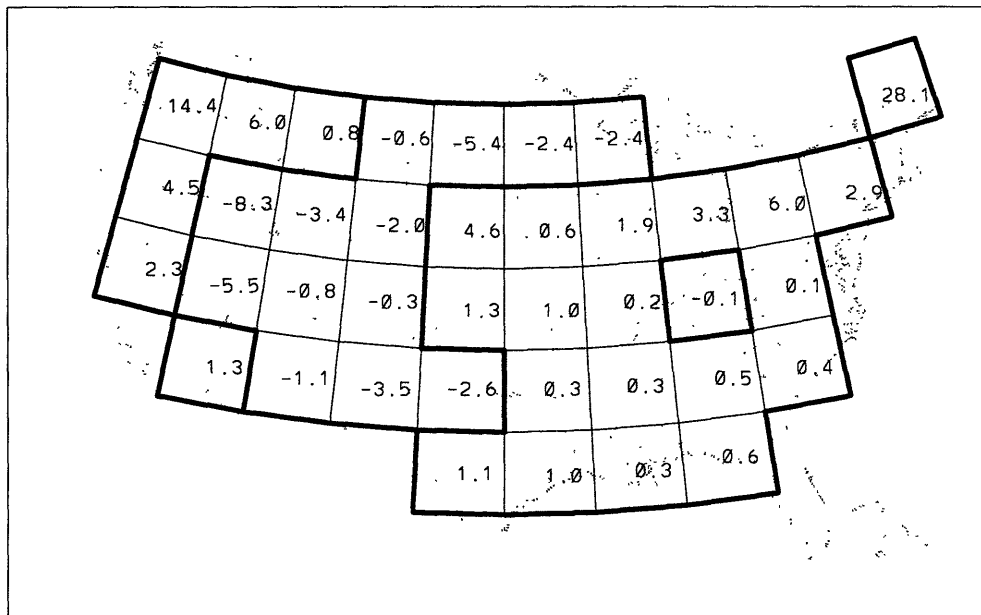
Figure 4-8: GCM grid area map over the contiguous United States showing the difference between annual average values of SIM1 and SIM2 for a) top soil layer saturation and b) combined lower soil layers saturation. Bold lines indicate regions of positive and negative difference.

112

a) SIM2-SIM1: EVAPORATION [%]
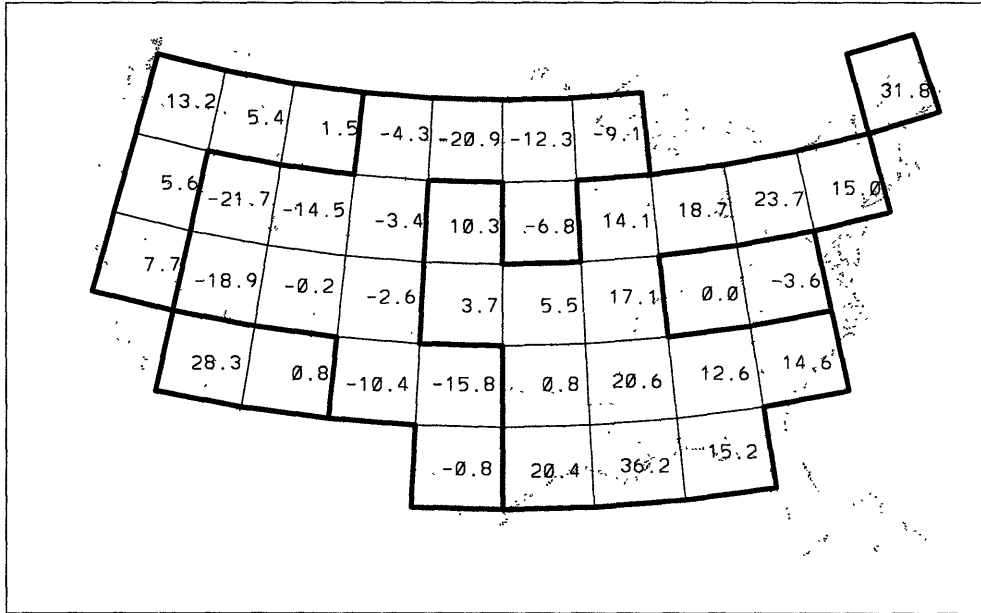
b) SIM2-SIM1: PRECIPITATION [%]
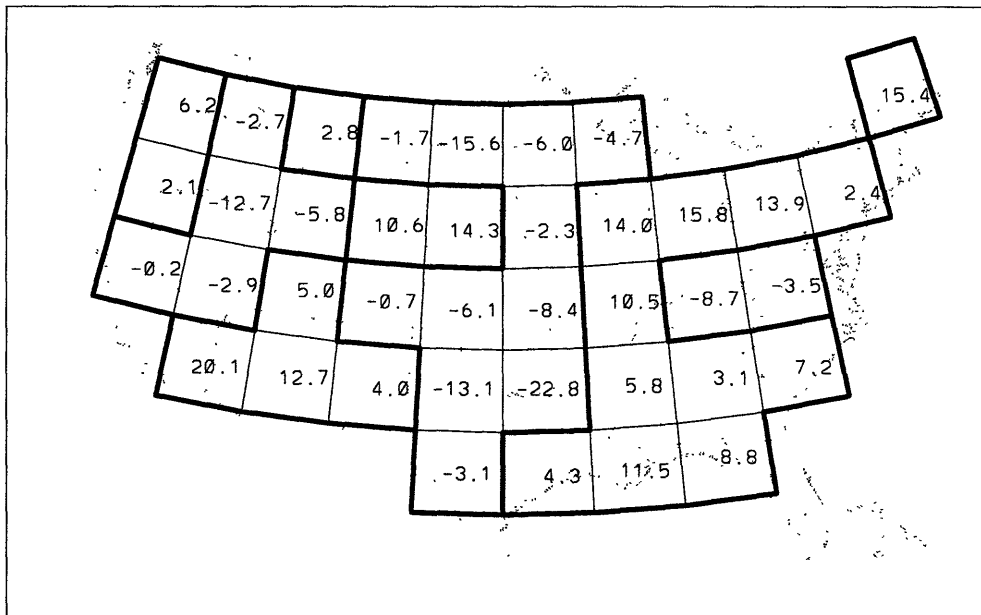
Figure 4-9: GCM grid area map over the contiguous United States showing the percent difference between annual average values of SIM1 and SIM2 for a) land surface evaporation and b) precipitation. Bold lines indicate regions of positive and negative difference.

a) SIM2-SIM1: SURFACE AIR TEMPERATURE [C]

b) SIM2-SIM1: LOWER LAYERS TEMPERATURE [C]

Figure 4-10: GCM grid area map over the contiguous United States showing the difference between annual average values of SIM1 and SIM2 for a) surface air temperature and b) combined lower soil layers temperature. Bold lines indicate regions of positive and negative difference.

114

corner. A sizable region with an increase in R is seen in the western Rockies. Surface runoff (Figure 4-7b) also shows these general regions, which helps to verify that their presence is not merely due to model variability and noise. Realistic spatial variations in fractional wetting apparently have a complex yet discernible influence, producing broad regions with similar responses that do not coincide directly with the $\bar{\kappa}$ perturbations. In fact, a general north-south division in $\bar{\kappa}$ differences seems to produce an east-west division in R and runoff.

Soil layer saturation differences are presented in Figure 4-8 The same three regions can again be clearly detected for the lower soil layers, but not for the top layer. This result is in agreement with the seasonal $\bar{\kappa}$ study, which also found noisy and patternless variations in the top soil layer saturation. This is in all likelihood due to the small storage capacity in the thin (10cm) top layer, which forces its saturation value to respond sharply and noisily to precipitation and diffusion, regardless of the fractional wetting value. Note that direction of the lower layers soil moisture changes (e.g. wetter in east and northwest) agree with the direction seen for R and runoff (less runoff and more infiltration in east and northwest).

Evaporation (Figure 4-9a) also portrays these three regions in accordance with the behavior expected from previous parameters. Note that evaporation corresponds with the lower soil layers and not the top layer, even though evaporation occurs mainly from the top layer. This is probably attributable to the diffusion process that occurs between soil layers. The thin top layer dries fairly quickly due to evaporation, causing upward diffusion of moisture from the lower layers. Therefore evaporation ultimately responds to the availablity of moisture in the reservoir represented by the lower layers, and the thin top layer merely acts as a conduit through which evaporation occurs.

It is rather remarkable that so many of the hydrologic parameters exhibit this clear east-west regionality in response to realistic spatial $\bar{\kappa}$ variations, considering the large inherent variability contained in these short GCM simulations. The regional fractional wetting variations are certainly having a significant impact, albeit the precise nature of this impact is difficult to determine.

115

Precipitation (Figure 4-9b) has a much noisier response to $\bar{\kappa}$. Grids with increased and decreased precipitation are more widely scattered, and broad regions with the same directional response are difficult to identify. The random nature of these spatial precipitation differences makes it very likely that they are simply due to the noise and inherent variability associated with these GCM simulations. Thus these realistic regional $\bar{\kappa}$ variations are unable to extend themselves far enough to influernce pecipitation. This conclusion is in agreement with the results of the previous seasonal $\bar{\kappa}$ investigations, which also saw little effect on precipitation.

Temperatures are shown in Figure 4-10. Both surface air and lower soil layers show a substantial decrease in temperature everywhere except for the northwest corner. The top soil layer temperature (not shown) also responds in this way. Although broad regions are easily identifiable here, they do not correspond to the three regions seen for the land surface parameters. Apparently the complex spatial interactions in the atmosphere manipulate the latent heat fluxes generated by the land surface, causing a disruption in the expected heat budget response. Atmospheric moisture transfer certainly affects clouds and consequently radiation in a complicated manner, making it difficult to relate the resulting temperature differences to land surface and fractional wetting changes.

In summary, GCM simulated climate responds to regional variations in fractional wetting in a clear but complex manner. No direct relationship can be detected between spatial $\bar{\kappa}$ variations and ensuing grid hydrologic and climatic parameter differences, due to the presence of independent seasonal $\bar{\kappa}$ variations within each grid and substantial spatial interaction between adjacent atmospheric columns. Instead three distinct broad regions can be detected over the contiguous U.S. that share similar hydrologic responses to these realistic spatial $\bar{\kappa}$ variations. These broad regions remain consistent for all land surface parameters (runoff ratio, runoff, soil saturation and evaporation), since no lateral interaction occurs between adjacent land surface areas. Temperature differences however are not consistent, since they are determined in part by the moisture and latent heat transferred from the surface to the atmosphere, which becomes suaceptible to spatial interaction in the atmospheric

116

column.

The dominance of temperature decreases indicates once again that the model climate is responding more to increases in $\bar{\kappa}$ than decreases. The soil moisture states of Figure 4-9 also show that most grids become wetter, signifying a greater response to $\bar{\kappa}$ increases. The same overall response of cooler and wetter surface conditions seen in seasonal $\bar{\kappa}$ investigations is seen in these regional investigations. This is understandable, since the limits that apply at low $\bar{\kappa}$ values are valid regardless of the location or month in which they occur. Therefore it can be concluded that the introduction of realistic regional and seasonal variability into GCM climate simulations results in cooler surface temperatures and drier land surface moisture states.

4.3 Comparison of Observational Data Sets used for GCM Validation

4.3.1 Introduction

One of the advantages of studying fractional wetting in a full GCM environment is the availability of observational data sets with which to validate model results. This feature is not available for the screening model, since it does not realistically represent the earth or a particular part of it. The myriad of processes, parameterizations and simplifications contained in current GCMs makes the simulated climate produced subject to substantial doubt and criticism in the scientific community. Therefore the data sets used to assess the accuracy of a GCM become a critical factor in determining its reliiabilty as a tool for understanding and predicting future hydrologic and climatic change scenarios.

Unfortunately, these observational data sets also contain inconsistencies and variability between sources, which raises questions about their own reliability. Hydrologic measurement is certainly not a precise science. Sources which use different instrumentation and collection procedures can yield noticeably different observations of the same parameter. The large spatial scale of observations required for GCM

117

validation further complicates the issue, since aggregation methods for point measurements become an important issue. The raw data must be processed in such a way that they become compatible with GCM diagnostics, which represent large land surface areas as homogeneous regions.

The principal goal of this research is to assess the impact of realistic fractional wetting variations on GCMs, and to see if the simulated climate improves toward observations as a result. A secondary aim is to look critically at observational data sets that can be used for GCM validation. We will first compare a wide range of applicable data sets for precipitation and runoff, and ascertain their reliability and any biases that they may contain. Temperature data will also be briefly discussed. Then we will focus on different data sets over the contiguous U.S. to be used for validation. Their compatibility with GCM grid area diagnostics will be discussed, and the validation results will be presented.

Most of the data described in this section is obtained from published results. The only exception is a set of point measurements of streamflow, precipitation and temperature over the contiguous United States compiled by Wallis et al. [1990]. The actual monthly data for over 1000 streamflow and climate (precipitation and temperature) stations over the period from 1948-1988, available on CD-ROM, was used for this study. The point data was collected into grid areas corresponding to the 39 GISS GCM grids used throughout this study. This data set will be the principal observational source for validating our GCM results. The reasons for this will become clear as it is described and compared to other data sources in the following sections.

4.3.2   Precipitation Data Sets

We begin by looking at observational data sets of land surface precipitation over the contiguous United States. For comparison purposes, some data sets that cover all of North America are also included. The following data sets are used; each is followed by a two letter abbreviation which will be used from this point on: *Wallis*

et al. [1990] (WA); *Guetter and Georgakakos* [1993] (GG); *Roads et al.* [1993] (RO); *Henning* [1989] (HE); *Baumgartner and Reichel* [1975] (BR). Table 4.1 lists each source along with the region measured and its precipitation value.

Precipitation is typically measured using raingages. They measure rainfall at a point, and weighted average procedures are usually employed to obtain mean areal precipitation values from the entire raingage network. Dcata arhives mentioned here are maintained by a number of different agencies, including the National Climatic Data Center (NCDC), National Center for Atmospheric Research (NCAR), and National Oceanographic and Atmospheric Administration (NOAA). The networks used in the archives can be of varying density, data quality, and record length, which could lead to inconsistent measurements of precipitation over the same area. Not surprisingly, the various sources in Table 4.1 produce precipitation measurements over a wide range of values, even for measurements of the same region.

Another important factor when obtaining areal average precipitation depths from point measurements is the way in which the data is aggregated. The GG data provides the mean areal precipitation over the entire contiguous U.S. using divisional data. The RO data first bins the point measurements into independent 2.5° nodes over the U.S., then averages the nodes together to obtain the overall U.S. value. The two methods account for the uneven distributioni of raingage networks in a different manner, yielding different results. The WA precipitation data was gridded in a manner similar to that of RO, as illustrated in Figure 4-11. All stations falling within a GISS grid area were averaged together to produce a grid area value; the 39 grid area values were then averaged to obtain the U.S. value listed in Table 4.1. Note that this gridded value matches very closely the gridded RO value.

The issue of gridding is clearly very important in obtaining precipitation values representing a large area. GCM diagnostics of large landsurface regions can only be obtained by averaging individual grid values. Therefore gridding should be applied to observed precipitation data before using it to validate GCM simulations.

Finally, it is important to note that raingages are not totally reliable as a precipitation measurement tool. They can lead to substantial underestimates of true

119

Table 4.1: Observational data sets of precipitation and runoff over the contiguous United States and North America.

Source	Location	Precipitation	Runoff
Wallis et al. [1990]	Contiguous U.S.	75.1 cm/yr	33.9 cm/yr
Roads et al. [1993]	Contiguous U.S.	76.7 cm/yr	18.3 cm/yr
Guetter and Georgakakos [1993]	Contiguous U.S.	89.0 cm/yr	21.0 cm/yr
Henning [1989]	North America	62.2 cm/yr	22.8 cm/yr
Baumgartner and Reichel [1975]	North America	64.5 cm/yr	24.2 cm/yr

Precipitation/Temperature Stations
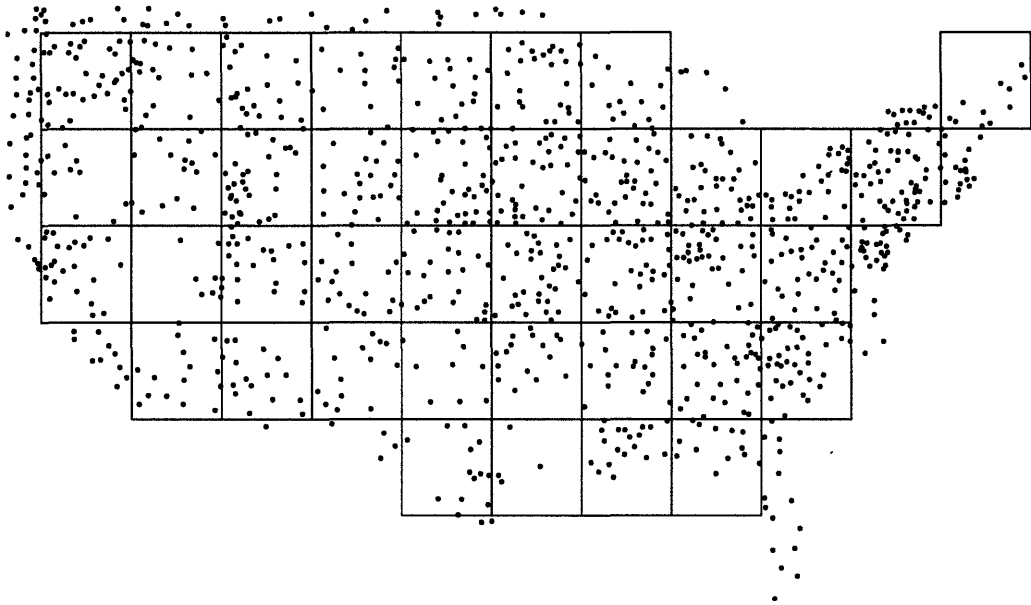
Figure 4-11: Location of 1036 climatological stations comprising the *Wallis et al.* [1990] data, along with grid area boundaries for the 39 GISS GCM grids over the contiguous U.S.

precipitation under conditions of high wind or snow. *Legates and Willmott* [1990] suggests increasing raingage measurements by 10-20% to account for this instrumentation error. This empirical adjustment was not applied in this study, so observed precipitation values used for GCM validation may be erroneously low.

4.3.3 Temperature Data Sets

Surface air temperature measurements are generally much more reliable than precipitation measurements. It can be measured easily and accurately, and average temperature fields are fairly smooth in time and space. Therefore much less disagreement is found between different data sources. However, since it is a point measurement, the gridding issues concerning precipitation also hold true for temperature. Temperature measurement networks should also be gridded before obtaining average values over a large region when comparing to GCM results.

There is one important consideration when obtaining the average surface air temperature of a large region. Although temperature measurements are taken at the surface, the surface elevation can vary substantially over a region the size of a GCM grid. Ambient air temperature is strongly related to elevation. This factor was accounted for in the WA data, since station elevation data was also provided. For every station in a grid, its average temperature was corrected to the grid's mean surface elevation. These adjusted temperatures were then averaged together to obtain a mean temperature at the grid mean elevation. An ambient lapse rate of 9.8°C/km was used for the adjustment, since the adiabatically-mixed boundary layer near the surface is characterized by this lapse rate.

Due to the high quality of temperature data in general, the WA data set is the only one considered here. The annual average over all 39 grids, after applying the elevation adjustment, is 10.53°C.

122

4.3.4 Runoff Data Sets

The five data sources used for land surface precipitation also provide runoff measurements. They are also listed in Table 4.1. Surface runoff has historically been a difficult parameter to validate in GCMs, since runoff data is usually available in the form of streamflow values in rivers. This is not directly compatible with GCM grid area diagnostics, since GCMs do not model rivers and river basins do not coincide with grid areas. Therefore validation is usually limited to large geographic areas, for which major rivers can be used that collect runoff from much of the region.

As indicated in Table 4.1, river outflow measurements over large surface areas are remarkably consistent. The only exception is the WA data set, which will be discussed below. Both the GG and RO measurements for the U.S., and the BR and HE measurements for North America, produce very similar values. In fact the GG and RO results both use the same set of 197 streamflow stations located on major rivers near the border of the contiguous U.S. The only difference between the measurements is that once again, RO bins the data into 2.5° nodes while GG does not. Like precipitation, gridded data is seen to yield a different runoff value than ungridded data, although the difference here is much less noticeable.

Unfortunately, a major flaw is contained in using major rivers as the data source for GCM validation. Although the streamflow in large rivers such as the Mississippi or the Colorado is generated from a large basin area that covers much of the contiguous United States, it is not a true representation of the runoff generated over the basin area. This is because major rivers are subject to diversion and regulation due to human interference. This substantially reduces the streamflow at the mouth of the river, resulting in an underestimation of the physically-induced true surface runoff. GCMs certainly do not account for these human interventions; they generate runoff based solely on the physical processes that are parameterized.

The WA streamflow attempts to account for this. The 1009 streamgages contained in this set all represent streams with little or no diversions or regulations. As a result, their representative basin areas are very small relative to GCM grid areas. The average basin area for this set is $1.7 \times 10^4 \text{km}^2$, while the GCM grid areas under

investigation have an area of about $2.5 \times 10^5 \text{km}^2$. Therefore these streamflows can essentially be considered as point measurements relative to the grid area, so that the runoff recorded by each streamflow gage within a grid area can be averaged together to produce a reliable grid area runoff value. All 39 grids can be averaged in the same way as the WA precipitation data, yielding an observed U.S. average runoff value that is substantially larger than the RO and GG values. Table 4.1 shows that this is indeed the case. Diversion and regulation clearly plays a major role in the determination of appropriate observational runoff data for use in GCM validation.

Figure 4-12 shows the location of each streamflow gage along with GCM grid area borders. The streamgages are much less evenly distributed than the raingages (Figure 4-11). As a result many grids, particularly in the west, have very sparse and uneven streamgage coverage. This may become an important factor in assessing the reliability of this data source, and will be discussed in more detail later. Furthermore, the WA data may have some biases also. The small basin areas and lack of human intervention imply small, first order streams, which typically occur in upland areas with high hillslopes. This may produce an overestimation of grid average runoff, since a large grid area in all likelihood does not consist entirely of steeply contoured land.

The main purpose of this section was to demonstrate that observational data sets can vary depending on their own particular characteristics. Therefore all data sets should be critically examined before using them for validation, in order to detect biases or incompatibilities with GCMs. One must recognize that discrepancies between model and observations may indicate problems with the data as well as weaknesses in the model.

Based on comparisons with other data sources and GCM output characteristics, the precipitation and runoff observations of *Wallis et al.* [1990] appear to be best suited for validation of the GCM simulations described earlier. Another advantage of using this data set is that since the raw monthly point data are available, validation of the annual cycle and spatial distribution of hydrologic response can also be performed. However, it is dangerous to presume that this data set is not without

Runoff Stations
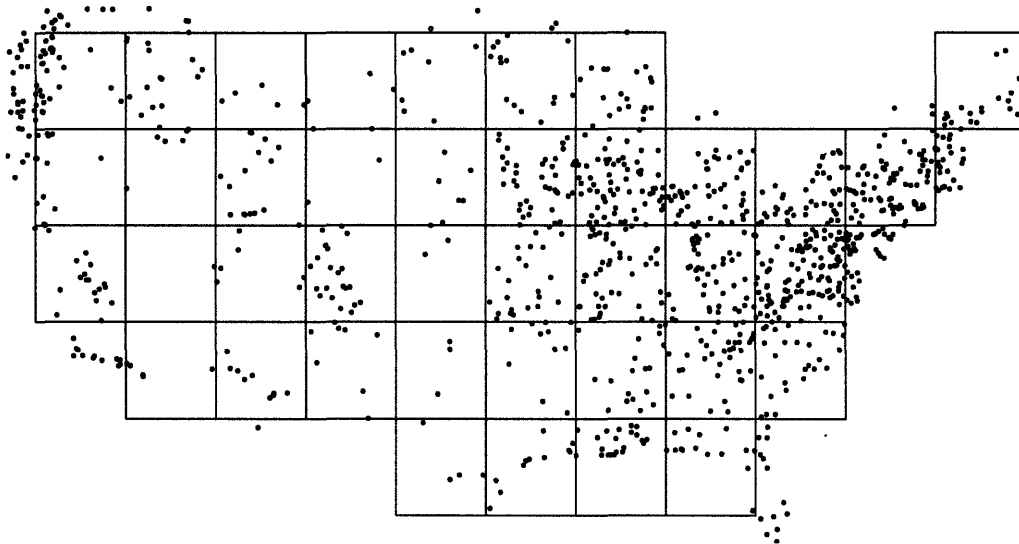
Figure 4-12: Location of 1009 streamflow stations comprising the *Wallis et al.* [1990] data, along with grid area boundaries for the 39 GISS GCM grids over the contiguous U.S.

limitations, especially when validating at such fine detail. It too must be applied critically.

The remaining sections of this work will focus on validating GCM runs SIMG, SIM1 and SIM2, primarily against the WA data set. The limitations and possible biases associated with these observations will be noted where appropriate. Also, the simulations will be validated against more than one data source whenever possible.

4.4 Validation of GCM Simulations

The validation exercise will take place at three different spatial and temporal scales. First, annual hydrologic and climatic parameter values will be compared for the contiguous U.S. as a whole, and also for three major river basins within the U.S. Major river basins represent the finest scale to date at which GCM simulations have been validated. Next, monthly annual cycles representing the entire U.S. will be compared. Finally, the annual value for each of the 39 grids comprising the contiguous U.S. will be studied. These last two scales are identical to those used in Section 4.2 to specifically study the effects of fractional wetting variations. They are at a level of temporal and spatial detail, respectively, beyond that of previous GCM validation exercises. This work represents the first attempt to validate GCM simulations at such detail, which is necessary if these models are to be used for studying global and regional hydrology.

4.4.1 Annual Parameter Values over the Contiguous United States and Major River Basins

Observed and simulated values of average annual precipitation are presented in Figure 4-13. The WA, RO and GG data sets have all been included for the entire contiguous U.S. The three major river basins being studied are the Mississippi, Colorado and Columbia. The boundaries of each river basin are designated according to a study by *Russell and Miller* [1990]. The WA data for grids within each basin has

126

Average Annual Precipitation
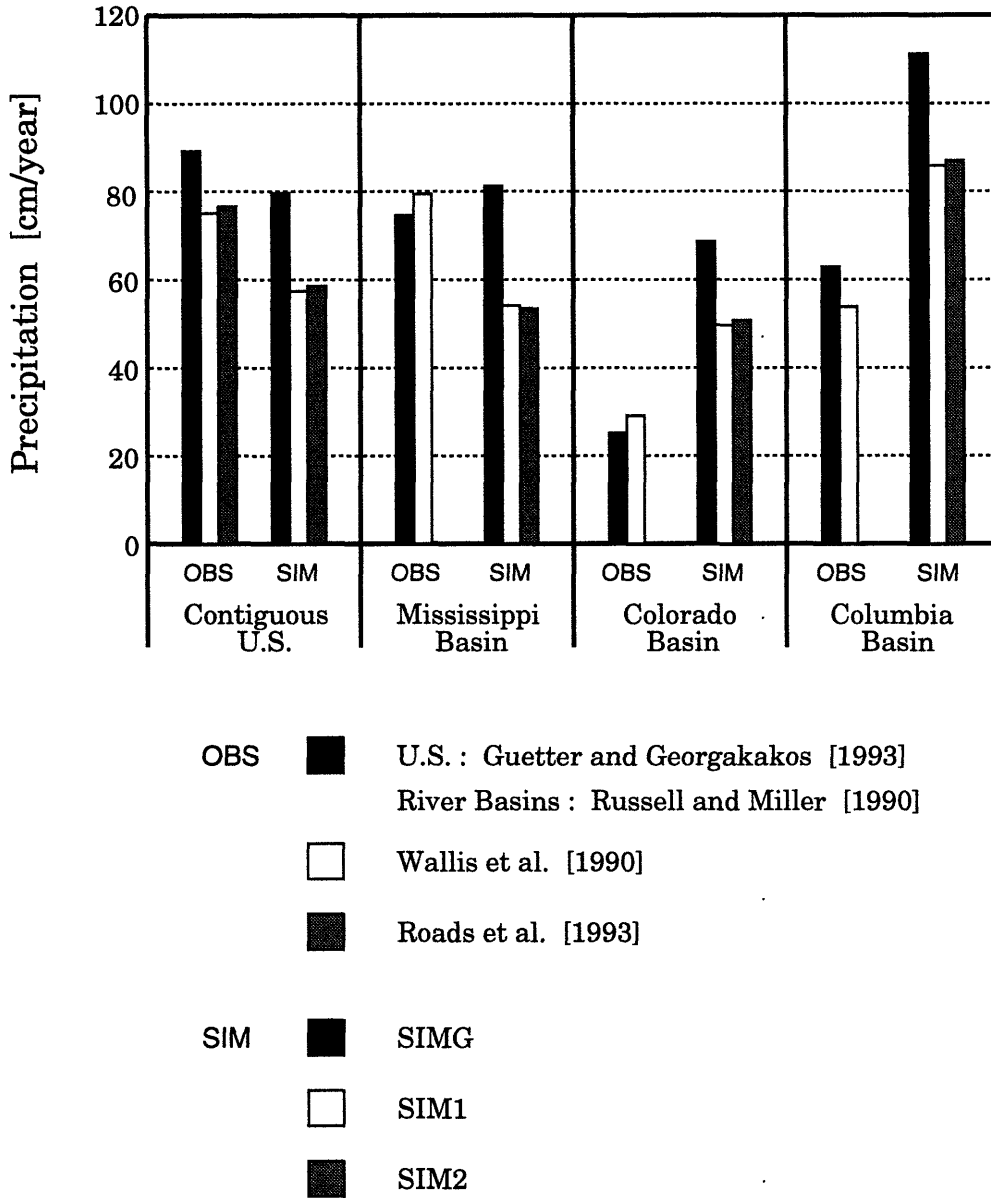
Figure 4-13: Observed and simulated average annual precipitation over the contiguous United States and three major river basins.

been used to obtain the observations for these regions. The *Russell and Miller* [1990] study also provides observed river basin precipitation and runoff values, so they are included in our validation and designated RM. The RM precipitation observations are gridded, and their runoff observations were collected at the outlet of the rivers, so they contain substantial human intervention.

Data from different precipitation sources do yield different values, as suggested earlier. This is true even for the RM and WA basin values, which are both gridded. However, in all cases the change in precipitation produced by introducing the *Entekhabi and Eagleson* [1989] scheme is substantially greater than these observational differences. This is evidenced by the dramatic decrease in precipitation between SIMG and SIM1. The ambiguity detected between different precipitation observation sources is minor compared to the room for improvement available in the simulations.

For some regions, improved hydrology leads to a better agreement between simulations and observations. In other cases SIM1 appears to be worse than SIMG. These results are hindered however by the fact that precipitation mechanisms in the GCM may not be sufficiently parameterized, which could cause errors not detectable here. Fractional wetting variations do not appear to have a major impact. This is not surprising since all $\bar{\kappa}$ variations in SIM2 occur about the same mean value used uniformly in SIM1. The same results concerning SIM1 and SIM2 is expected for all parameters discussed in this section. Changes in the annual value due to nonlinearities discovered in Chapter 3 cannot be accurately determined due to the short duration of the GCM simulations.

Surface runoff is presented in Figure 4-14. The influence of diversions and regulation on runoff observations is apparent; the WA data produces significantly higher annual runoff in all regions. In most cases, the final simulation run SIM2 agrees rather well with the WA data, and represents an improvement over SIMG. The only exception is the Columbia Basin, in which WA gives an extremely high value. Here the RM observations appear much more reasonable. This may be explained by problems with the WA data, which will be discussed in detail later.

Average Annual Surface Runoff
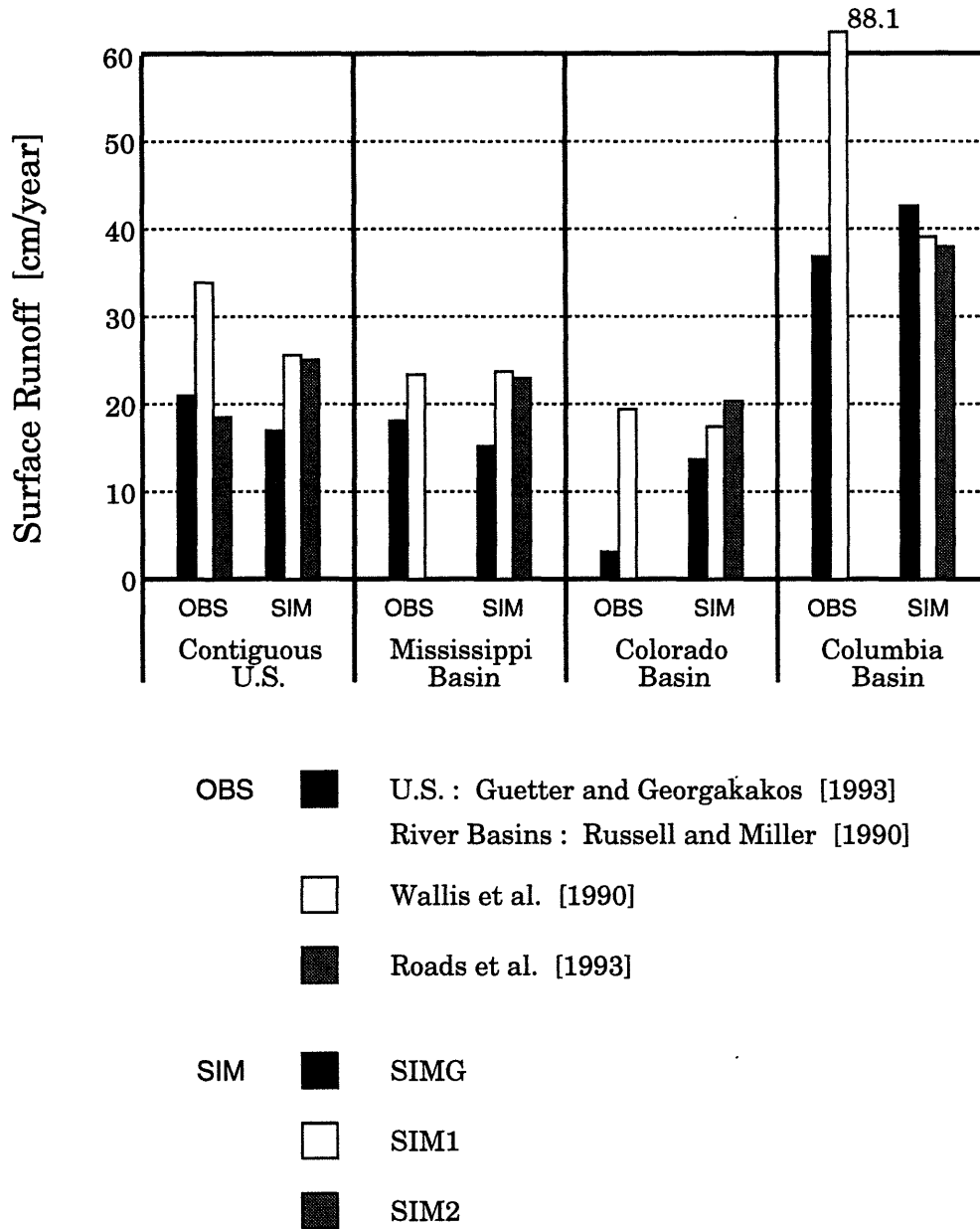
Figure 4-14: Observed and simulated average annual surface runoff over the contiguous United States and three major river basins.

SIM1 overall leads to substantially higher runoff than SIMG. This is an expected consequence of improved land surface hydrology, and has been discussed in the literature [*Johnson et al.*, 1993]. The Columbia Basin again provides an exception. Here runoff actually decreases slightly, probably in response to the large decrease in precipitation forcing seen in Figure 4-13. Again, $\bar{\kappa}$ variations represented by SIM2 have a negligible influence.

The importance of diversion and regulation is clearly exemplified by the Colorado Basin. Due to the high demand for water in this arid region, the Colorado river is subject to an exceptionally high degree of human intervention. This leads to the very small runoff value given by RM, which sharply contrasts with all simulation runs. The WA data is free from intervention, so its runoff value is much higher, and is much more in line with the simulations. Using WA, the simulations steadily improve as hydrology and $\bar{\kappa}$ improvements are incorporated, while they appear to be getting worse if the incorrect RM data was used instead. Outflow measurements for major rivers are an inappropriate data source for GCM runoff validation, especially if the rivers are subject to substantial diversions and regulation.

Land surface evaporation is shown in Figure 4-15. For the observations, evaporation was simply calculated as the residual of precipitation minus runoff. The WA evaporation is lower than other sources, due to the large increase in runoff and relatively small change in precipitation. WA evaporation is not presented for the Columbia Basin, since for this region the observed annual runoff actually exceeds precipitation. This violation of basic mass balance certainly implies an error in the WA data or the way in which it is used. The WA data will be closely inspected in the next section. As expected, a strong reduction in evaporation is seen in SIM1, and little change is seen in SIM2. Agreement with observations is generally poor for all simulations, due in part to the fact that observations are a residual, while simulations represent an actual evaporation value. However, the strong reduction in evaporation resulting from improved hydrology does represent an overall improvement.

Figure 4-16 presents the average annual runoff of Figure 4-14 divided by the average annual precipitation of Figure 4-13. This parameter will be used as a surro-

130
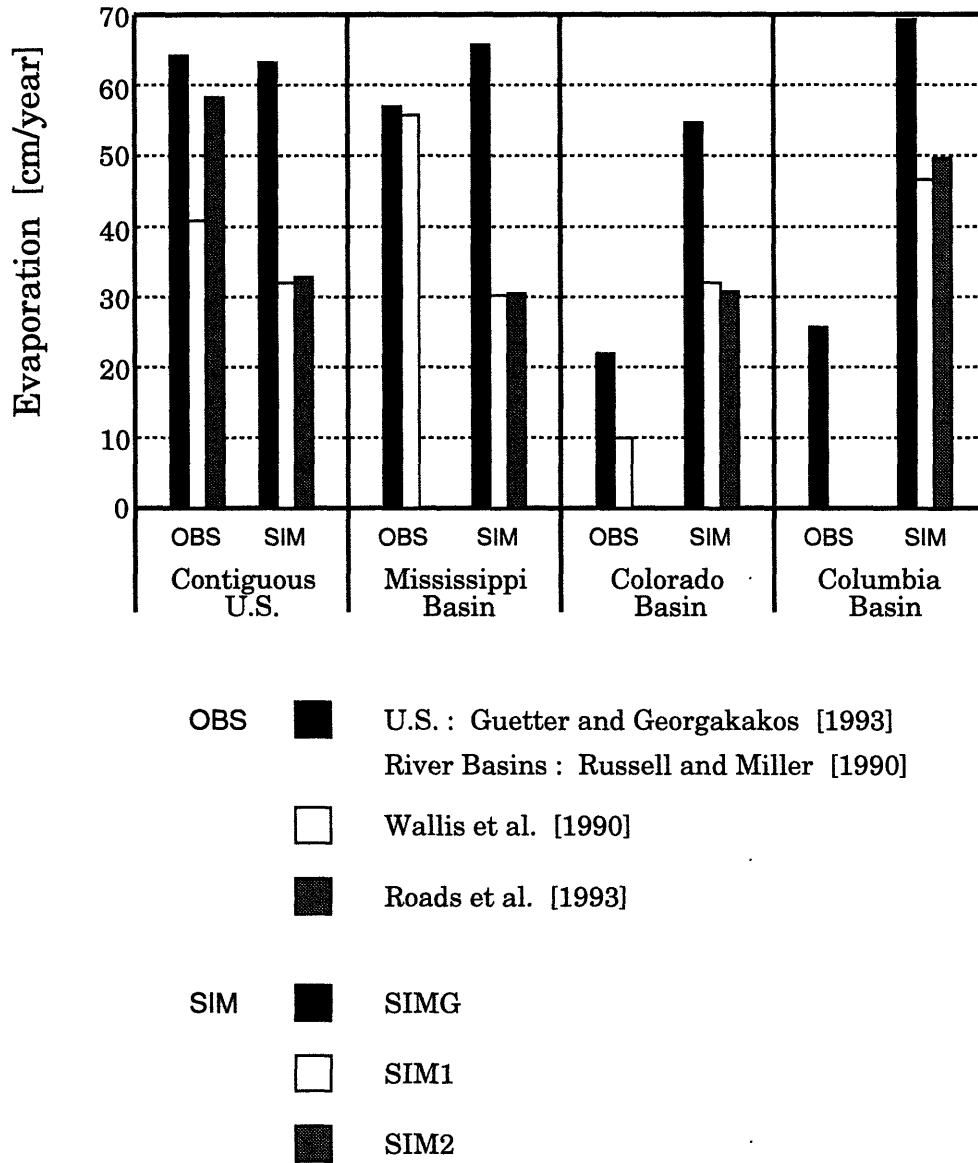
Figure 4-15: Observed and simulated average annual land surface evaporation over the contiguous United States and three major river basins.

Surrogate Runoff Ratio
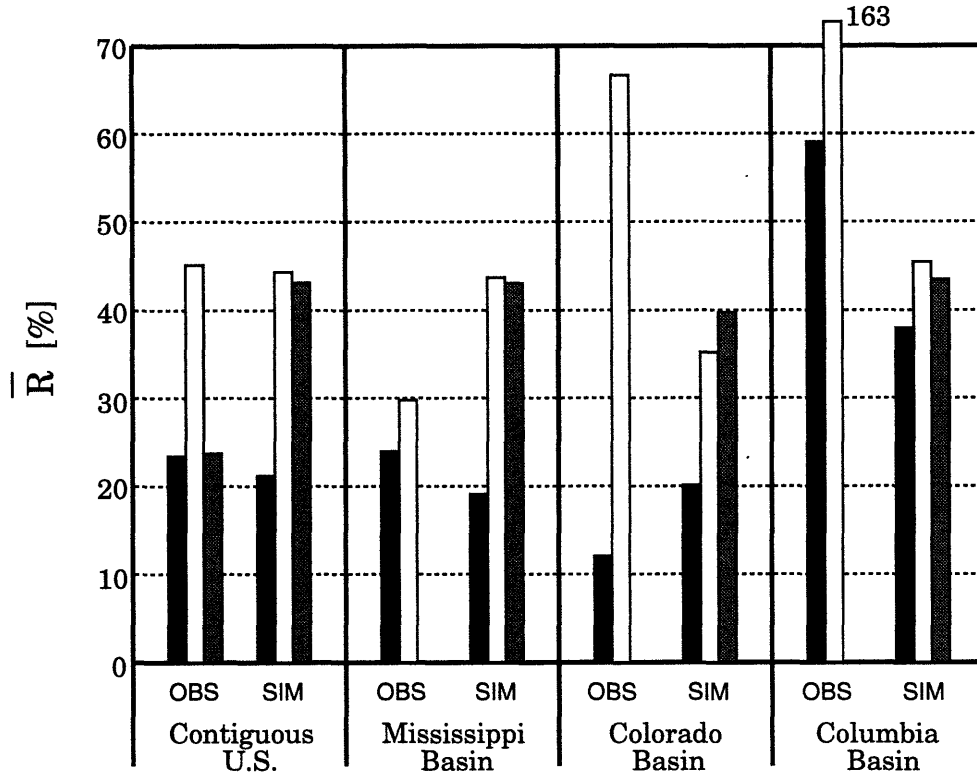
Figure 4-16: Observed and simulated average annual surrogate runoff ratio, $\bar{R}$, over the contiguous United States and three major river basins. $\bar{R}$ is calculated as average annual runoff divided by average annual precipitation.

gate to the true climatic runoff ratio R, since it can be calculated for all simulations and observations. Evaluation of the true R parameter requires that monthly time series of precipitation and runoff be available, so that R can be calculated for each month in the series. We will use the symbol $\bar{R}$ to designate this surrogate parameter. Observed $\bar{R}$ values incorporate both the human intervention error in runoff and the gridding/data source error in precipitation. Note that the RO data over the U.S. matches the WA data in terms of precipitation since both sources are gridded. However, RO matches not WA but GG in terms of runoff, since both contain diversions and regulation. When combined in $\bar{R}$, the RO data agrees with GG and not WA. This implies that the human interve ntion factor on runoff is greater than the gridding/data source factor on precipitation. This provides further evidence that previous GCM runoff validations have used inappropriate data sources.

Since WA gives more runoff than precipitation over the Columbia Basin, $\bar{R}$ for this region is greater than 1. This is physically impossible, and will be explained in the next section. The expected increase in $\bar{R}$ between SIMG and SIM1 is clearly evident, as is the negligible change between SIM1 and SIM2. However, simulated $\bar{R}$ still appears to be too low over the Colorado and Columbia Basins, even accounting for the WA error in the Columbia Basin. These regions are characterized by substantial snowfall, so this error may be due to the unsophisticated and unrealistic snowfall and snowmelt parameterizations currently employed by the GISS GCM.

Finally, surface air temperature is shown in Figure 4-17, with WA as the sole observation source. SIM1 yields higher temperatures, due in part to the decrease in evaporation and latent heat flux associated with increased runoff (see Figure 3-3). This increase leads to a fair improvement over SIMG. SIM2 produces slight changes. They may be significant due to the low variability in temperature fluctuations, but no statistical tests can be performed to verify this. In most cases this potentially significant change represents an improvement over SIM1.

133

Average Annual Surface Air Temperature
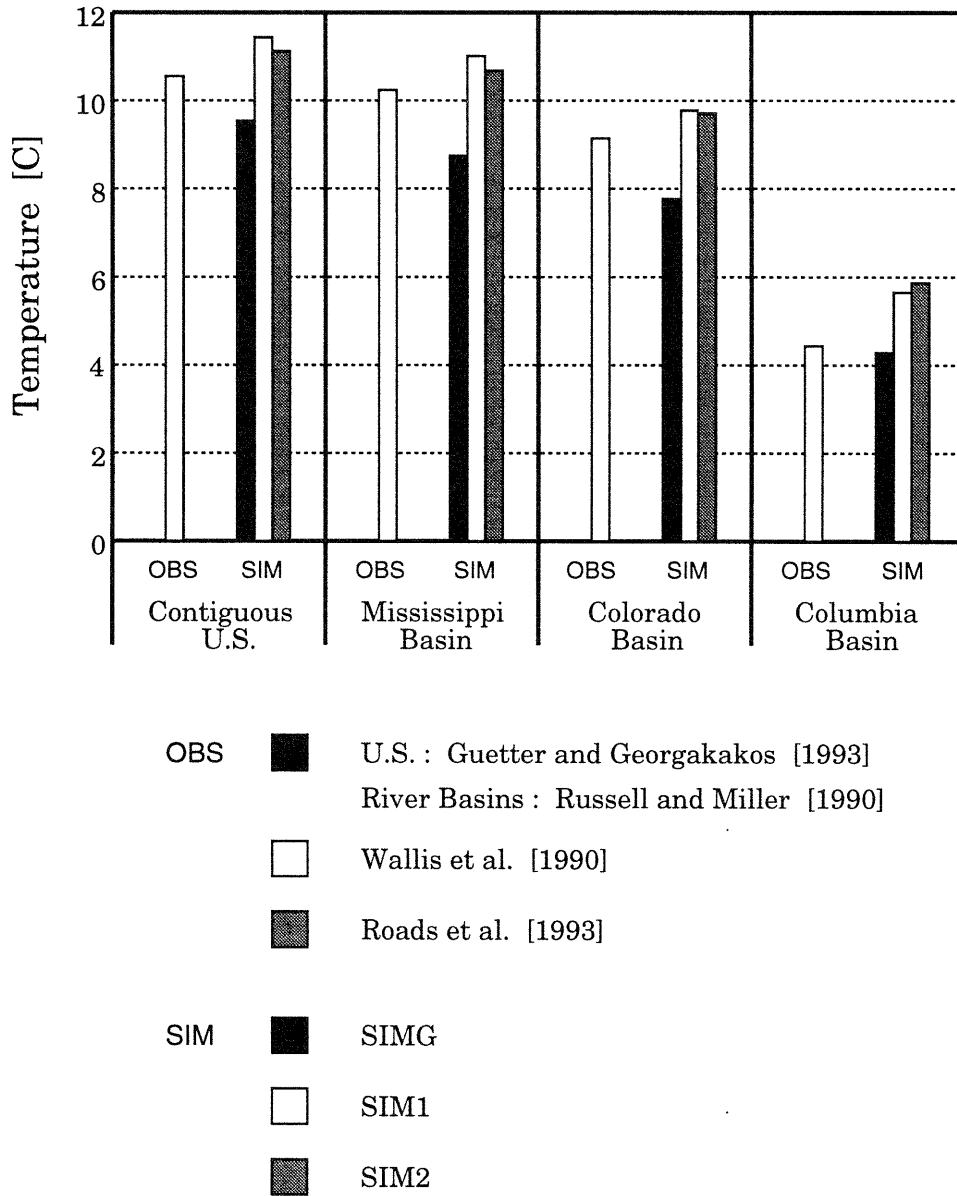
Figure 4-17: Observed and simulated average annual surface air temperature over the contiguous United States and three major river basins.

4.4.2 Inspection of the *Wallis et al.* [1990] Observational Data Set

The WA data set fails to satisfy basic mass balance principles over the Columbia Basin. Specifically, observed annual surface runoff exceeds the observed annual precipitation forcing. A number of different factors exist which may explain why this error occurs. Since the WA data set is broken down into individual grid areas, and since this data set will be used for grid-scale validation, it is reasonable to search for the causes of this error by looking at annual values for individual grids. Station networks and grid boundaries were previously shown in Figures 4-11 and 4-12. The ratio of average annual runoff to average annual pecipitation ($\bar{R}$) for each grid is shown in Figure 4-18. Bold lines indicate grids where runoff exceeds precipitation. As seen in Figure 4-18, $\bar{R}$ exceeds 1 in four northwestern U.S. grids. This area coincides with the Columbia Basin.

A number of potential sources of error can be identified in this data set. The precipitation stations (Figures 4-11) are much more evenly distributed throughout the contiguous U.S. than the streamflow stations (Figures 4-12). In particular, streamflow coverage is very sparse and uneven in the western half of the U.S. Some grids have but a few streamgages to represent the entire grid, which certainly is insufficient for such a large area. Sparse data networks can yield a very poor estimate of the mean areal value, since much of the grid is not represented. This is especially true if a straight, equally weighted average of all stations is taken as the grid value, as is the case here.

Poorly distributed networks also present problems. These large grid areas must be treated as homogeneous units by a GCM, but in truth hydrologic parameters can vary greatly throughout the grid area. Substantial gradients in runoff and precipitation may exist within the grid area, due for example to orography or proximity to oceans. If such gradients occur in a grid with an uneven station network, the conditions over the densely covered portion of the grid will be unfairly weighted, and the average value will not accurately portray the grid as a whole.

The extreme northwest grid covering Washington and Oregon provides a clear example of this bias. This grid's precipitation network is dense and evenly dis-

OBSERVED SURROGATE RUNOFF RATIO [%]
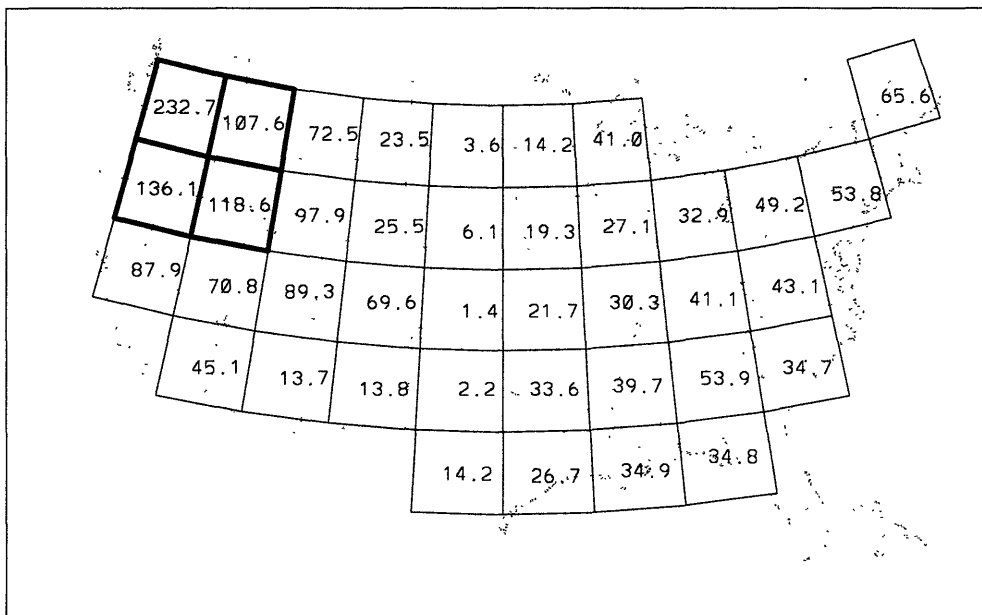
Figure 4-18: Observed ratio of average annual runoff to average annual precipitation ($\bar{R}$) for individual grids over the contiguous U.S. from data compiled by *Wallis et al* [1990].

tributed. The streamflow stations however are located primarily on the western edge of the grid, nearer to the coast. Only three out of 27 streamgages are in the eastern half of the grid. Climatic conditions can vary substantially within this grid. The western half consists of a humid and mild climate, with hight precipiation and runoff totals. The eastern half is a mountainous region, which is more arid. The grid average precipitation represents both climates equally, while the grid average runoff essentially represents the much wetter western edge. Therefore the calculated runoff will be substantially larger than the true grid mean value. The gradient is sharp enough that the biased runoff value exceeds the reasonable precipitation value, resulting inan $\bar{R}$ value greater than 1.

The extent and direction of the resulting bias can be in either direction, depending on the particular climatic and network characteristics of a grid. Although four grids yield a $\bar{R}$ value greater than 1, a number of other grids have extremely high values that approach 1. For example, while the $\bar{R}$ value of 87.9% for the southwestern grid representing central California and part of Nevada is not physically impossible, it is nonetheless an unrealistically high value. Also, a number of grids have an $\bar{R}$ value that is unrealistically low. For example, the grid comprised of North and South Dakota has an $\bar{R}$ value of 3.6%. Individual storms can have extreme runoff ratios, depending on storm intensity and ambient soil moisture conditions. Average annual values over large areas, however, simply do not reach such extremes. Notice that all grids with unreasonably high or low values of $\bar{R}$ are located in the west, and have sparse and/or unevenly distributed streamflow networks. In fact, a few of these grids also have relatively poor precipitation networks, again in the west.

This source of error can be eliminated with denser networks. This is the fundamental goal of all data collection projects: to obtain better, longer, more thorough data. Quality streamflow networks are generally more difficult to obtain, since they are dependent on river location, accessibility, and upstream conditions. Also, corresponding basin areas must be determined, which is not always a simple task. Another means of improvement would be to use a weighted average scheme to obtain the grid mean areal value, such as Theissen Polygons. This would help to eliminate the

137

bias towards densely covered portions of a grid. Using a finer gridding resolution will also aid in this respect. However, excessively small grid areas may lead to grids that have no stations within its boundaries. Even with the 4°x5° grid areas used here, some grids have only a few stations.

Another potential error involves the fact that the precipitation and streamflow measurements are made up of different networks. Therefore even if both networks are sufficiently dense and uniform, they may still represent different conditions due to say elevation. Precipitation stations are generally located at low or moderate elevations, where they are more accessible. The streamflow stations were selected to be free from diversions and regulation. These small first-order streams may be located primarily in higher elevations. Thus the streamflow stations in this data set may be at a collectively higher elevation than the precipitation stations. If that is the case, precipitation events induced by orographic lifting will not be captured by low lying raingages, but the runoff generated by these events will be captured by the high elevation streamgages. If orographic precipitation is a major factor, this may explain why $\bar{R}$ is unrealistically high in much of the mountainous western U.S.

The WA data set included station elevations for both raingages and streamgages. To determine the impact of elevation differences, the average elevation of all stations in each grid were calculated, for both streamflow and precipitation. In 29 of the 39 grids the average raingage elevation exceeded the average streamgage elevation. There were very few grids which showed a major elevation discrepancy in either direction. Apparently uncontrolled streams exist that are low enough to not pose a problem to precipitation measurement. The ten grids that did have higher streamgage elevation did not coincide with grids in which $\bar{R}$ approached or exceeded 1. Thus elevation discrepancies between streamflow and precipitation networks cannot be used to explain the extreme $\bar{R}$ value observed for some grids.

A final possible error source concerns the quality of the precipitation measurements. It was noted earlier that raingages have a tendency to underestimate precipitation, especially under conditions of high wind, or if the precipitation is in the form of snowfall. If precipitation measurements are too small, the calculated $\bar{R}$

would consequently be too large. For regions with substantial snowfall or stormy weather, the precipitation error may be enough to cause $\bar{R}$ to exceed 1. Note that in Figure 4-18 the four grids with $\bar{R} > 1$ are located in the northwest U.S., a region with significant storminess and snowfall. This error can explain erroneously large $\bar{R}$ values, but not the extremely small values.

The WA data set was chosen to be the most applicable data source for GCM validation out of all sources discussed earlier. However even this data set is not without faults or limitations, especially when validation is being conducted at the grid scale. Many of the errors noted here are due to poor network coverage or particular climatic conditions in certain grids. If the contiguous U.S. is treated in its entirety, thesde indiviual grid errors get muted when averaged over all 39 grids. They only become apparent wihen indivdual grids are studied to reveal violations of physical laws. These errors can be traced to general data quality issues. Although GCMs represent grid areas as homogeneously , they are still larrge, heteogeneous regions, and sufficient data must be provided to obtain observations that represent the average condition over the entire grid area.

4.4.3 Annual Cycle over the Contiguous United States

We now attempt to validate the GCM simulations at scales applicable to global and regional hydrology. Monthly annual cycles of precipitation, surface runoff, land surface evaporation, runoff ratio and surface air temperature representing the entire contiguous U.S. are presented in Figures 4-19-4-23. Each figure displays the three runs SIMG, SIM1 and SIM2, along with the observations of WA. The WA data set is the only one used for these validations, since the raw data was available on a monthly basis over a 40 year period, and could be processed to produce monthly values and individual grid values.

As indicated in Figure 4-19, the observed precipitation cycle is reproduced very poorly by all of the simulations. SIMG bears no resemblance to observations at all. The inclusion of improved land surface hydrology in SIM1 greatly affects the modeled precipitation cycle, but it only exhibits a slight improvement towards

139
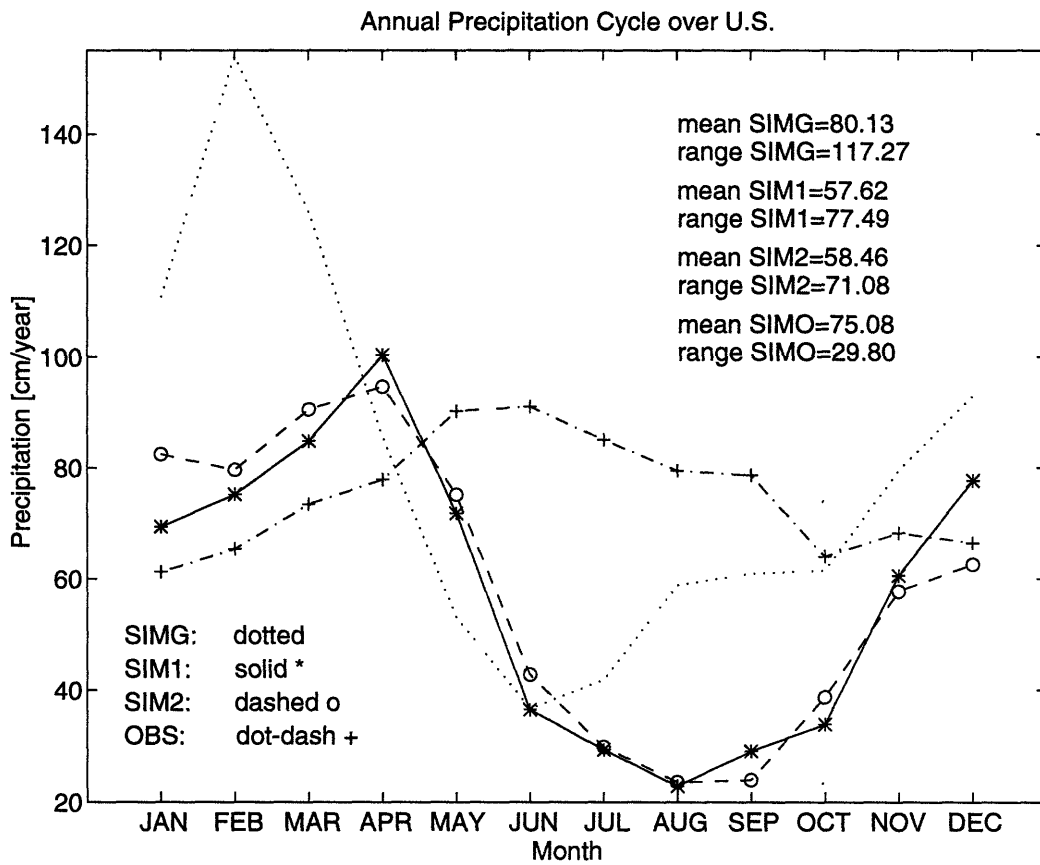
Figure 4-19: Observed and simulated monthly annual cycle of precipitation over the contiguous United States.
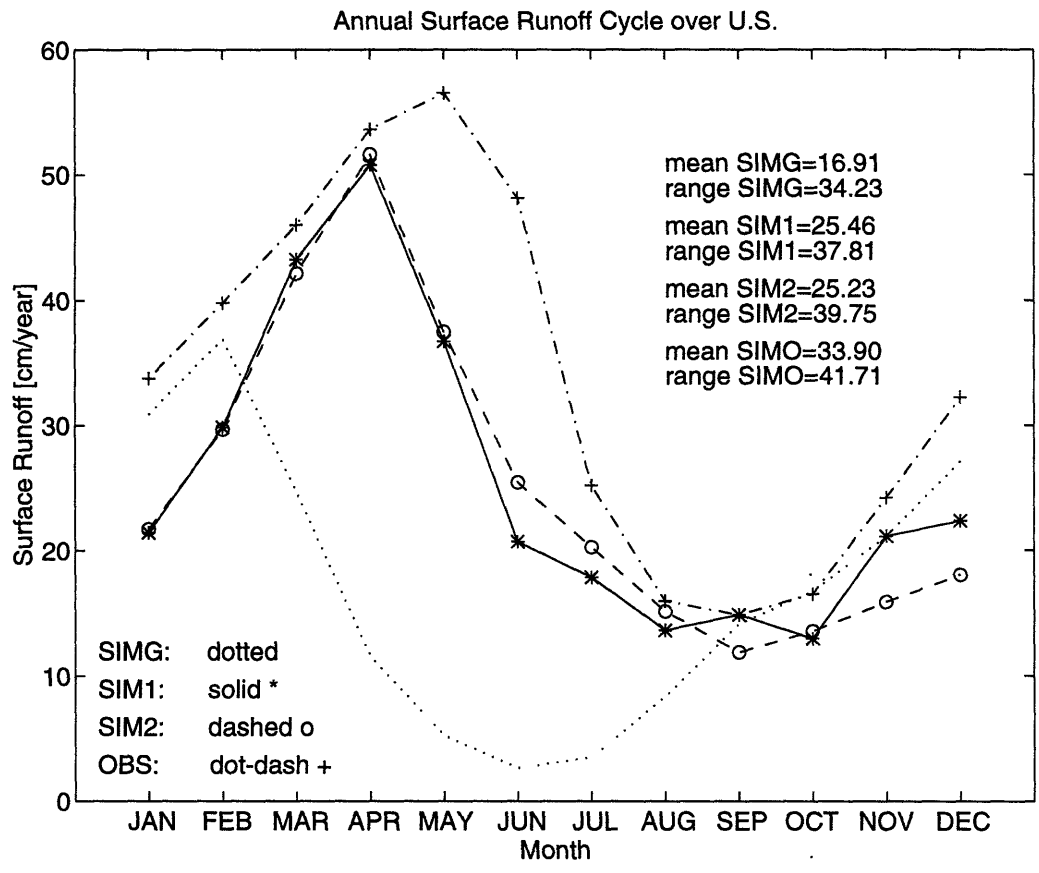
Figure 4-20: Observed and simulated monthly annual cycle of surface runoff over the contiguous United States.
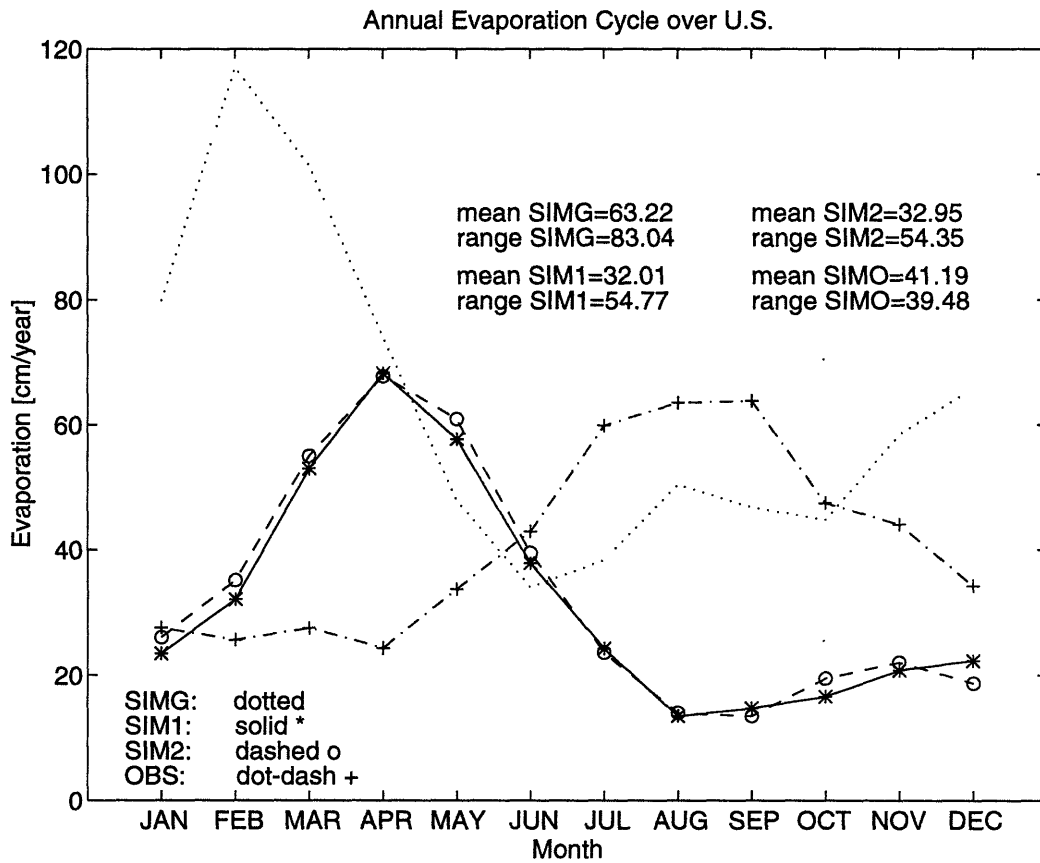
Figure 4-21: Observed and simulated monthly annual cycle of land surface evaporation over the contiguous United States.
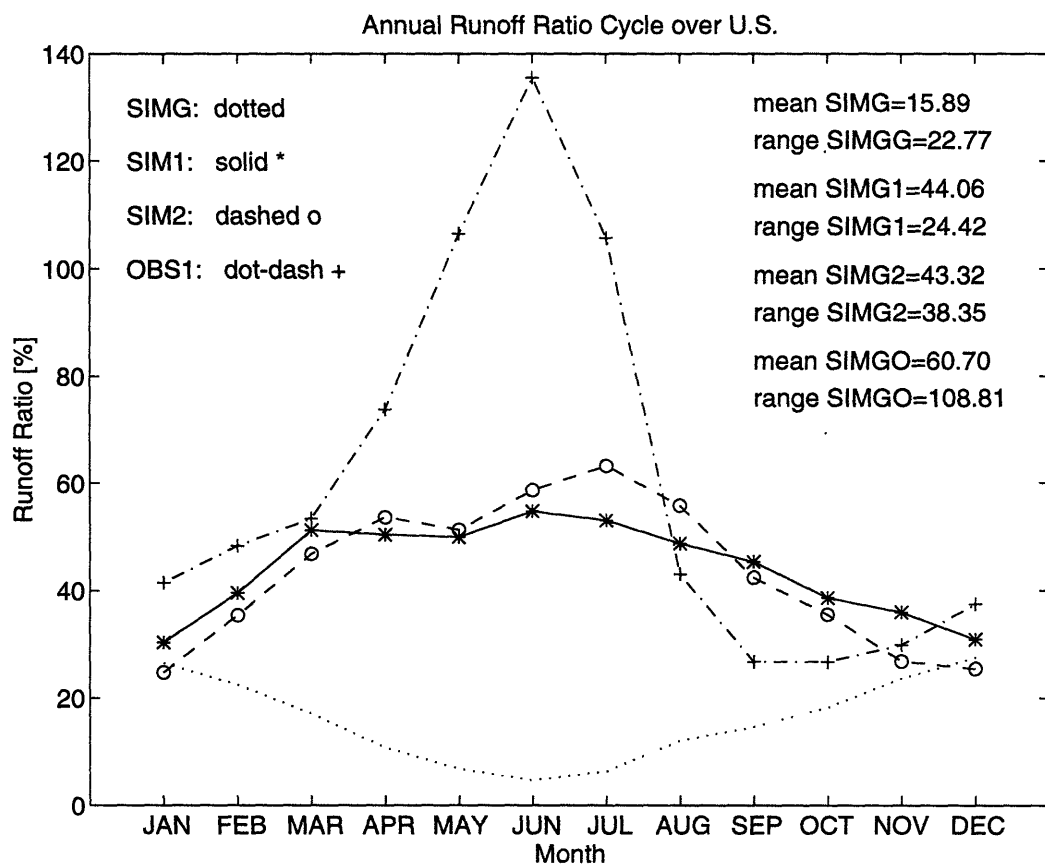
Figure 4-22: Observed and simulated monthly annual cycle of runoff ratio over the contiguous United States.
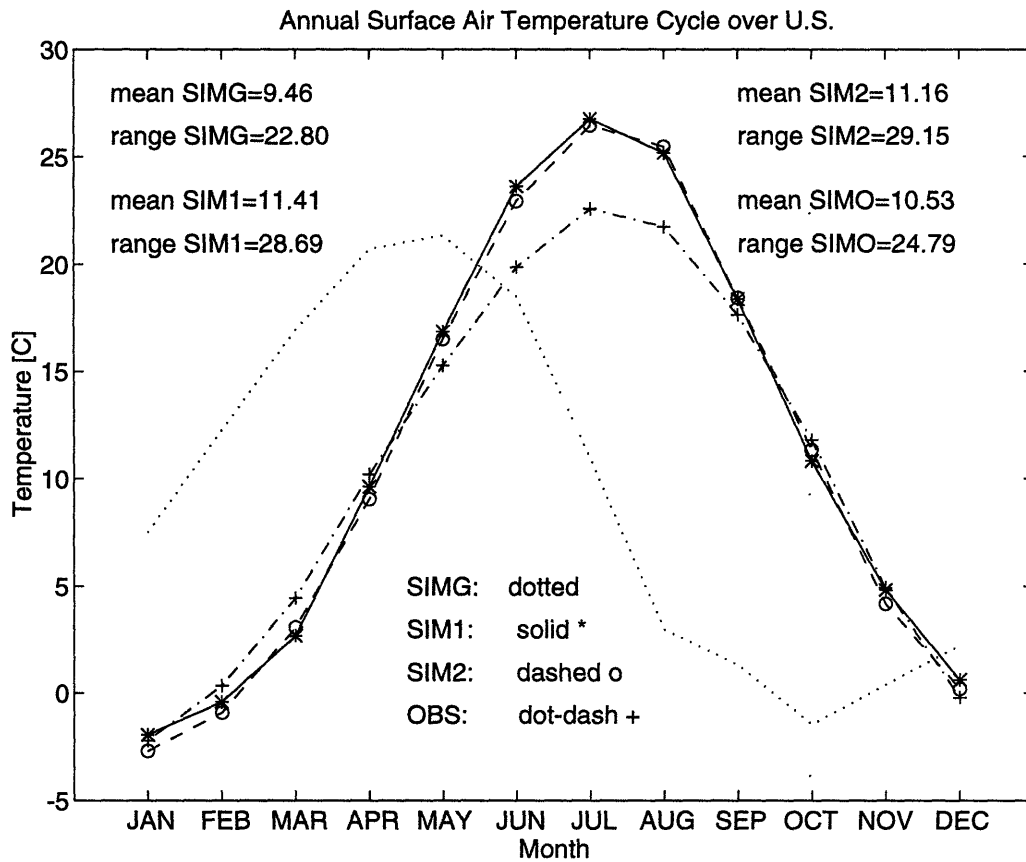
Figure 4-23: Observed and simulated monthly annual cycle of surface air temperature over the contiguous United States.

observations. The annual range of values is reduced, but is still too large. The summer and autumn months contain the greatest discrepancy; here the high observed precipitation sharply contrasts with the low simulated precipitation. As indicated in Section 4.2, the introduction of realistic fractional wetting variations in SIM2 has hardly any affect on the precipitation cycle.

Note the difference in validation results when analyzing annual cycles as opposed to just annual averages. The observed mean of 75.08 cm/yr is much closer to the SIMG mean of 80.13 cm/yr than the SIM1 and SIM2 means of around 58 cm/yr. Looking only at the means would imply that the introduction of improved hydrology is detrimental to simulated precipitation. However when the annual cycles are compared, SIMG is clearly is not better than SIM1 or SIM2. None of the simulations perform well, but SIM1 and SIM2 at least produce a more reasonable range of values. Also, the winter and spring months are simulated fairly well by SIM1 and SIM2, whereas SIMG is completely out of phase with the observations.

The WA precipitation data is of reasonably high quality, due to the gridding procedure applied, and the dense and evenly distributed raingage network. However, the observations may be too small in the winter, since raingages underestimate precipitation under conditions of wind and snow. If this is true, then SIM1 and SIM2 may actually be simulating winter and spring precipitation very well, since it generates values slightly higher than the underestimated observations. This implies that summer precipitation in particular is not modeled well by the GCM. Since summertime rainfall is dominated by moist-convective processes, an improvement in the GCM moist-convection parameterization is needed.

Surface runoff however, is dramatically improved using improved hydrology, as indicated in Figure 4-20. Despite the network density problems associated with the WA data set, the data nonetheless shows a very reasonable annual cycle with peak values during the spring, due to snowmelt. In all likelihood, grids with positive and negative biases in observed runoff cancel each other out, or are suppressed when averaged over the entire U.S. SIM1 and SIM2 also exhibit this springtime maximum, but the simulated peak occurs one month earlier. Also, SIM1 and SIM2 generally

underestimate runoff during winter and spring, when snowfall and snowmelt are most likely. Summer and autumn months are reproduced rather well. Thus the treatment of snowfall and snowmelt processes in the GCM appear to be insufficient. This is not surprising, since these processes have not received much attention, and are currently parameterized very crudely. In any case, the improvement over SIMG is clear.

Section 4.2 indicated the presence of noticeable changes in surface runoff from June through December due to the inclusion of realistic fractional wetting variations. These monthly changes can be seen in Figure 4-20, but they appear to be very minor compared to the change induced by improved hydrology. One expectation of seasonal $\bar{\kappa}$ variations was that it would result in an improvement in the simulated annual cycle for relevant parameters such as surface runoff. However, SIM2 does not produce a substantial overall improvement towards observations. Nor does $\bar{\kappa}$ affect the characteristics of the annual cycle. The changes induced by $\bar{\kappa}$ are small relative to the range of values seen over the annual cycle.

Observed land surface evaporation (Figure 4-21) is reproduced very poorly by all simulations. Although SIM1 and SIM2 show a much more reasonable annual range than SIMG, their cycles still appear to be completely out of phase with the observed cycle. However, the reliability of the observed evaporation cycle is questionable. It is computed simply as the residual of precipitation minus surface runoff, so it includes the errors contained in both data sets. Therefore the accuracy of the simulated evaporation is difficult to assess. The slight overall increase in evaporation due to $\bar{\kappa}$ seen in Section 4.2 has a negligible impact on the shape of the annual cycle.

Runoff ratio is presented in Figure 4-22. In this figure the actual runoff ratio parameter R is utilized, not the surrogate value $\bar{R}$. The WA data allows for the determination of R, since monthly values of precipitation and surface runoff were available over the same 40 year period. Grid area R values were calculated for each month of the data set by taking the ratio of that month's runoff and precipitation for each grid, generating a 40 year monthly time series of R for each grid.

The observed R annual cycle shows a huge rise in the late spring and early

146

summer. This is due in part to snowmelt processes, which can still be substantial well into the spring at higher elevations. Certain months show an observed R greater than 1. This is not physically impossible, but merely indicates a substantial amount of accumulated snow on the surface. Mass balance requires only the annual mean R to be below 1. The peak in observed R agrees generally with the peak in observed surface runoff, although the R peak occurs later. Since R involves both precipitation and runoff, it too is subject to data set errors in both parameters. This may also help to explain the magnitude of the observed R peak. Although a spring peak is expected due to snowmelt, an average value over the entire U.S. should not have a peak that is so large and occurs so late, since much of the U.S. receives little or no snowfall. The observed annual mean R value is 60.7%, which is intuitively too high; errors in the data are a likely cause of this phenomenon.

None of the simulations contain this spring peak R due to snowmelt. The lack of a rise in R during the spring in the simulated cycles provides further evidence that snowfall and snowmelt are inadequately parameterized in the GISS GCM. SIM1 and SIM2 however do show a noticeable improvement over SIMG in terms of the expected general annual cycle. R is expected to be highest in the summer and lowest in the winter, since the summertime is dominated by moist-convective processes, which have more intense precipitation and generate more runoff. Winter precipitation on the other hand is characterized by less intense large-scale supersaturation type events. Compared to other parameters, R exhibits the most detectable change in annual cycle due to $\bar{\kappa}$. SIM2 clearly increases R in the summer and decreases it in the winter, magnifying the range of its annual cycle. A noticeable though still small improvement towards observations is seen in SIM2.

Surface air temperature is shown in Figure 4-23. The WA temperature observations are very reliable, due to the general high quality of temperature measurements and the density of the temperature gage network. SIMG appears to be about two months out of phase with the observations. Introducing improved hydrology seems to correct this lag error. Included in hydrology improvements utilized by SIM1 and SIM2 is a realistic soil moisture diffusion scheme. This moisture diffusion within

the soil column also affects the seasonal heat balance due to evaporation and latent heat flux. Heat conduction between soil layers is explicitly modeled in SIMG to produce an annual cycle in the heat budget. However this moisture diffusion process provides an additional source of seasonal heat storage, which is necessary to generate the observed temperature lag and reproduce the observed annual cycle in surface air temperature.

Unfortunately, an additional consequence of this improvement is an overestimation of temperature in the summer months. This is probably a result of the failure by SIM1 and SIM2 to reproduce observed summer precipitation and evaporation. These simulations underestimate summer evaporation, which leads to an increase in the less efficient sensible heat flux and consequently increases temperatures. Also, the underestimated summertime precipitation may lead to too little atmospheric moisture, which would allow more solar radiation to reach the surface. This was shown during the screening model simulations of Chapter 3 to be a potentiaay important factor. SIM2 was shown in Section 4.2 to decrease temperatures, but Figure 4-23 indicates that this derease is minor and insufficient to improve upon the overestimation seen in the summer months.

4.4.4 Annual Values for Individual GCM Grid Areas

We conclude the validation exercise by studying average annual parameter values for individual GCM grid areas over the contiguous U.S. Validation at grid scale is necessary for global and regional hydrology, but nonetheless represents an ambitious effort since GCMs were developed primarily for assessing broad global climatic patterns. Also, the sparsity of streamflow data over the western U.S. in the WA data set makes grid scale observations there very unreliable.

To simplify the analysis, only the difference between SIM2 and the WA observations will be presented in this section. Appendix D contains the actual grid values for all three simulations and the WA observations. The discussion will refer to these appendix figures as well as the difference figures included in this section. The anal-

148

ysis will focus on determining if the problems concerning the GCM simulation and data set quality mentioned in the annual cycle validation can also be detected here.

Precipitation is shown in Figures 4-24 and D-1-D-2. Observed precipitation in the contiguous U.S. is characterized by a humid eastern half and an arid western half, with a clear vertical division along the center of the country. SIM2 does not reproduce this characteristic, but instead generates a wider and more disperse range of values. As a result, precipitation is overestimated in the west and underestimated in the east. The extent of the difference varies from grid to grid, but the greatest error is seen in the southeast, where precipitation is severely underestimated. This region experiences a significant amount of moist-convective precipitation, indicating that this process is poorly parameterized in the GCM. Note that this conclusion agrees with the annual cycle validation, which showed that the moist-convective summer months underestimated precipitation.

Surface runoff is presented in Figures 4-25 and D-3-D-4. Annual values are presented here over the entire U.S., which does not contain any perpetually frozen regions. Therefore the effects of snowmelt do not play a role in this part of the analysis. Since runoff observations in the west are generally sparse, uneven and unreliable, the difference between SIM2 and the observations is very ambiguous in this region. For example, the underestimation of runoff in the far west is due to a large extent to the excessive observed runoff in this region, as indicated by surrogate runoff ratios greater than 1 shown in Section 4.4.2. The east, which has much more reliable runoff data, shows a consistent underestimation of observed surface runoff, despite the changes brought upon by land surface hydrology and fractional wetting improvements. This result is closely related to the underestimation of precipitation in this region. As for precipitation the greatest degre of underestimation occurs in the southeast grids. Insufficient precipitation forcing will lead to insufficient runoff generation, regardless of the land surface hydrology. Therefore this underestimation of surface runoff may be attributable to inadequate treatmernt of GCM precipitation processes.

Land surface evaporation is presented in Figures 4-26 and D-5-D-6. Once again

149

data quality is suspect in the west. Therefore the large overestimation of evaporation in the west may be due in par to erronesously low observed evaporation in this region. Remember that observed evaporation is determined simply as the residualt of precipitation minus runoff. In general the evaporation maps appear to correspond with the precipitation maps discussed earlier, with humid areas consequently producing more evaporation. Although land surface hydrology can affect the partitioning of precipitation into runoff and evaporation, the magnitude of the evaporative flux is still highly dependent on the magnitude of the precipitation forcing.

Runoff ratio is presented in Figures 4-27 and D-7-D-8. The grids with the greatest difference all reside in the western half of the U.S., where runoff data is known to be poor. Abnormally high R observations are found in the far west, and these grids show severe underestimation of R by the simulations. Conversely, grids closer to the center of the U.S. exhibit an overestimation by the simulations; these grids contain most of the abnormally low observed R values. Thus the large R differences in the western U.S. between SIM2 and simulations appear to be caused by problems with the validation data as much as with insufficiencies in the GCM land surface hydrology parameterization. East of the Mississippi River, where streamflow data is substantially better, the extent of the difference in R decreases dramatically. In this region, most of the grids seem to simulate observed runoff ratio values fairly well.

Surface air temperature is shown in Figures 4-28 and D-9-D-10. A clear majority of grids overestimate observed annual temperature. This coincides with the seasonal response of the U.S. as a whole, in which temperature was overestimated in the summer but reproduced rather well in all other months. The summer temperature overestimation was related to summer precipitation and evaporation underestimations, which were in turn related to the parameterization of moist convection. The annual grid temperature differences agree with this conclusion, since the most substantial overestimation of surface air temperature occurs in the southeast, where moist-convective processes dominate. In general though, SIM2 reproduces observed surface air temperature over U.S. grids very well compared to the hydrologic parameters. A general decrease in temperature with latitude and elevation can be seen for

150

all simulations and the observations. On the other hand, observed spatial hydrologic characteristics like the east/west delineation of humid and arid regions in the U.S. are not simulated by the GCM.

For all parameters, the difference between SIM2 and the observations is substantially greater than the difference between SIM1 and SIM2. This is true for virtually every grid, and in many cases their magnitudes differ by over an order of magnitude. Thus, although regional fractional wetting variations have a measurable impact at the grid scale, these changes do not alter the spatial characteristics of the GCM simulation. Like seasonal variations, there ii no discernable improvement towards observations.

Overall, the GCM simulations do not appear to reproduce obsoerved hydrolgic and climatic features very well at the grid scale. Unfortunately, this result is clouded by the lack of sufficient data to validate grids in the western U.S. Some of the errors can be traced to the parameterization of physical processes other than land surface hydrology, such as moist-convective precipitation. The same can also be said for the annual cycle validation exercise conducted in the previous section. In that exercise snowfall and snowmelt was also identified as a process in need of improvement. Clearly, significant advances in GCM physical parameterizations and also validation data quality must be made before successful and reliable validations of GCM simulations can be conducted at these scales.

SIM2-OBS: PRECIPITATION [cm/yr]

									17.8	
33.6	39.2	24.7	28.9	6.8	-22.2	-32.1				-15.5
27.9	23.5	32.0	32.2	-2.6	-30.9	-36.7	-30.4	-16.5		
-21.0	13.0	34.5	50.4	-6.1	-57.2	-65.6	-64.8		-36.5	
	-1.1	15.6	44.6	-3.6	-72.3	-100.7	-89.7	-56.5		
				-25.0	-67.1	-121.6	-97.2			
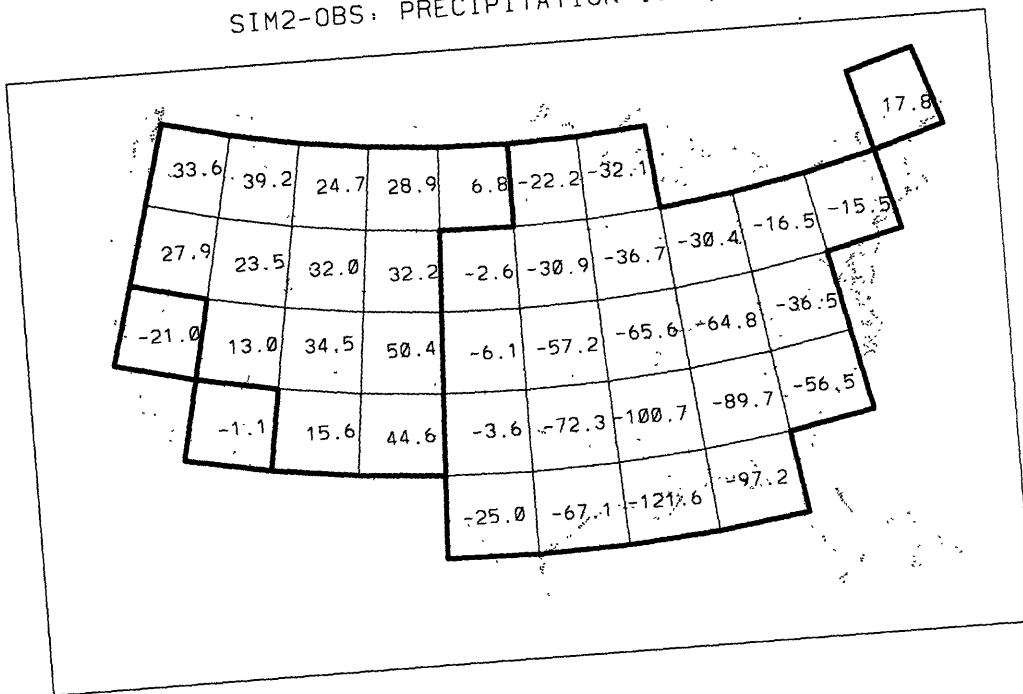
Figure 4-24: Difference between SIM2 and observations [*Wallis et al.*, 1990] of precipitation for individual U.S. grid areas.

152

SIM2-OBS SURFACE RUNOFF [cm/yr]

Figure 4-25: Difference between SIM2 and observations [*Wallis et al.*, 1990] of surface runoff for individual U.S. grid areas.

SIM2-OBS: EVAPORATION [cm/yr]

Figure 4-26: Difference between SIM2 and observations [*Wallis et al.*, 1990] of land surface evaporation for individual U.S. grid areas.

SIM2-OBS RUNOFF RATIO [%]

Figure 4-27: Difference between SIM2 and observations [*Wallis et al.*, 1990] of runoff ratio for individual U.S. grid areas.

155

SIM2-OBS: SURFACE AIR TEMPERATURE [C]

Figure 4-28: Difference between SIM2 and observations [*Wallis et al.*, 1990] of surface air temperature for individual U.S. grid areas.

Chapter 5

Conclusions

5.1 Summary of Results

The primary goal of this work is to assess the role played by fractional rainfall coverage in the parameterization of land surface hydrology employed by atmospheric general circulation models. Many previous studies of GCM hydrology schemes point to fractional wetting as an influential parameter. Better treatment of this parameter has the potential to substantially improve GCM climate simulations, possibly to a level at which they may be used to study global and regional hydrology.

In Chapter 2, a conditional probability approach is utilized to derive a methodology for accurately estimating the fractional wetting parameter over fixed land surface areas. This method uses long term hourly station precipitation measurements as the data source, and a correction procedure is included to account for the possibility of sparse data within the land area. This methodology is applied to 39 rectangular land surface areas corresponding to the GISS 4°x5° GCM grid areas over the contiguous United States, since the required precipitation data is readily available over this region. A monthly fractional wetting climatology is produced which contains noticeable seasonal and regional variations that conform to expected characteristics. The mean value over all grids and months is .082, which is significantly lower than prescribed values used in previous studies. This result confirms the speculation that

the current practice of prescribing a uniform value of $\bar{\kappa}$ over all GCM grid areas is an invalid simplification. A monte-carlo simulation study is also conducted to verify the validity of the derived methodology.

The influence of these observed fractional wetting variations is investigated within a variety of environments in Chapter 3. Off-line analyses of the *Entekhabi and Eagleson* [1989] land surface hydrology parameterization, which incorporates $\bar{\kappa}$, indicate that the runoff ratio R is extremely sensitive to $\bar{\kappa}$ in the climatologically expected range of relevant parameter values. Other parameters such as grid average precipitation intensity and surface soil saturation are also found to be influential to R.

Simulations using a one-dimensional climate model designed for hydrologic screening are performed, and they reveal a complex relationship between $\bar{\kappa}$ and simulated climate filled with interactions, nonlinearities and feedbacks. A perpetual-day version of the screening model is utilized to perform a sensitivity analysis on $\bar{\kappa}$, within the expected range of .02-.18. Two negative feedback processes are hypothesized that inhibit the functional relationship between $\bar{\kappa}$ and R. One involves a change in the precipitation forcing generated by the model, and the other involves a change in the surface soil saturation. The impact of these negative feedbacks increases in magnitude as $\bar{\kappa}$ values decrease.

Seasonally varying simulations are conducted which study the influence of realistic monthly fractional wetting variations on simulated climate. Only the soil saturation feedback is observed in this environment, due to the constantly changing conditions which prevent the precipitation forcing from reaching an equilibrium with altered $\bar{\kappa}$ values. However, other limiting factors are identified at the land surface which also serve to inhibit the influence of small $\bar{\kappa}$ values. Two such factors are the physical soil moisture limitations at low saturation values, and the realistically parameterized, nonlinear relationship between soil saturation and evaporation.

The net result of these interactions and feedbacks is a "linearization" of the $\bar{\kappa}$-R relationship in the screening model. A smooth, sinusoidal monthly variation in $\bar{\kappa}$ about an annual mean of .08 affects the monthly R cycle in a similar manner, with

decreases in $\bar{\kappa}$ producing increases in R. However, land surface parameters that react to R, such as soil saturation and evaporation, are seen to respond more strongly to months with increases in $\bar{\kappa}$ than in months with decreases. Surface sensible and latent heat fluxes react similarly, since the moisture and heat budgets are coupled through evaporation. More remote parameters like surface temperatures and precipitation are not directly affected. Instead, the seasonal variations in $\bar{\kappa}$ lead to cooler temperatures and increased precipitation over most of the year, which reflect an overall increase in $\bar{\kappa}$.

The screening model simulations produce clear, patterned, physically-based hydrologic and climatic responses to seasonal fractional wetting variations. These results justify the investigation in Chapter 4 of observed regional and seasonal $\bar{\kappa}$ variations in a full GCM, using the actual monthly $\bar{\kappa}$ values that were estimated over the contiguous U.S. Seasonal variations in this environment produce a land surface response that is similar to the screening model in many respects, and results in cooler temperatures and wetter soils. The direct monthly response to $\bar{\kappa}$ changes by land surface parameters is clouded however by the increased climatic variability contained in GCMs and the limited duration of the GCM simulations. In addition, physical processes not modeled by the screening model, such as snowfall and snowmelt, lead to some discrepancies between screening model and GCM results.

Regional variations in fractional wetting do not produce corresponding grid scale changes in R. Seasonal variations in $\bar{\kappa}$ within each grid and spatial interaction between adjacent atmospheric columns lead to a much more complex relationship. This intricate response produces three distinct regions over the U.S. that share similar responses by R and land surface parameters. Temperature and precipitation responses do not portray these regions, since they are more remotely related to $\bar{\kappa}$, and are subject to atmospheric mixing. Another interesting result is that most grids exhibit a decrease in temperature and an increase in soil saturation in response to these spatial $\bar{\kappa}$ variations. Indeed, all climate simulations share this general behavior, especially for temperature. Therefore, it can be concluded that the introduction of realistic fractional wetting values containing regional and seasonal variability results in a

slightly cooler and wetter climate.

A second objective of this work, pursued in Section 4.3, is to critically assess observational data sets that are used for GCM validation. An important factor concerning precipitation data is the gridding of raingage data. Data sets that bin the station data into smaller groups before averaging over a large area produce different mean areal values than sets that are not binned. Since GCMs produce values for individual grid areas, binned data is more applicable and should be used for validation. Another important point is that raingages usually underestimate precipitation, especially under conditions of wind or snow. Thus raingages may contain a negative bias that could influence the validation of GCM simulations.

Runoff data sets can exhibit a tremendous bias based on the locations of streamflow gages used. Streamgage measurements taken at the outlet of major rivers are subject to substantial upstream diversions and regulation, which reduces the streamflow and thus underestimates the true runoff generated at the landsurface. Data from smaller rivers devoid of such human interventions are shown to produce much higher runoff depths. This undisturbed data is more applicable to GCM simulations, since the models only parameterize the physical response at the land surface.

Data quantity is also an important issue for any parameter, especially when using point measurements to obtain average values over a large area. This factor becomes even more important when validations are conducted at the grid scale. Validating at larger regional or continental scales allows for the suppressing of errors induced by poor or sparse data in an individual grid. Positive and negative biases are demonstrated that result from sparse or unevenly distributed streamgage networks within a grid area. For many grids this leads to unrealistically high or low runoff values. For a few grids a large positive bias is produced which leads to the violation of basic mass balance principles.

In general, all data sets contain errors or other insufficiencies that prevent them from being perfectly compatible with GCM simulated parameters. Therefore care must be taken when selecting data sets for GCM validation exercises, and each set must be critically analyzed to determine its limitations. Validations should be

160

performed using a variety of data sets whenever possible.

The validation exercises performed here clearly demonstrate how different data sets can result in different interpretations of the simulated climate. This is particularly true for surface runoff, where a large discrepancy in observed runoff exists in the Colorado River Basin, since this river is subject to significant diversions and regulation. Precipitation data sets on the other hand appear to vary very little relative to the changes induced by different simulations.

GCM validations of annual values over the entire contiguous United States are reasonably successful, which is in agreement with previous studies. Unfortunately, validation at finer scales applicable to global and regional hydrology are not as successful. Annual cycles and spatial patterns of many relevant parameters do not agree with observed values. Precipitation and evaporation simulations are generally poor, while runoff and runoff ratio results are mixed. Surface air temperature is the only parameter found to reproduce observed values consistently, but it is not directly related to land surface hydrology or fractional wetting. However, these discrepancies may be due to errors in the observed data as much as to problems with the GCM simulations.

Finally, although realistic variations in fractional wetting are shown to have a clear and explainable effect on simulated climate, even in a GCM environment, the magnitude of the induced changes is very small. These changes are barely noticeable in the validation of annual cycles presented in Section 4.4.3. For almost all parameters, $\bar{\kappa}$ has virtually no impact on the shape of the simulated annual cycle, and does not lead to improved reproduction of the observations. The only exception is seen in the runoff ratio; for this parameter the amplitude of the annual cycle is magnified, but it still fails to capture the main features of the observed cycle. The same negligible impact is seen in the grid-scale validation of Section 4.4.4. Spatial parameter characteisrtics are unaltered, and no improvement towards observations can be identified.

5.2 Discussion

The preceding research has clearly demonstrated the role of fractional wetting in the atmospheric General Circulation Model hydrologic processes. Realistic regional and seasonal variations in $\bar{\kappa}$ are found to have identifiable impacts on simulated hydrologic and climatic parameters. However, the magnitude of these impacts is not large enough to produce substantial changes in the overall climate or its regional or seasonal patterns. Consequently, detailed $\bar{\kappa}$ variability over individual grids and months may not be necessary in GCMs. Values representing larger, climatically similar regions and three month seasons may be sufficient.

However, one should not discount the influence of $\bar{\kappa}$ variations entirely. This analysis was limited to the contiguous United States due to data availability constraints. On a global scale, this region has fairly consistent climatic characteristics dominated by moderate temperatures, seasonalities, and prevailing westerly winds. Yet clear and physically reasonable variations are detected over this region. Other regions of the globe have substantially different climates, e.g. tropical rainforests or areas with distinct wet and dry seasons. Different $\bar{\kappa}$ values are certainly expected in these regions. Considering the wide range of spatial and temporal climatic characteristics present throughout the world, one would definitely expect a much wider range of fractional wetting values than that obtained here over the contiguous United States.

Over the course of the GCM validation exercises, a number of deficiencies were detected in the GCM simulations irrelevant of fractional wetting or the land surface hydrology parameterization. In particular, the moist-convection and snowfall/snowmelt parameterizations employed by the GISS GCM have been identified as being in need of improvement. Many problems with the validation of land surface parameters can be traced to summer months and the southeast U.S., where moist-convective precipitation dominates. If the precipitation forcing is inaccurate, it will lead to errors in the surface fluxes that are not due to the land surface partitioning of precipitation.

162

Many of the errors seen in simulated surface runoff correspond to grids and months in which snowmelt is substantial. Surface snowpack can have a substantial influence on surface fluxes, since it provides an additional reservoir for evaporation and increases the surface albedo. Also, melted snow is partitioned into infiltration and runoff in a different manner than precipitation events, since the infiltration capacity is rarely exceeded. Unfortunately, the processes of snowfall, snowpack evolution, and snowmelt are currently parameterized very crudely in GCMs. It clearly must receive additional attention and improved treatment if the GCM land surface-atmosphere boundary is to be faithfully represented in GCMs.

Improved treatment of these and other processes will lead to more successful validation of GCMs, particularly at more detailed monthly and grid area scales. However, the fine scale validation exercises conducted here have also demonstrated the need for improvement in validation data sets. Dense, high quality and long term data networks are required; observational errors caused by sparse or otherwise poor data is also detrimental to successful model validation. Substantial improvements are needed in both GCM parameterizations and observational data sets before GCMs can be validated at a scale useful to global and regional hydrology.

5.3   Suggestions for Future Research

It is apparent from this work that further improvements in atmospheric GCMs can best be obtained by improvements in the moist-convection and snowfall/snowmelt parameterizations, and not by detailed investigations of parameters involving the runoff ratio at the land surface. A number of potential future research directions concerning fractional wetting are nonetheless worth mentioning, since $\bar{\kappa}$ variations may still be influential on a global scale. Also, fractional wetting has other applications outside of GCMs. For example, it can be useful in aggregating or disaggregating various data sources to produce spatial storm structure characteristics.

As mentioned earlier, $\bar{\kappa}$ can be obtained on a global scale; if not for individual grids and months then for larger regions and seasons. A global data $\bar{\kappa}$ climatology

would have many uses, but its determination is limited by the absence of the required precipitation data over much of the world. However, it may be possible to correlate $\bar{\kappa}$ calculated in regions with sufficient precipitation data to other more readily quantifiable climatic characteristics. This analogy can then be used to approximate $\bar{\kappa}$ in other regions that share these climatic characteristics.

Extended GCM simulations would improve upon the analysis of $\bar{\kappa}$ effects by providing increased statistical reliability. Many of the simulation features, or lack of features, were attributed to statistical noise, and may be eliminated with longer runs. An alternative is to develop significance tests applicable to limited duration runs. This could potentially allow modelers to determine the length of a simulation needed to produce significant results prior to the run. Reliable significance tests would also eliminate some of the ambiguity and skepticism currently associated with GCMs.

Statistical tests can also be developed and applied to the $\bar{\kappa}$ estimation procedure. Although the values estimated in Chapter 2 yield clear annual cycles and spatial patterns, the range of values obtained over the U.S. is small. Although it is unlikely, statistical checks would verify that the observed patterns are not mere coincidences produced by noise.

Finally, the $\bar{\kappa}$ estimation procedure was developed for specified land surface areas. One unaccounted for consequence of this is that there are instances when a precipitation event does not occur entirely over one grid, but instead covers portions of two or three grids. Since precipitation processes in GCMs are modeled entirely within individual atmospheric columns, these "edge effects" are nonexistent in the simulations. Since the GCM grids used here are fairly large relative to typical storm sizes, this edge effect associated with the estimated $\bar{\kappa}$ values may not be significant. Nonetheless, an additional correction procedure can be derived relating fractional storm coverage over a region to mean storm area. This larger mean storm area would then be the parameter that gets implemented into the GCM, since it represents the storm area characteristics for the general region represented by the corresponding GCM grid.

164

References

Abramopoulos, F., C. Rosenzweig, and B. Choudhury, 1988: Improved ground hydrology calculations for GCMs–Soil water movement and evapotranspiration, *J. of Climate, 1(9)*, 921-941.

Avissar, R. and R. Pielke, 1989: A parameterization of heterogeneous land surfaces for atmospheric numerical models and its impact on regional meteorology, *Mon. Weather Rev., 117*, 2113-2136.

Barancourt, C., J.D. Creutin and J. Rivoirard, 1992: A method for delineating and estimating rainfall fields, *Water Resour. Res., 28(4)*, 1133–1144.

Baumgartner, A and E Reichel, 1975: *The World Water Balance*, Elsevier Scientific, New York.

Bradley Jr., A.A. and J.A. Smith, 1993: The hydrometeorological environment of extreme storms in the southern plains of the United States, *Fourth International Conference on Precipitation; Hydrological and Meteorological Aspects of Rainfall Measurement and Predictability*, Iowa City, Iowa, page 41.

Braud, I., J. D. Creutin and C. Barancourt, 1993: The relation between the mean areal rainfall and the fractional area where it rains above a given threshold, *J. Appl. Meteor., 32*, 193–202.

Carson, D.J., 1982: Current parameterizations of land surface processes in atmospheric general circulation models, *Landsurface Processes in Atmospheric General Circulation Models*, P.S. Eagleson (Ed.), Cambridge University Press, London, 67–108

Collier, C.G., 1993: The application of a continental-scale radar database to hydrological process parameterization within atmospheric general circulation models, *J. Hydrol., 142*, 301–318.

Crow, E.L., F.A. Davis and M.W. Maxfield, 1960: *Statistics Manual*, Dover, New York, 288 pages.

Dickinson, R.E., A. Henderson-Sellers, P.J. Kennedy and M.F. Wilson, 1986: *Biosphere-Atmosphere Transfer Scheme (BATS) for the NCAR Community Climate Model*, NCAR Technical Note TN-275STR, 69 pages.

Drake, A., 1967: *Fundamentals of Applied Probability*, McGraw-Hill, New York, 283 pages.

Eagleson, P.S., 1978: Climate, soil, and vegetation 2. the distribution of annual precipitation derived from observed storm sequences, *Water Resour. Res., 14(5)*, 713–721.

Eagleson, P.S., 1984: The distribution of catchment coverage by stationary rainstorms, *Water Resour. Res., 20(5)*, 581–590.

Eagleson, P.S. and W. Qinliang, 1985: Moments of catchment storm area, *Water Resour. Res., 21(8)*, 1185–1194.

Eagleson, P.S., 1986: The emergence of global-scale hydrology, *Water Resour. Res., 22(9)*, 6S–14S.

Earthinfo NCDC (National Climatic Data Center) hourly precipitation records, 1989: *Earthinfo*, Boulder, CO.

Eltahir, E.A.B. and R.L. Bras, 1993: Estimation of the fractional coverage of rainfall in climate models, *J. of Climate, 6*, 639–644.

Entekhabi, D. and P.S. Eagleson, 1989: Landsurface hydrology parameterization for atmospheric general circulation models including subgrid scale variability, *J. of Climate, 2(8)*, 816–831.

Entekhabi, D., 1994: A simple model of hydrologic cycle and climate: 1. Model construct and sensitivity to landsurface boundary, in press *Advances in Water Resources*.

Entekhabi, D., K. L. Brubaker and P.S. Eagleson, 1994: A simple model of hydrologic cycle and climate: 2. Observational evidence for the parameterization of atmospheric heat and moisture divergence, in press *Advances in Water Resources*.

Famiglietti, J.S. and E.F. Wood, 1990: Evapotranspiration and runoff from large land areas, land surface hydrology for atmospheric general circulation models, *Landsurface-atmospheric Interactions for Climate Modeling*, E.F. Wood (Ed.), Kluwer Academic Publishers, 179–205.

GARP, 1975: The physical basis of climate and climate modeling, *GARP Publication Series No. 16*, WMO/ICSU, Geneva.

Guetter, A.K. and K.P. Georgakakos, 1993: River outflow of the conterminous United States, 1939–1988, *Bulletin of the American Meteorological Society, 74(10)*, 1873–1891.

Gupta, V.K. and E.C. Waymire, 1993: A statistical analysis of mesoscale rainfall as a random cascade, *J. Appl. Meteor., 32*, 251–267.

Hansen, J., G. Russell, D. Rind, P. Stone, A. Lacis, S. Lebedeff, R. Ruedy and L. Travis, 1983: Efficient three-dimensional global models for climate studies: models I and II, *Monthly Weather Review, 111(4)*, 609–662.

Henderson-Sellers, A. and K. McGuffie, 1987: *A Climate Modeling Primer*, J. Wiley and Sons, New York, 217 pages.

Henning, D., 1989: *Atlas of the Surface Heat Balance of the Continents*. Gebruder Borntraeger, 402 pages.

Hoffman, R.N., 1981: A computer program which calculates radiative fluxes and heating rates in model atmospheres, *Scientific Report No. 4, Project for the Study of Climatic Fluctuations, Volcanic Aerosols and Carbon Dioxide Changes* Department of Meteorology and Physical Oceanography, Massachusetts Institute of Technology, 124 pages.

Johnson, K.D., D. Entekhabi and P.S. Eagleson, 1993: The implementation and validation of improved land surface hydrology in an atmospheric general circulation model, *J. of Climate, 6(7)*, in press.

Koster, R.D. and M.J. Suarez, 1992: Modeling the land surface boundary in climate models as a composite of independent vegetation stands, *J. Geophys. Res., 97*, 2697–2715.

Legates, D.R. and C.J. Willmott, 1990: Mean seasonal and spatial variability in global surface air temperature, *Theo. Appl. Climatol., 41*, 11–21.

Lopez, R.E., D. Atlas, D. Rosenfield, J.L. Thomas, D.O. Blanchard and R.L. Holle, 1989: Estimation of areal rainfall using the radar echo area time integral, *J. Appl. Meteor., 28*, 1162–1175.

Pitman, A.J., A. Henderson-Sellers and Z.L. Yang, 1990: Sensitivity of regional climates to localized precipitation in global models, *Nature, 346(23)*, 734–737.

Roads, J.O., S.C. Chen, A.K. Guetter and K.P. Georgakakos, 1993: Large-scale aspects of the United States hydrologic cycle, *Bulletin of the American Meteorological Society*, in press.

Russell, G.L. and J.R. Miller, 1990: Global river runoff calculated from a global atmospheric general circulation model, *Journal of Hydrology, 117,* 2414–254.

Schneider, S.H., and R.E. Dickinson, 1974: Climat Modeling, *Reviews of Geophysics and Space Physics, 12(3),* 447–493.

Sellers, P.J., Y. Mintz, Y.C. Sud and A. Delcher, 1986: A simple biosphere model (SiB) for use within general circulation models, *J. Atmos. Sci., 43(6),* 505–531.

Thomas, G. and A. Henderson-Sellers, 1991: An evaluation of proposed representations of subgrid hydrologic processes in climate models, *J. of Climate, 4,* 898–910.

Wallis, J.R., D.P. Lettenmaier and E.F. Wood, 1990: A daily hydro-climatological data set for the continental U.S., *IBM Reasearch Report RC 16607 (#70451),* 20 pages.

Wang, W.C., and P.H. Stone, 1980: Effect of ice-albedo feedback on global sensitivity in a one-dimensional radiative-convective climate model, *J. of Atmospheric Sciences, 37,* 545–552.

Warrilow, D.A., A.B. Sangster and A. Slingo, 1986: Modeling of land surface processes and their influence on European climate, DCTN 38, Dynamical Climatology, Meteorological Office, Bracknell, Berkshire, 92 pages.

Waymire, E. and V.K. Gupta, 1981: The mathematical structure of rainfall representations 1. A review of the stochastic rainfall models, *Water Resour. Res., 17(5),* 1261–1272.

Appendix A

Estimated Fractional Wetting Values over the Contiguous United States

The fractional wetting climatology over the contiguous United States developed in Chapter 2 is presented here. Monthly $\bar{\kappa}$ values for each of 39 U.S. grids are shown as 12 GCM grid area maps, one for each month.

FRACTIONAL WETTING: JANUARY
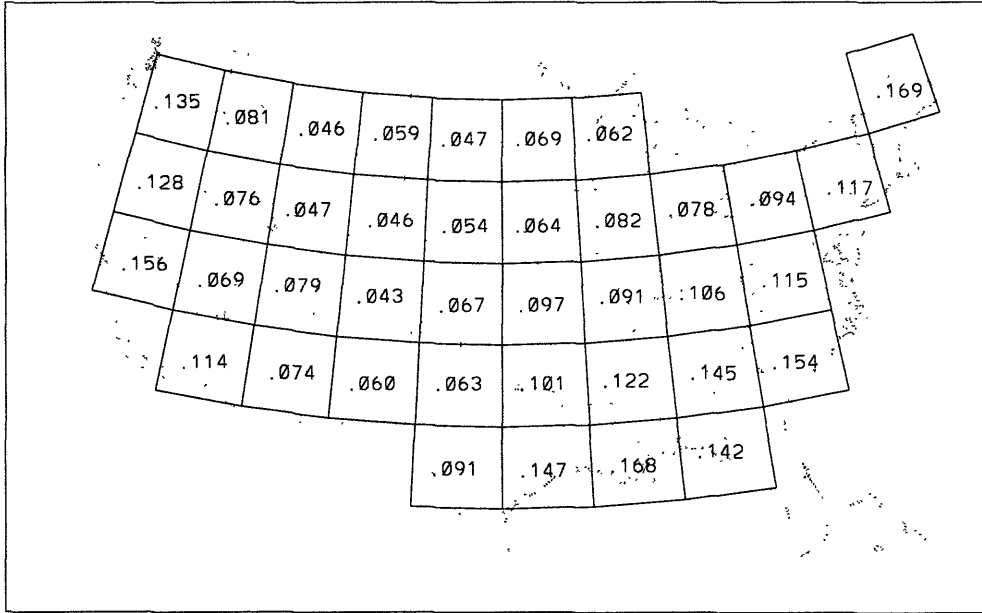
FRACTIONAL WETTING: FEBRUARY
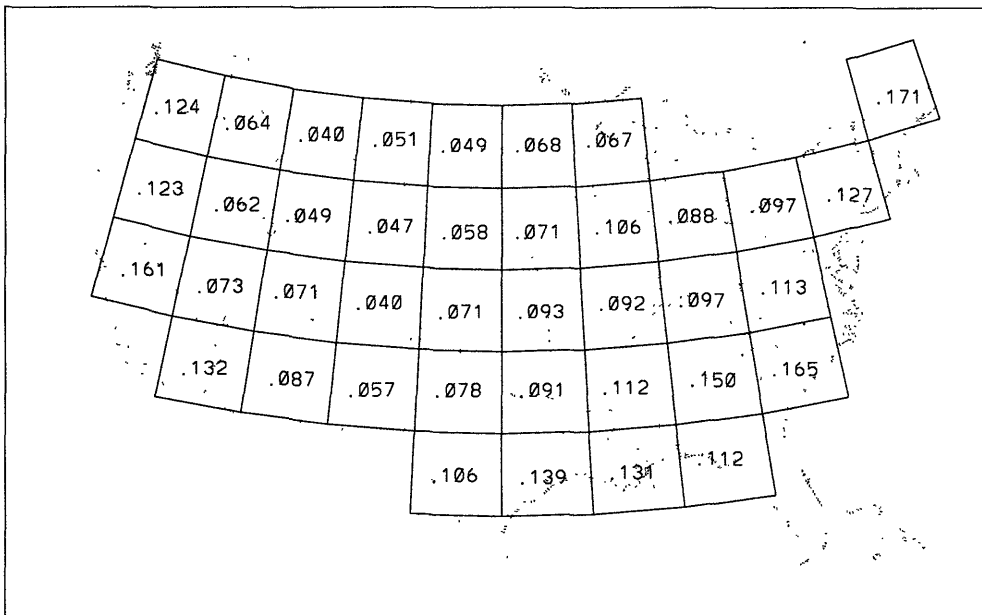
Figure A-1: GCM grid area maps over the contiguous United States showing estimated fractional wetting values for January and February

170

FRACTIONAL WETTING: MARCH
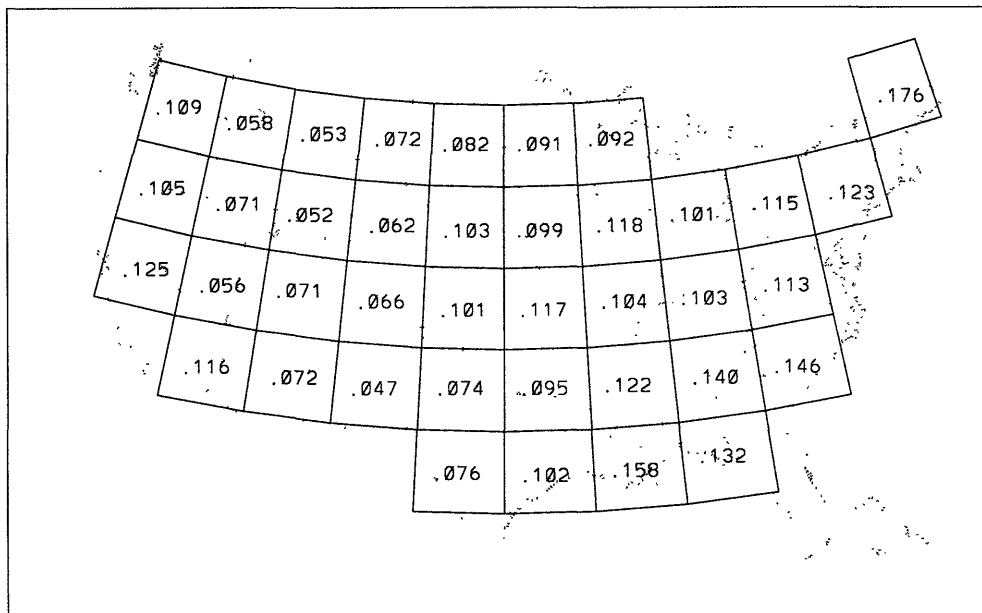
FRACTIONAL WETTING: APRIL
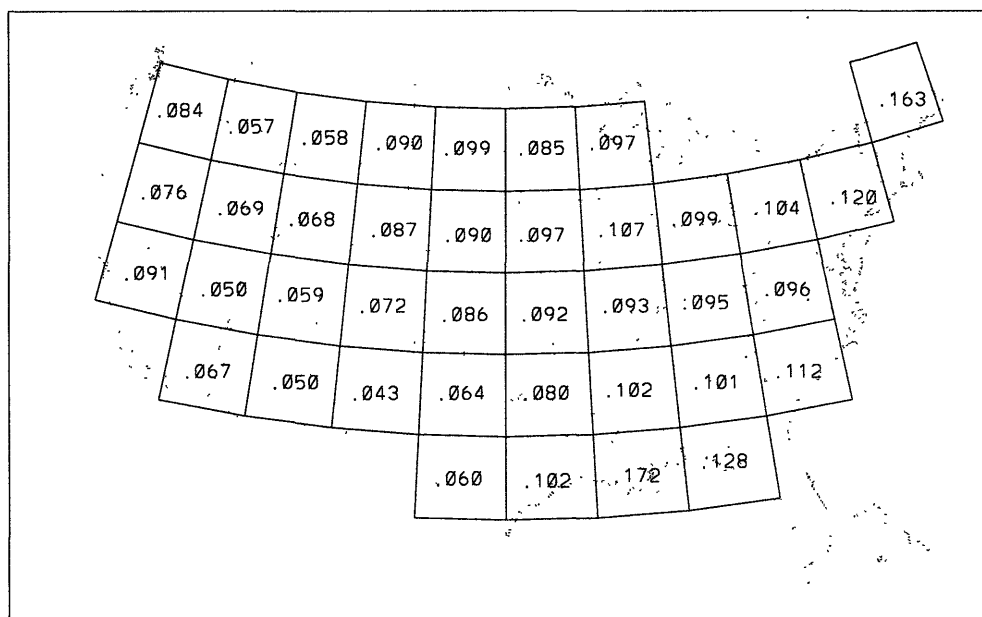
Figure A-2: GCM grid area maps over the contiguous United States showing estimated fractional wetting values for March and April

171

FRACTIONAL WETTING: MAY
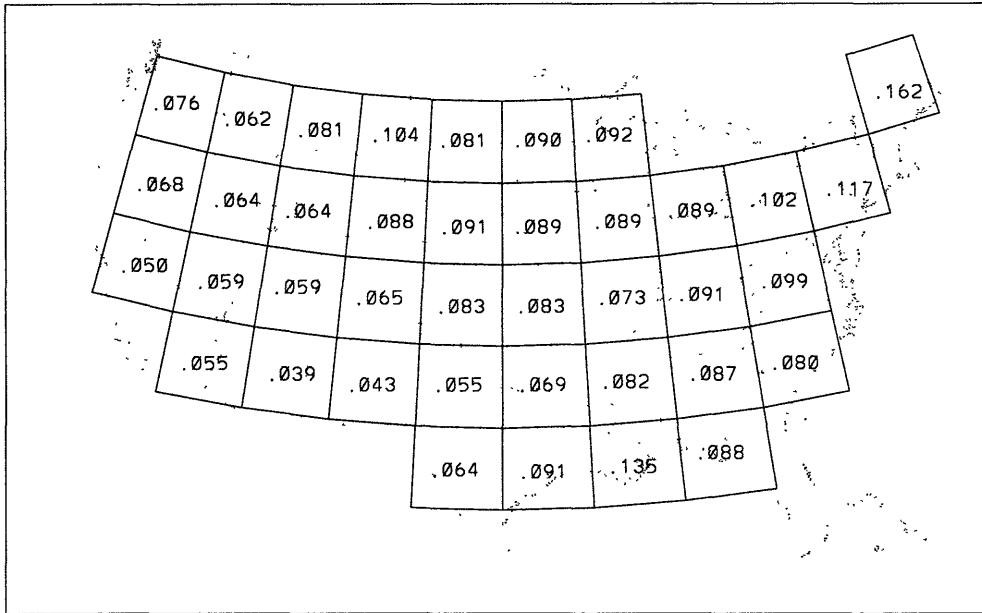
FRACTIONAL WETTING: JUNE
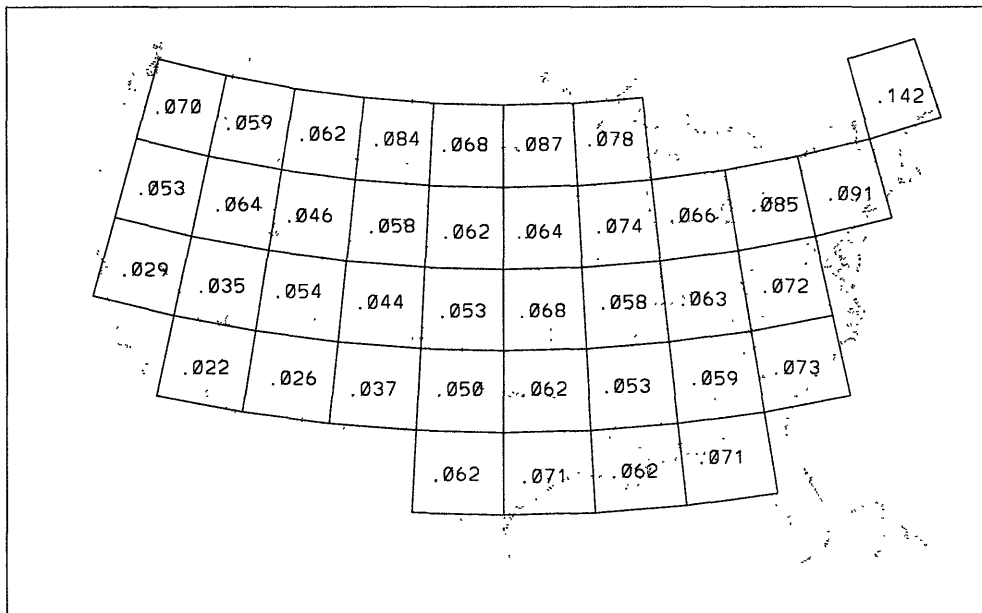
Figure A-3: GCM grid area maps over the contiguous United States showing esti-
mated fractional wetting values for May and June

172

FRACTIONAL WETTING: JULY
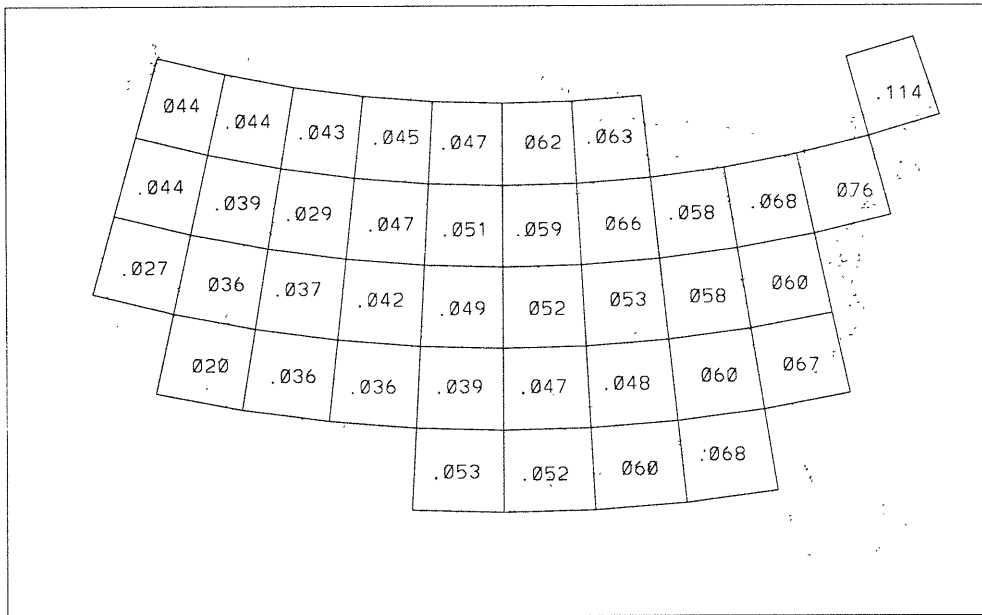
FRACTIONAL WETTING: AUGUST
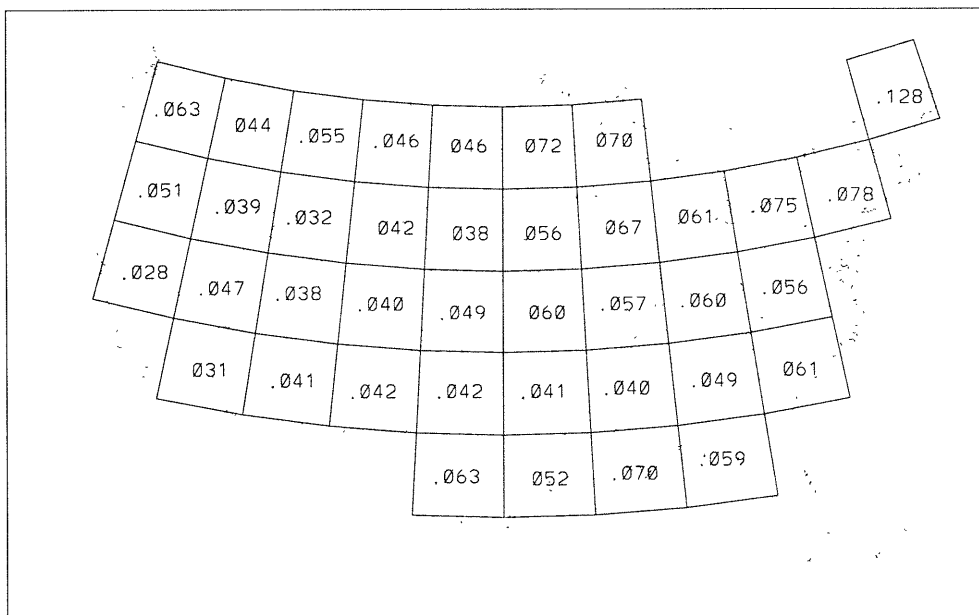
Figure A-4: GCM grid area maps over the contiguous United States showing estimated fractional wetting values for July and August

173

FRACTIONAL WETTING: SEPTEMBER
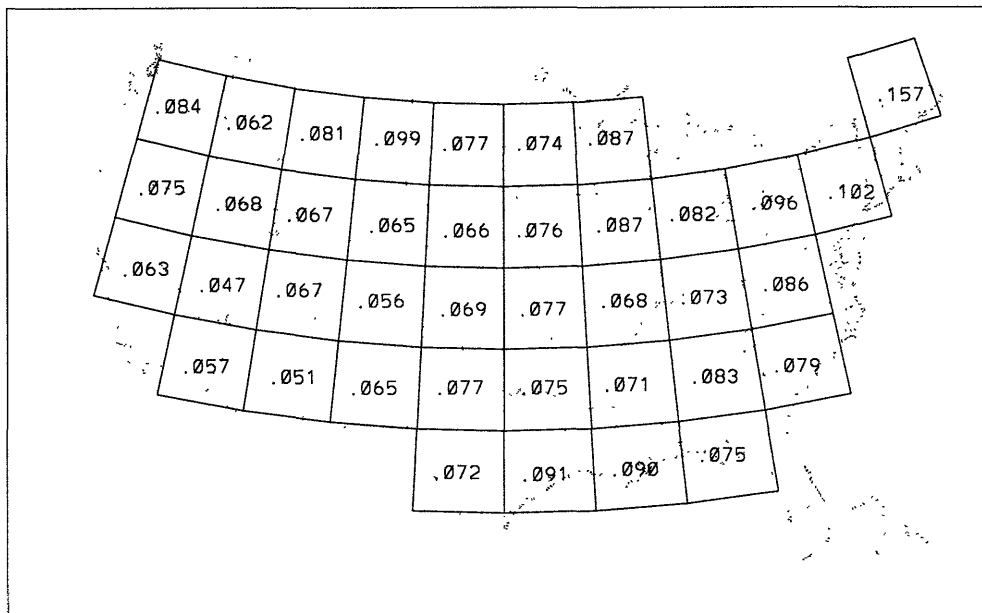
FRACTIONAL WETTING: OCTOBER
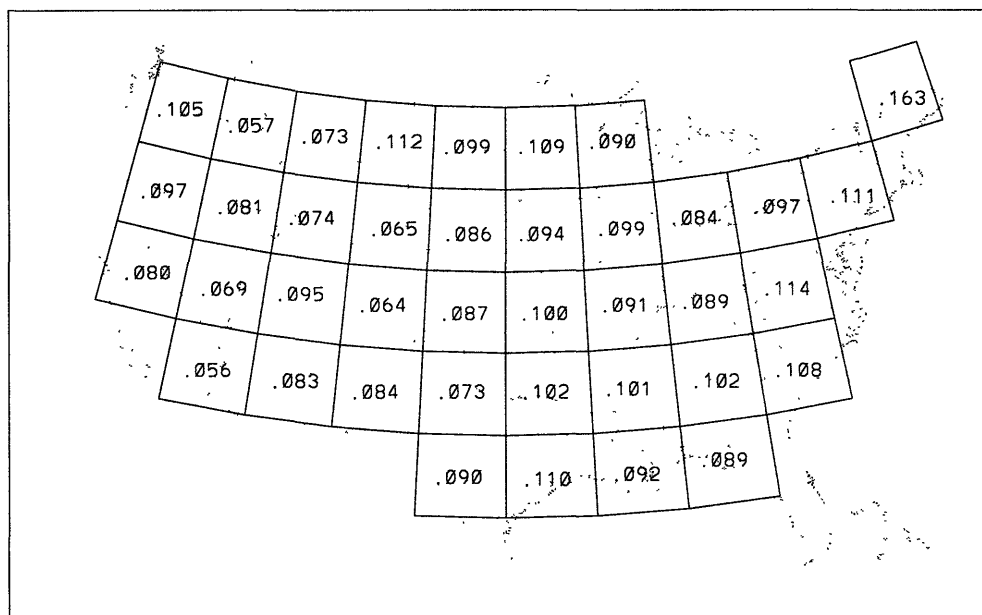
Figure A-5: GCM grid area maps over the contiguous United States showing esti-
mated fractional wetting values for September and October

FRACTIONAL WETTING: NOVEMBER

.128 .066 .048 .064 .058 .089 .083 .175
.119 .077 .054 .070 .092 .098 .114 .105 .111 .117
.120 .061 .082 .059 .102 .121 .113 .115 .113
.110 .097 .065 .075 .103 .120 .121 .118
.096 .122 .147 .110
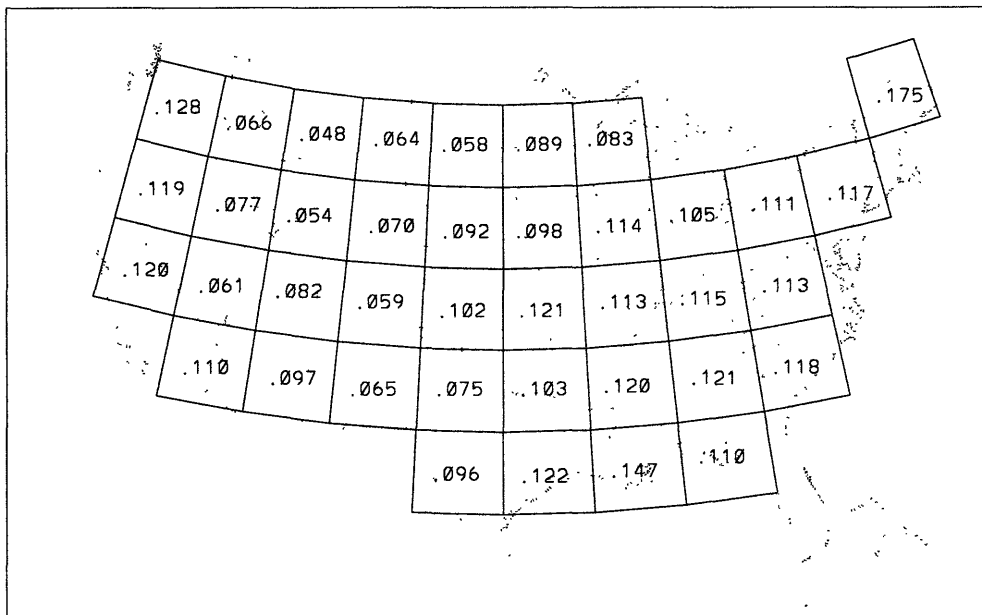
FRACTIONAL WETTING: DECEMBER

.146 .074 .043 .056 .047 .068 .072 .186
.127 .075 .051 .048 .060 .074 .108 .105 .109 .117
.127 .055 .079 .052 .085 .111 .119 .099 .111
.117 .090 .070 .080 .110 .126 .142 .148
.087 .130 .190 .128
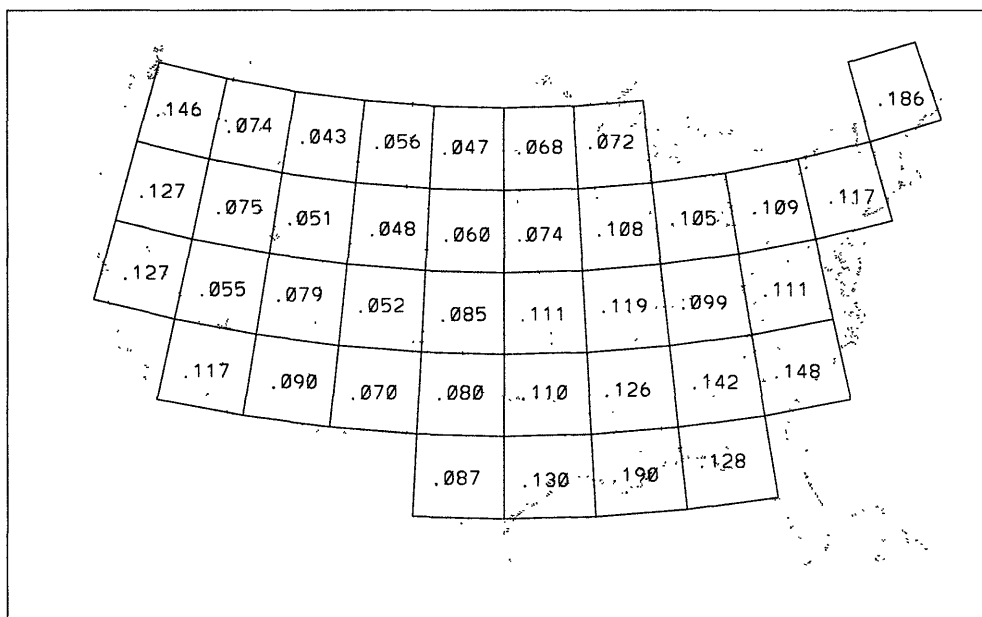
Figure A-6: GCM grid area maps over the contiguous United States showing estimated fractional wetting values for November and December .

175

Appendix B

Heat Conduction Through Three Soil Layers

Heat conduction through three soil layers in the screening model is achieved by assuming ground temperature to be a quadratic function of depth through the entire soil column, as depicted in Figure B-1. The origin of the vertical coordinate system is located between the top and middle layers for computational simplicity. The depth of each soil layer is prescribed, hence z_1, z_2 and z_3 are known. General temperature functions for each layer can be written:

$$T_1(z) = a_1 z^2 + b_1 z + c_1 \tag{B.1}$$

$$T_2(z) = a_2 z^2 + b_2 z + c_2$$

$$T_3(z) = a_3 z^2 + b_3 z + c_3$$

where

$$T_1(0) = T_2(0) \tag{B.2}$$

$$T_2(-z_2) = T_3(-z_2) \tag{B.3}$$

Heat flux between adjacent layers is the temperature gradient at the interface multiplied by the soil thermal conductivity λ, assumed here to be constant at a value of
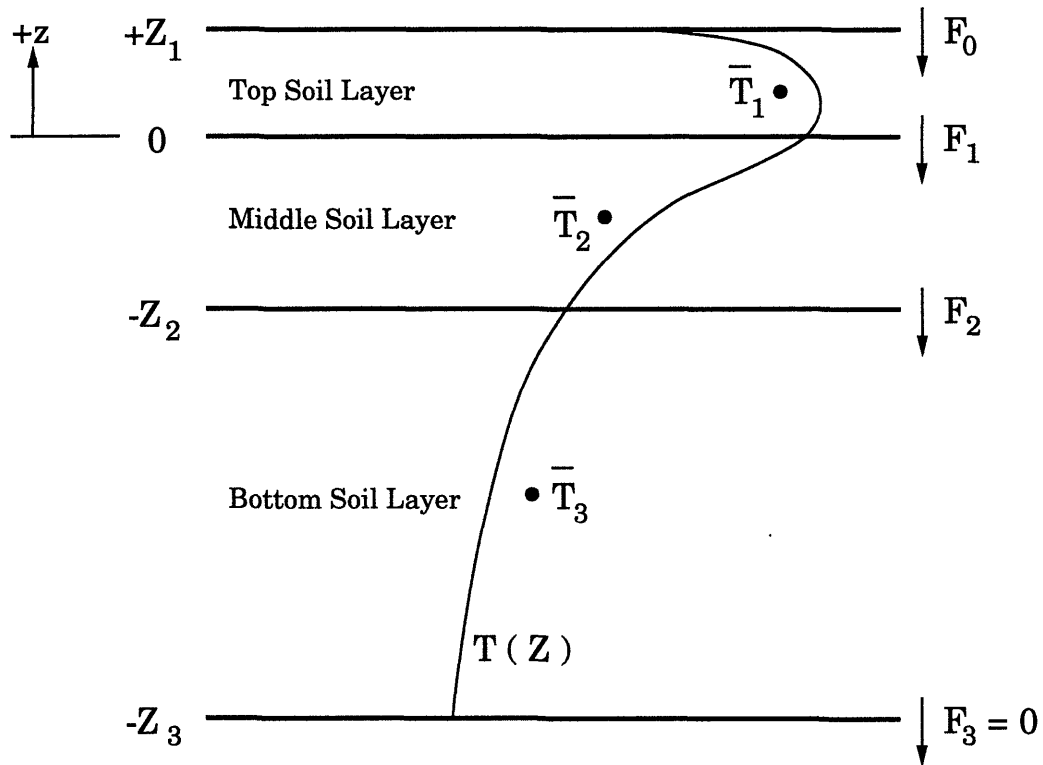
Figure B-1: Schematic representation of the three-layer soil column utilized by the screening model heat conduction parameterization, with associated heat fluxes and parabolic temperature profile.

0.42 W/mK. F_0 is the ground heat flux computed from the surface energy balance, and it is assumed that no heat flux occurs out of the bottom of the soil column ($F_3 = 0$).

$$F_0 = \lambda \frac{dT_1}{dz} \Big|_{z_1} \tag{B.4}$$

$$F_1 = \lambda \frac{dT_1}{dz} \Big|_0 = \lambda \frac{dT_2}{dz} \Big|_0 \tag{B.5}$$

$$F_2 = \lambda \frac{dT_2}{dz} \Big|_{-z_2} = \lambda \frac{dT_3}{dz} \Big|_{-z_2} \tag{B.6}$$

$$F_3 = \lambda \frac{dT_3}{dz} \Big|_{-z_3} = 0 \tag{B.7}$$

The mean temperature of each layer computed by the model is obtained by taking the integral of the temperature profile over the entire thickness of the layer, and dividing by the thickness.

$$\bar{T}_1 = \frac{1}{z_1} \int_0^{z_1} T_1 dz \tag{B.8}$$

$$\bar{T}_2 = \frac{1}{z_2} \int_{-z_2}^0 T_2 dz \tag{B.9}$$

$$\bar{T}_3 = \frac{1}{z_3 - z_2} \int_{-z_3}^{-z_2} T_3 dz \tag{B.10}$$

Equations B.2-B.10 represent nine equations which can be used to solve for the nine unknown coefficients in equation B.1. After the coefficients are determined, equations B.5 and B.6 can be used to solve for the heat flux between adjacent layers as:

$$F_1 = \lambda b_1 = \lambda b_2 \tag{B.11}$$

$$F_2 = \lambda[-2a_2 z_2 + b_2] = \lambda[-2a_3 z_2 + b_3] \tag{B.12}$$

Appendix C

Cloud Cover Parameterization in the Screening Model

The following is an abbreviated version of the screening model cloud cover parameterization as described in *Entekhabi and Eagleson* [1989]. Cloud cover at each time step is estimated using an arbitrary function that depends on temperature and humidity. It is assumed that the temperature T throughout the grid element is normally distributed in space. The mean $\bar{T}$ is the temperature maintained by the model, and the standard deviation σ_c is prescribed. The dew-point temperature T^* of the airmass can be obtained from the vapor pressure e maintained by the model using the Clausius-Clapeyron equation:

$$e = e_s(T^*) = e_{so}exp[\frac{\lambda}{R_v}(\frac{1}{T_o} - \frac{1}{T_*})]$$

(C.1)

Solving for T^*,

$$T^* = [\frac{1}{T_o} - \frac{R_v}{\lambda}log[\frac{qP}{e_{so}(\epsilon + q)}]]^{-1}$$

(C.2)

where

$$q = \frac{\epsilon e}{P - e}$$

T^* is less than $\bar{T}$ since the airmass is usually not saturated, and will approach $\bar{T}$ as atmospheric humidity increases. T^* is used as a threshold temperature for cloud cover in the grid element. Given the assumed spatial distribution for T, the fraction

179

of the grid with a temperature below T^* is considered to be the cloud fraction. In other words, the cloud fraction is equal to $F_T(T^*)$, which is the cumulative density function of the normally distributed random variable T with mean $\bar{T}$ and standard deviation σ_c, evaluated at the value T^*.

Appendix D

Annual Parameter Values for Individual GCM Grid Areas

Several primary diagnostic parameters are presented here as average annual values for individual GCM grid areas over the contiguous U.S. The parameters presented are precipitatiom, surface runoff, evaporation, runoff ratio and surface air temperature. For each parameter, four maps are presented. They represent the *Wallis et al.* [1990] observations and the three simulations SIMG, SIM1 and SIM2. For the evaporation maps, land surface evapotranspiration is shown for the observations, SIM1 and SIM2. SIMG however contains the grid area evaporation value. A discrepancy therefore occurs in grids with substantial ocean or lake coverage, since water surfaces evaporate at the much higher potential rate.

OBSERVED PRECIPITATION [cm/yr]
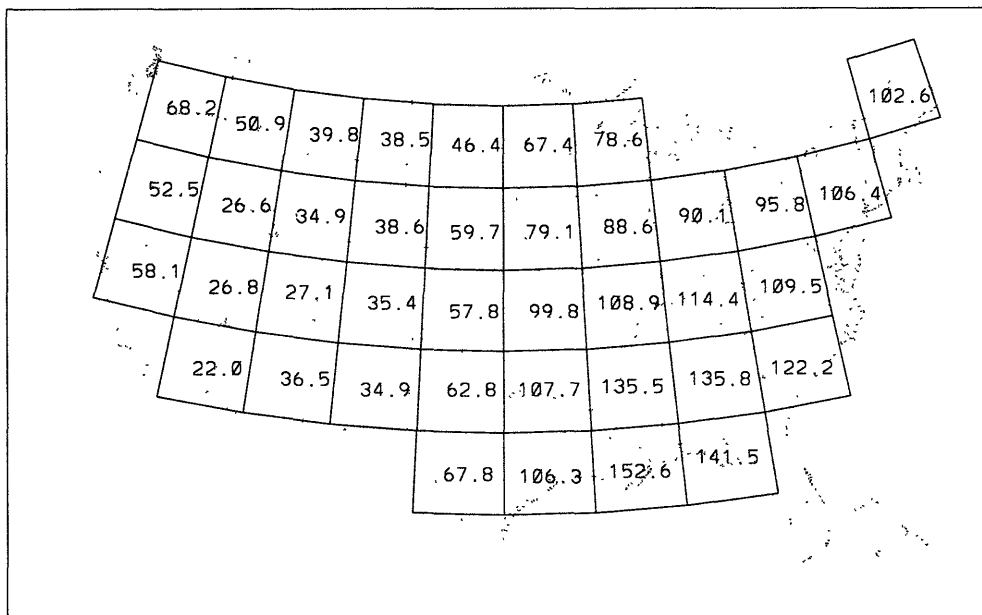
SIMG: PRECIPITATION [cm/yr]
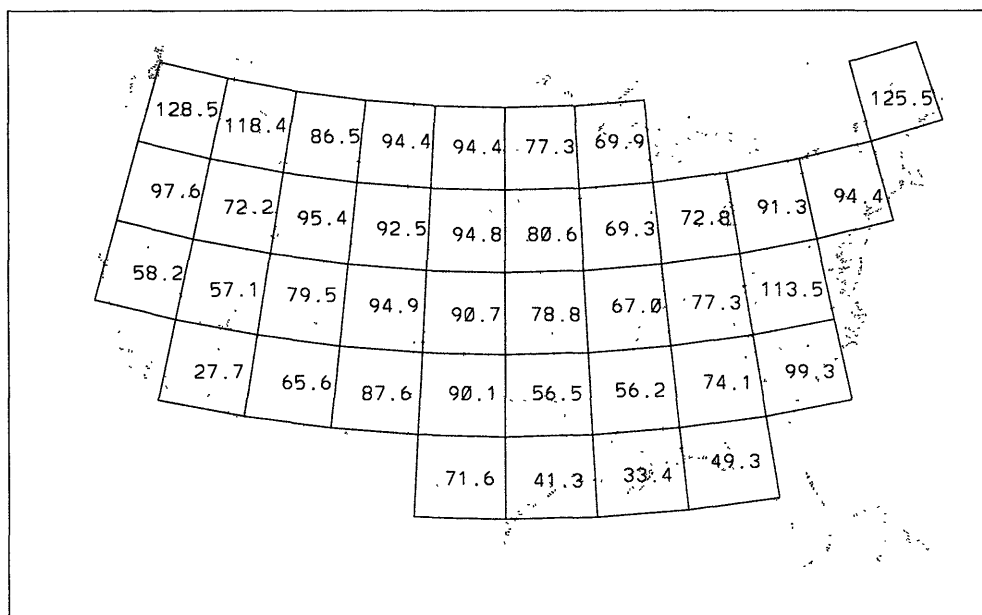
Figure D-1: GCM grid area maps over the contiguous United States showing precipitation for *Wallis et al.* [1990] observations and SIMG

SIM1: ANNUAL PRECIPTATION [cm/yr]
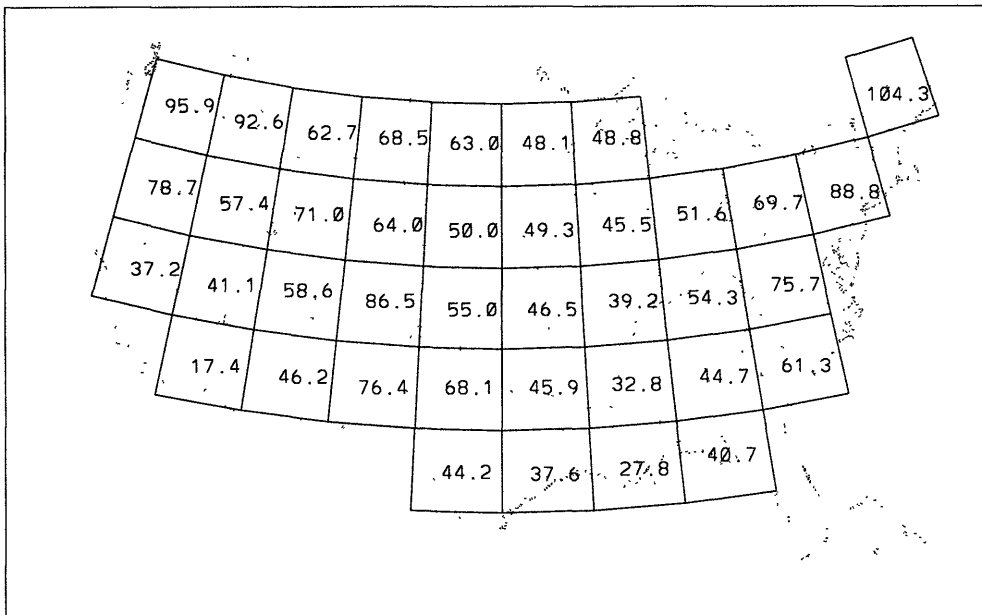
SIM2: PRECIPITATION [cm/yr]
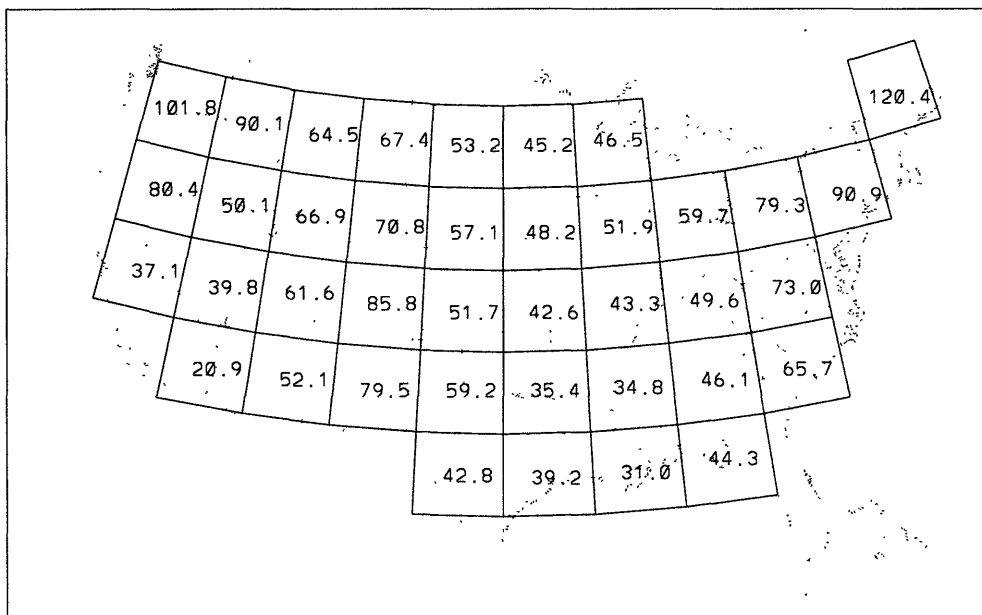
Figure D-2: GCM grid area maps over the contiguous United States showing precipitation for SIM1 and SIM2

183

OBSERVED RUNOFF [cm/yr]
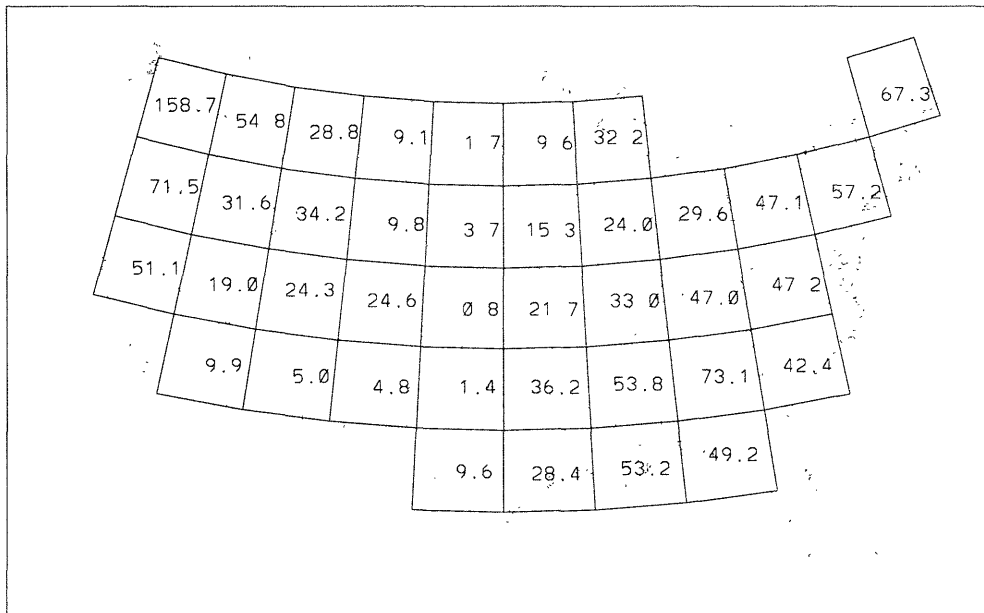
SIMG: SURFACE RUNOFF [cm/yr]
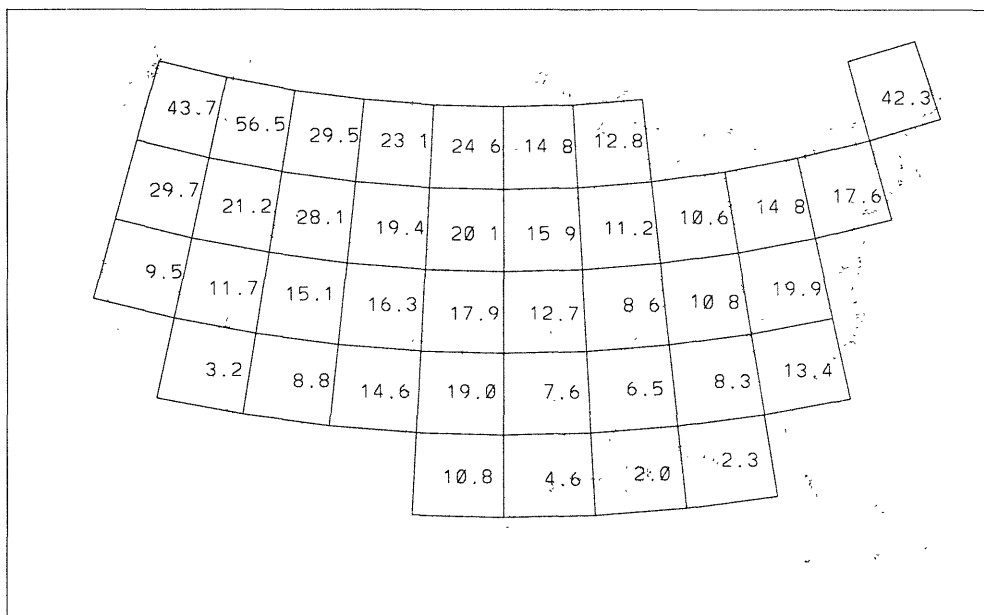
Figure D-3: GCM grid area maps over the contiguous United States showing surface runoff for *Wallis et al.* [1990] observations and SIMG

SIM1: ANNUAL SURFACE RUNOFF [cm/yr]
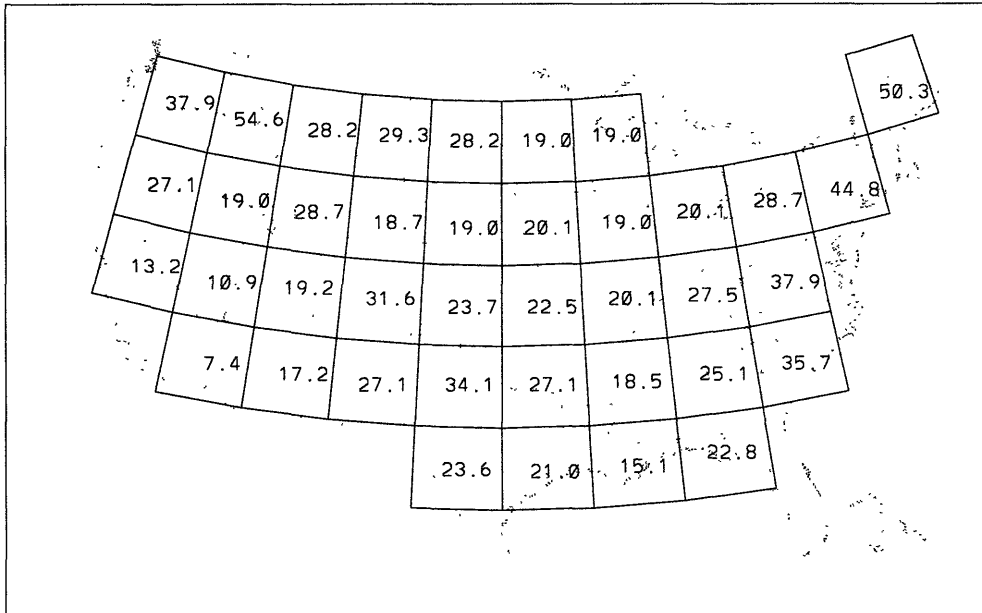
SIM2: SURFACE RUNOFF [cm/yr]
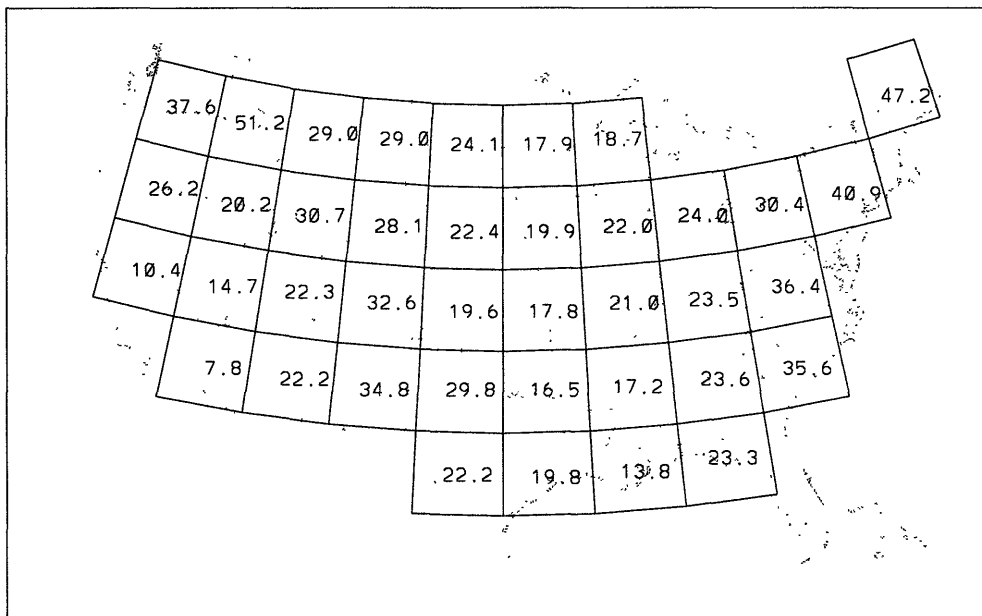
Figure D-4: GCM grid area maps over the contiguous United States showing surface
runoff for SIM1 and SIM2

OBSERVED LAND EVAPORATION [cm/yr]
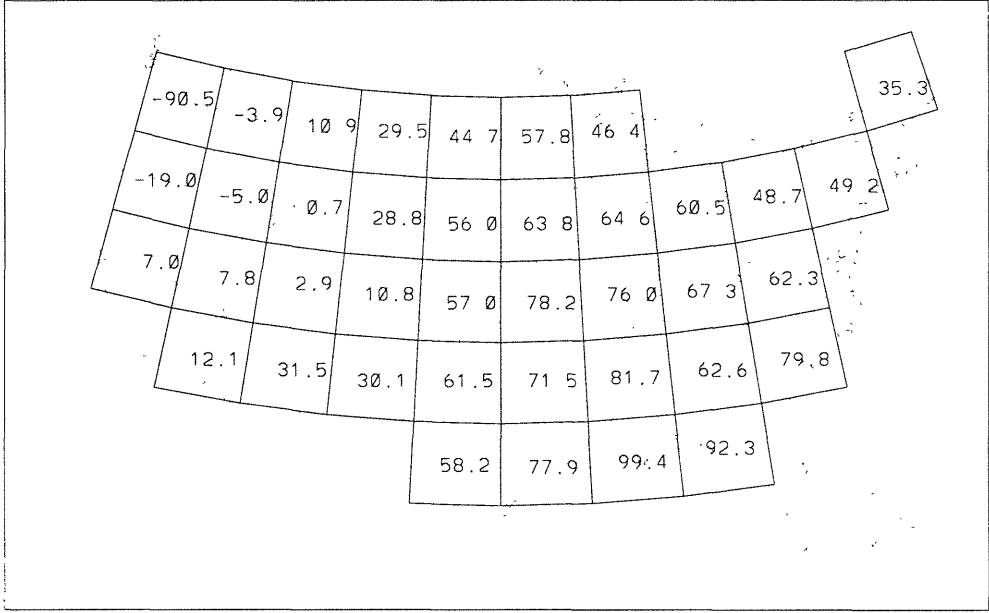
SIMG: GRID EVAPORATION [cm/yr]
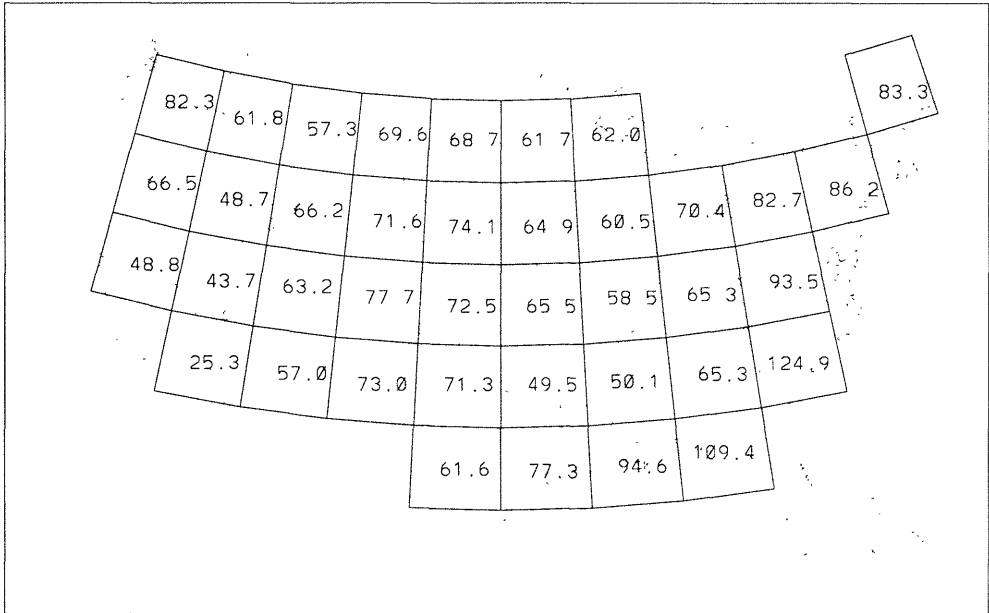
Figure D-5: GCM grid area maps over the contiguous United States showing evaporation for *Wallis et al.* [1990] observations and SIMG

186

SIM1: ANNUAL LAND SURFACE EVAP [cm/yr]
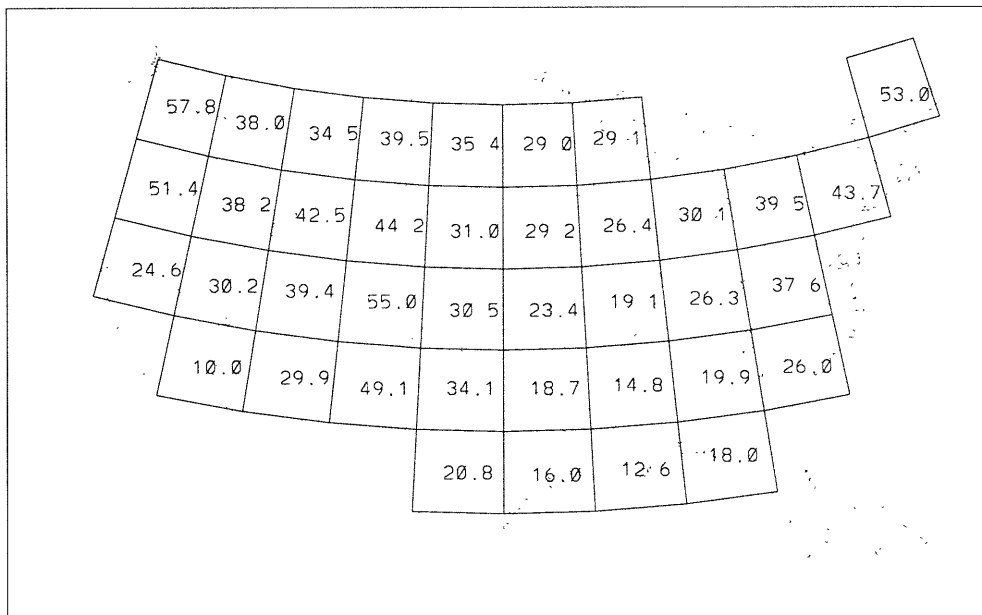
SIM2: LAND SURFACE EVAP [cm/yr]
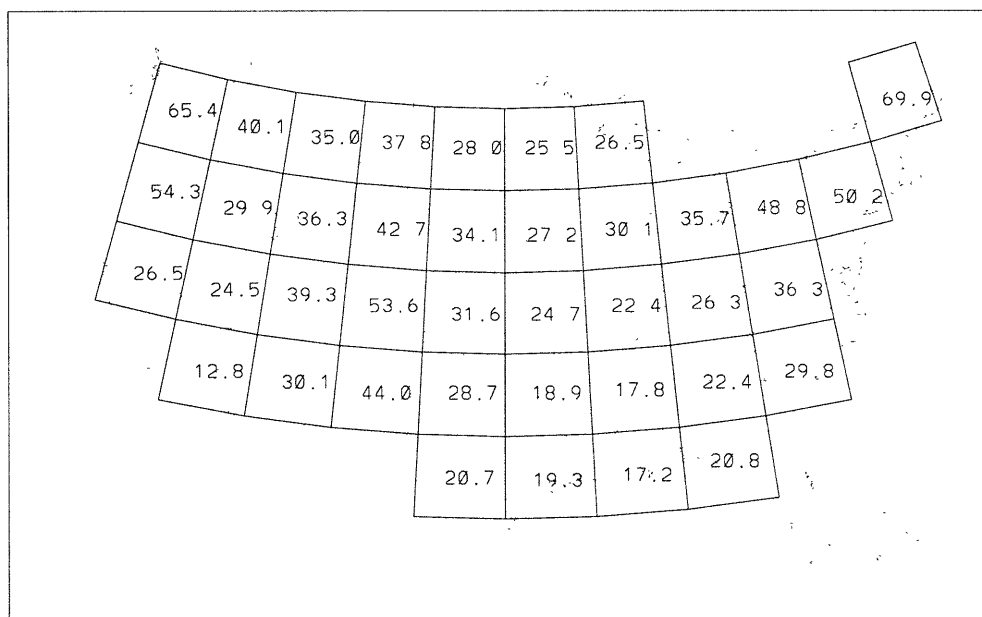
Figure D-6: GCM grid area maps over the contiguous United States showing evaporation for SIM1 and SIM2

187

OBSERVED RUNOFF RATIO [percent]
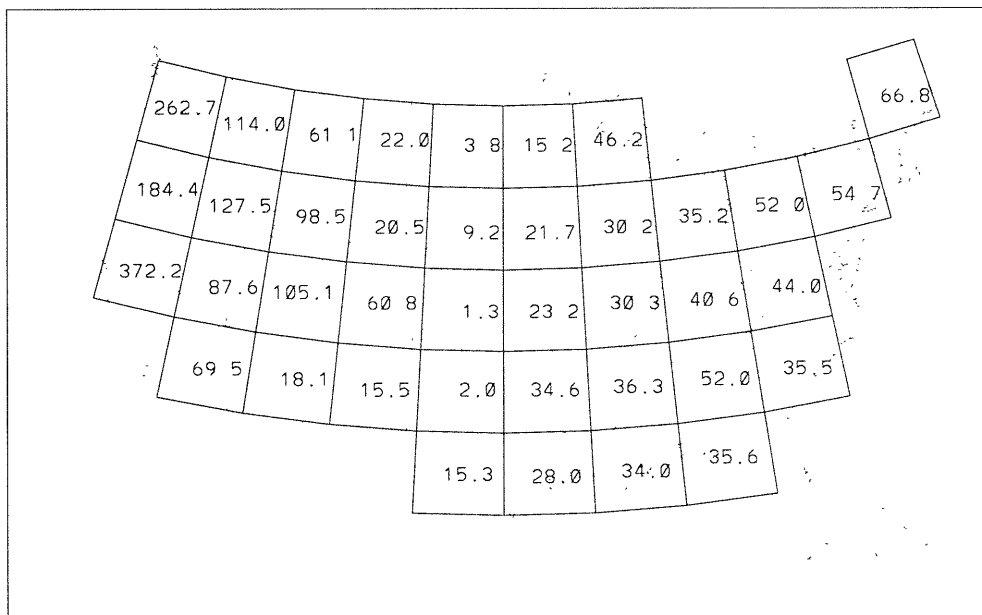
SIMG. RUNOFF RATIO [percent]
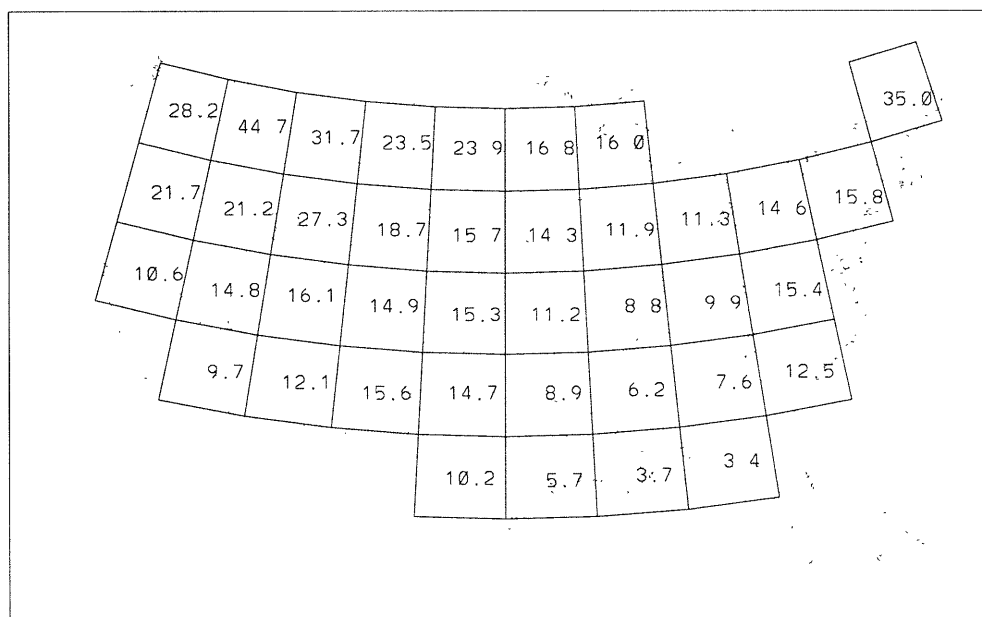
Figure D-7: GCM grid area maps over the contiguous United States showing runoff ratio for *Wallis et al.* [1990] observations and SIMG

SIM1: ANNUAL RUNOFF RATIO [percent]
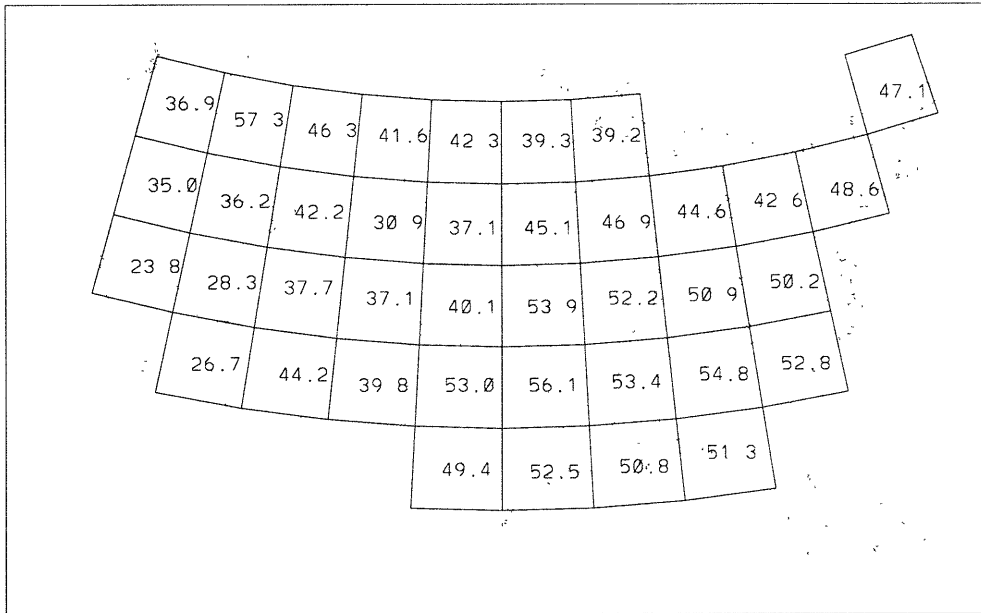
SIM2: RUNOFF RATIO [percent]
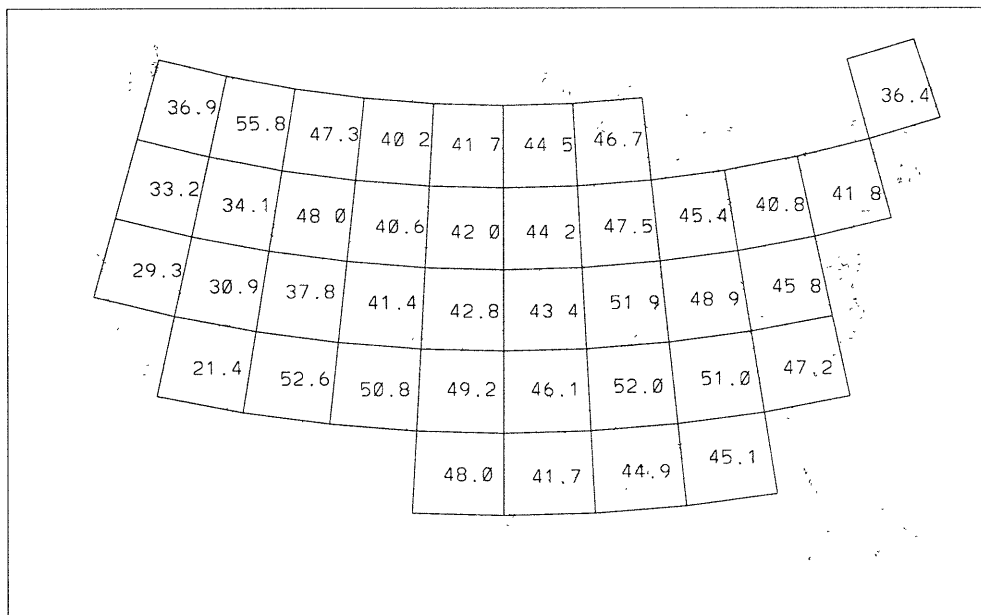
Figure D-8: GCM grid area maps over the contiguous United States showing runoff ratio for SIM1 and SIM2

OBSERVED SURFACE AIR TEMPERATURE [C]
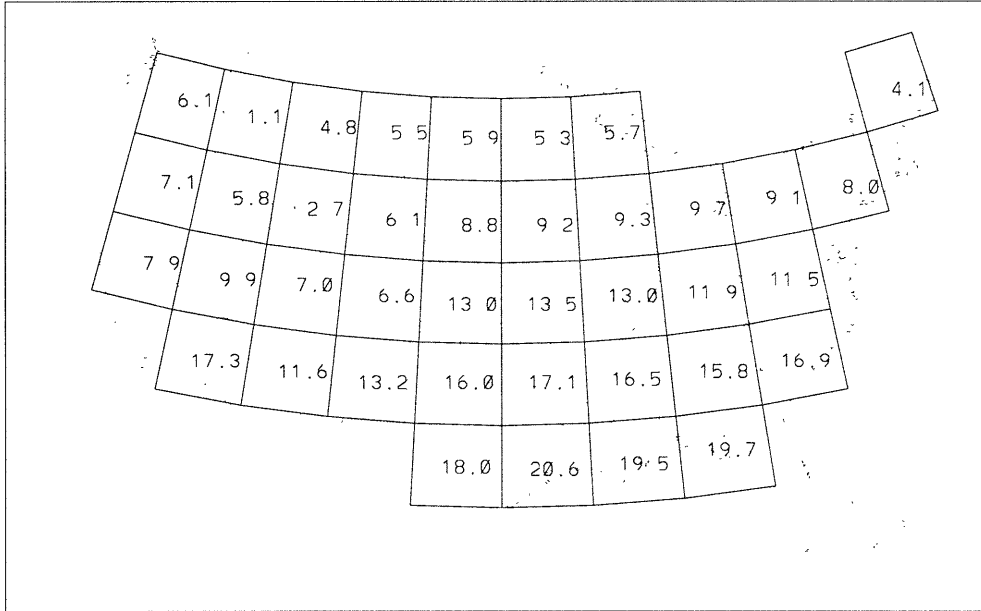
SIMG: SURFACE AIR TEMP [C]
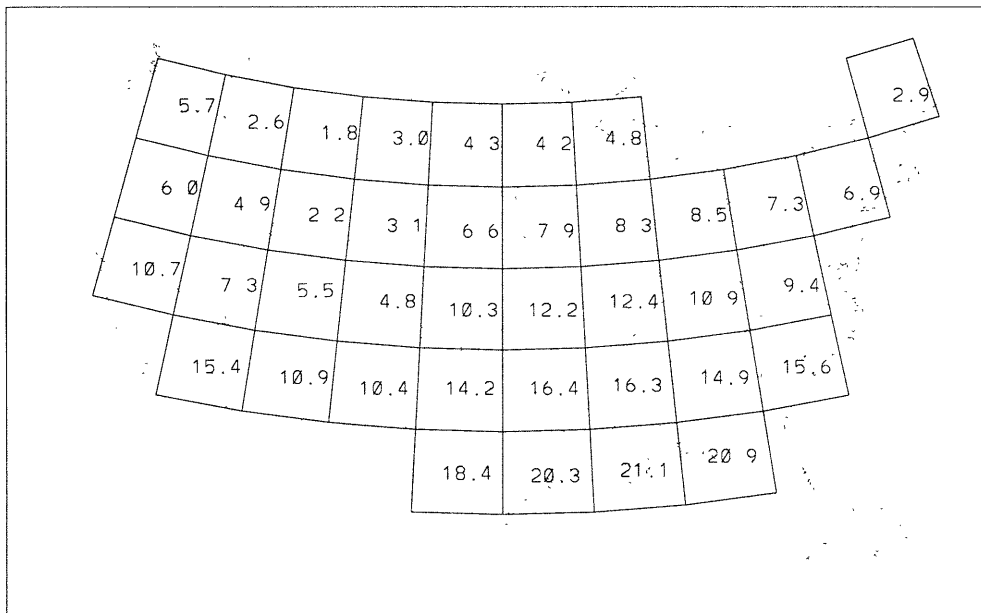
Figure D-9: GCM grid area maps over the contiguous United States showing surface air temperature for *Wallis et al.* [1990] observations and SIMG

SIM1: ANNUAL SURFACE AIR TEMP [C]
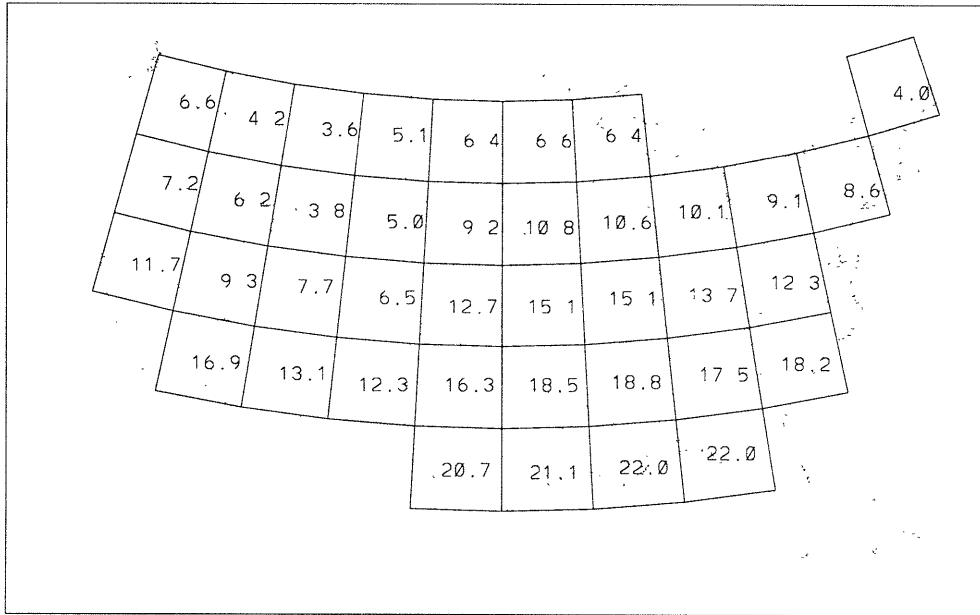
SIM2· SURFACE AIR TEMP [C]
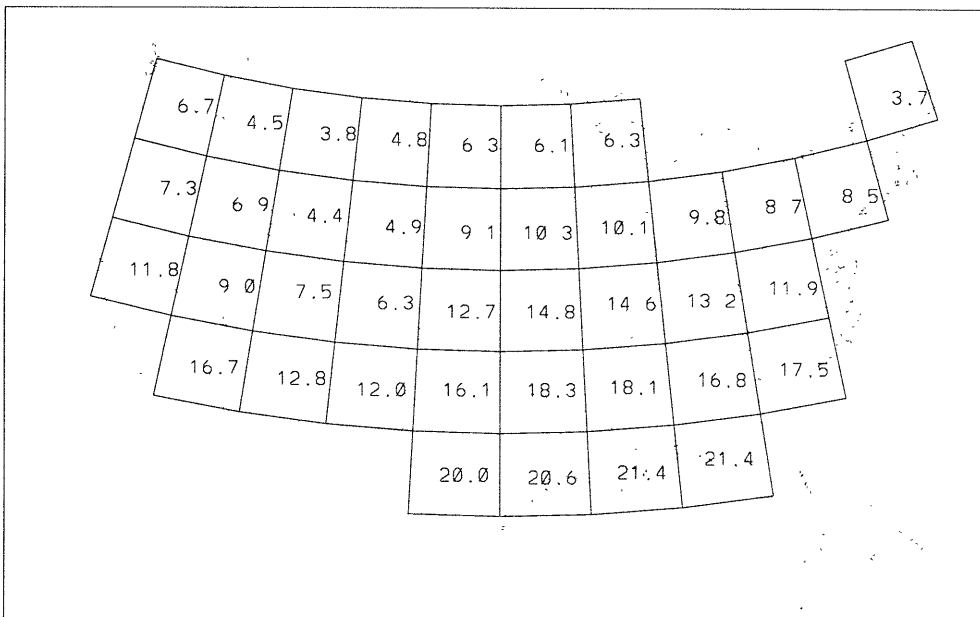
Figure D-10: GCM grid area maps over the contiguous United States showing surface air temperature for SIM1 and SIM2